REPUBLIQUE DU CAMEROUN
Paix-Travail-Patrie

UNIVERSITE DE YAOUNDE I

CENTRE DE RECHERCHE ET DE FORMATION DOCTORALE EN SCIENCES, TECHNOLOGIES ET GEOSCIENCES

UNITE DE RECHERCHE ET DE FORMATION DOCTORALE EN PHYSIQUES ET APPLICATIONS

B.P 812 Yaoundé
Email: crfd_stg@uy1.uninet.cm

REPUBLIC OF CAMEROON
Peace-Work-Fatherland

THE UNIVERSITY OF YAOUNDE I

POSTGRADUATE SCHOOL OF SCIENCES, TECHNOLOGY AND GEOSCIENCES

RESEARCH AND POSTGRADUATE TRAINING UNIT FOR PHYSICS AND APPLICATIONS

P.O. Box 812 Yaoundé
Email: crfd_stg@uy1.uninet.cm

LABORATORY OF MECHANICS, MATERIALS AND STRUCTURE
LABORATOIRE DE MECANIQUE, MATERIAUX ET STRUCTURE

STOCHASTIC RESONANCE PHENOMENON IN DEFORMABLE SUBSTRATES: EFFECTS OF COUPLING, CHAIN SIZE AND POTENTIAL SHAPE

Thesis submitted in partial fulfillment of the requirements for the award of the degree of Doctor of Philosophy (Ph.D.) in Physics,

option: Fundamental mechanics and complex systems

By

WADOP NGOUONGO YANNICK JOEL

Registration Number: **07W005**

Master of Science in Physics

Under the direction of

DJUIDJE KENMOE G.

Associate Professor

Under the supervision of

KOFANE Timoléon Crépin

Professor

2021

UNIVERSITE DE YAOUNDE I
UNIVERSITY OF YAOUNDE I

FACULTE DES SCIENCES
FACULTY OF SCIENCE

DEPARTEMENT DE PHYSIQUE
DEPARTMENT OF PHYSICS

ATTESTATION DE CORRECTION DE LA THESE DE DOCTORAT/Ph.D

Nous, Professeur **FEWO Serge Ibraid** et Professeur **WOAFO Paul**, respectivement Examinateur et Président du jury de la Thèse de Doctorat/Ph.D de Monsieur **WADOP NGOUONGO Yannick Joel** Matricule **07W005**, préparée sous la direction du Professeur **Germaine DJUIDJE KENMOE épouse ALOYEM KAZE** et sous la supervision du Professeur **KOFANE Timoléon Crépin,** intitulée : « **Stochastic resonance phenomenon in deformable substrates : effects of coupling, chain size and potential shape**», soutenue le **Vendredi, 23 Juillet 2021**, en vue de l'obtention du grade de Docteur/Ph.D en Physique, Spécialité **Mécanique, Matériaux et Structures**, attestons que toutes les corrections demandées par le Jury de soutenance ont été effectuées.

En foi de quoi, la présente attestation lui est délivrée pour servir et valoir ce que de droit.

Fait à Yaoundé le 29 SEP 2021

Un Examinateur

Pr. FEWO Serge Ibraïd

Le Président du Jury

Pr. WOAFO Paul

Le Chef de Département de Physique

UNIVERSITE DE YAOUNDE I * FACULTE DES SCIENCES * DEPARTEMENT DE PHYSIQUE
Le Chef de Département
Adjaka Jean-Marie Bienvenu
Professeur

University of Yaounde I

Faculty of Science

Department of Physics

STOCHASTIC RESONANCE PHENOMENON IN DEFORMABLE SUBSTRATES: EFFECTS OF COUPLING, CHAIN SIZE AND POTENTIAL SHAPE

Submitted and defended in Fulfillment of the Requirements for the Degree of Doctor of Philosophy/PhD in Physics
Option: Fundamental Mechanics and Complex Systems

By

WADOP NGOUONGO Yannick Joel
Registration number: 07W005
Master in Physics

Director
Prof. Germaine DJUIDJE KENMOE épouse ALOYEM
Professor, University of Yaounde I (Cameroon)

Supervisor
Prof. Timoléon Crépin KOFANE
Professor, University of Yaounde I (Cameroon)

Laboratory of Mechanics, Materials and Structures

Dedication

This work is dedicated to:

- My Lord God for all he has done for me.
- My late father **NGOUONGO Emmanuel**.
- My dear mother **WOGUEP Gisèle**.

Acknowledgements

The accomplishment of this thesis would not be possible without the assistance and the help of somebody. So, I would like to express my sincere gratitude to:

♣ My Director Professor Germaine DJUIDJE KENMOE, for motivating discussions and great time we had during my dissertation. She gave me the opportunity to work in the Mechanics Lab and showed me the way to postgraduate study. In spite of huge academic and administrative duties, she always found time to discuss with me and answer my queries.

♣ My supervisor Professor Timoleon Crepin KOFANE, Head of the Laboratory of Mechanics, Materials and Structures for his high human qualities, guidance and constant support during this research work. I am very grateful for the quality of his teaching and for his constructive comments.

♣ The head of Department of Physics Professor Jean Marie Bienvenu NDJAKA, I am very grateful for the quality of his teaching and for his constructive comments.

♣ Professor Clement TCHAWOUA, for his teaching and his encouragements.

♣ Professors Serge Ibraid FEWO, and Martin SIEWE SIEWE for their encouragement and their moral support.

♣ Professors NANA NBENDJO, Paul WOAFO, Serge Sylvain ZEKENG, Thomas BOUETOU BOUETOU, for their teachings and their visions of the evolution of Science.

♣ Doctor Rosalie WOULACHE, for her teaching and for her constructive comments.

♣ The teaching staff of the Department of Physics, Faculty of Science and University of Yaounde I for their teaching during my higher education, I specially express my acknowledgements.

♣ Thanks to the official editors and referees of Journal of Statistical Physics, and Physica A, for their detailed review, constructive criticism and excellent advice during the evaluation of my different publications.

♣ Thanks to Doctor Alain TOGUEU MOTCHEYO who is among a brilliant people who gave me his encouragement.

♣ Thanks to my late father NGOUONGO, my mother WOGUEP GISELE, my big sister KODJOUO Myriam Lore, my small sister SOTCHE Davina, my small brothers KAMNANG Sylvain, CHIMI Jovani, NOUMI Cyril, my fiancy NGAMENI Myriam, my uncles NGUEPKAM Joseph and YANKAP Richard and my brother in law FONKOU

Désiré for their love and availability.

♣ Thanks to Phd students of the Laboratory of Mechanics, Materials and Structures, specially to Paul NDY Von Kluge, Andre Marie FOPOSSI MBEMMO, Maxime Fabrice KEPNANG PEBEU, TEMGOUA DJOUATSA Diane Estelle and Dieudonné ZANGA.

♣ Thanks to the students of Nanoscale group specially to Paul NDY Von Kluge, Medine DJOLIEU FUNAYE, A. D. KENNE, A. F. MOYO TALA, H. W. KEPDJIEP NGANSOP.

♣ Thanks to all my family (uncles, aunts, cousins, nephews, nieces,...) for their love and availability.

♣ Thanks to all the unmentioned persons who have contributed even a little to this work. I did not forget you.

¡==========

Contents

List of Figures

List of Abbreviations

SR : **S**tochastic **R**esonance
SAR: **S**tochastic **A**nti**R**esonance
ASDP: **A**symmetric **D**eformable **P**otential
DWDP: **D**ouble-**W**ell **D**eformable **P**otential
RP: **R**emoissenet-**Peyrard**
PSD: **P**ower **S**pectral **D**ensity
HLA: **H**ysteresis **L**oop **A**rea
SNR: **S**ignal-to-**N**oise **R**atio
FFT: **F**ast **F**ourier **T**ransform
FK: **F**renkel-**K**ontorova
RK4: **F**ourth-order **R**unge **K**utta
PT: **P**arity-**T**ime
VR: **V**ibrational **R**esonance
AGWN: **A**dditive **G**ausssian **W**hite **N**oise
JJ: **J**osephson **J**unction

¡==========

Abstract

In this work, we focus our attention on the beneficial role of noise by exploring the stochastic resonance phenomenon which allows to amplify the weak signal in the artificial Brownian motors. In order to approach the realistic systems, we put forward the occurrence of this phenomenon in the periodic deformable substrate potentials introduced some years ago by Remoissenet and Peyrard.

Firstly, we present a theoretical prediction of the stochastic resonance of an underdamped Brownian particle in a periodic nonsinusoidal potential subjected to a periodic external field. This phenomenon is demonstrated through an investigation of the hysteresis loop area (HLA) which is equivalent to the input energy lost by the system to the environment per period of the external force and clearly studied as a function of the damping coefficient as well as the shape of the potential. It is observed that SR is evident in some range of the shape parameter of the potential, but cannot be observed in the other range. Specially, variation of the shape potential affects significantly and not trivially the heigh of the energy barrier as well as the occurrence of SR. The finding results show crucial dependence of the temperature of occurrence of SR on the shape of the potential. It is noted that the maximum of the input energy generally decreases with dissipation coefficient.

Secondly, we study the dynamics of a particle in the asymmetric deformable potential (ASDP) and double well deformable potential (DWDP). The SR is numerically studied in each both the systems in terms of hysteresis loop area. The average input energy displays a double SR peak as a function of temperature in the ASDP and one peak of SR which occurs at low temperature in the DWDP. We show that as a function of the potential shape, the input energy can be confined to two narrow bands however and the input energy distribution can get a bimodal nature. The presence of Chaos is also investigated in the DWDP system where we demonstrate that the Chaos can destroy the SR phenomenon.

Finally, in connection with SR and SAR phenomena, we analyse the dynamics of a chain of N particles coupled in a periodic sinusoidal potential which is a special case of the deformable Remoissenet-Peyrard potential. The dependence of the coupling pa-

rameter as well as the system size on SR and SAR is presented. The role played by the coupling on the SR is considered. We show that there is a range of coupling parameter where only SAR is observed, after this range the SR can occur, however, there also exists a range where neither SAR nor SR appear. It is noted that the maximum and the minimum of the average input energy increases with the coupling parameter. Also demonstrate that there exists an optimal value of the number of particles N for which the average input energy of the first particle reaches the saturation.

Keywords: Stochastic resonance; stochastic antiresonance; hysteresis loop area; non-sinusoidal Remoissenet-Peyrard deformable potential; double-well deformable potential; asymmetric deformable potential; chaos; coupled particles; noise; chain size; coupling; potential shape.

Résumé

Dans ce travail, nous focalisons notre attention sur le rôle bénéfique du bruit en explorant le phénomène de résonance stochastique qui permet d'amplifier les faibles signaux dans les moteurs Browniens artificiels. Dans le but d'aborder des systèmes plus réels, nous mettons en évidence l'apparition du phénomène de résonance stochastique (RS) dans les potentiels à substrat déformables périodiques introduits il y a quelques années par Remoissenet et Peyrard.

Dans un premier temps, nous présentons une prédiction théorique de la résonance stochastique d'une particule Brownienne amortie dans un potentiel non-sinusoïdal pério dique soumis à une force d'excitation périodique. Ce phénomène est démontré par une étude de l'aire de la boucle d'hystérésis (HLA) qui équivaut à l'énergie perdue par le système dans l'environnement par période de la force d'excitation est clairement étudiée en fonction du coefficient de frottement ainsi que la forme du potentiel. On observe que la RS est évident dans un certain intervalle du paramètre de forme du potentiel, mais ne peut pas être observé dans l'autre intervalle. En particulier, la variation de la forme du potentiel affecte de manière significative et non-triviale la hauteur de la barrière d'énergie du potentiel ainsi que l'apparition de la RS. Les résultats montrent une dépendance cruciale de la température d'occurrence de la RS à la forme du potentiel. Il est à noter que le maximum de l'énergie d'entrée diminue généralement avec le coefficient de frottement.

Deuxièmement, nous étudions la dynamique d'une particule dans un potentiel défor mable asymétrique (ASDP) et un potentiel double-puits déformable (DWDP). La RS est numériquement étudié dans chacun des deux systèmes en termes d'aire de la boucle d'hystérésis. L'énergie d'entrée moyenne montre un double pic de résonance en fonction de la température dans le modèle ASDP et un seul pic de résonance qui se produit aux basses températures dans le modèle DWDP. Nous montrons qu'en fonction de la forme du potentiel, l'énergie d'entrée peut toutefois être limitée à deux bandes étroites et la distribution d'énergie d'entrée peut avoir une nature bi-modale. La présence du chaos est aussi exploré dans le système DWDP où nous démontrons que le chaos peut détruire le Phénomène de RS.

Enfin, en relation avec les phénomènes de résonance stochastique et d'antirésonance

stochastique (ARS), nous analysons la dynamique d'une chaîne de N particules couplées dans un potentiel sinusoïdal périodique qui est un cas particulier du potentiel déformable de Remoissenet-Peyrard. La dépendance du paramètre de couplage ainsi que de la taille du système par rapport à la RS et la ARS est présentée. Le rôle joué par le couplage sur la RS est pris en compte. Nous montrons qu'il existe une gamme de paramètres de couplage où seul l'ARS est observé. Après cette plage, la RS peut se produire. Cependant, il existe également une plage où ni l'ARS ni la RS ne se produit. Il est à noter que le maximum et le minimum de l'énergie d'entrée moyenne augmente avec le paramètre de couplage. Nous démontrons également qu'il existe une valeur optimale du nombre de particules N pour laquelle l'énergie d'entrée moyenne de la première particule atteint la saturation.

Mots clés: Résonance stochastique; antirésonance stochastique; aire de la boucle d'hystérésis; potentiel déformable de Remoissenet-Peyrard non-sinusodal; potentiel double-puits déformable; potentiel déformable asymétrique; chaos; particules couplées; bruit; taille de la chaine; couplage; forme du potentiel.

General Introduction

These recent years, theoretical Physics has attracted considerable interest for the advanced technological. This is mainly due to various observations made in the nature. In order to clarify certain of these different observations and provide them some physical explanations, the researchers in Physics have produced the good mathematical models based on the laboratory experiments. One omong these fundamental models is the system constituted by one or many trapped particles. When this particle is trapped in a potential well and driven by an external force, a variety of phenomena can be realized such as synchronization [1, 2, 3, 4], chaos and bifurcation [5, 6, 7, 8] and recently vibrational resonance [9]. The effect of resonance is to produce a large vibration. Adding the noise (thermal fluctuation force) the system can exhibit several behaviors such as negative mobility [10], diffusion [11] and stochastic antiresonance (SAR) [12]. The general trend of a noise is to weaken the effect of a signal. Static on a radio-station, ancillary conversations in a crowded room and flashing neon light along a busy thoroughfare all tend to obscure or disturb from the desired information. Now, it has been realized that certain noise-induced phenomena are of great use in various contexts. One such noise-induced phenomenon which has a wide range of applications in various branches of science and engineering is stochastic resonance (SR).

Stochastic resonance is one of the most shining and relatively simple examples of this type of nontrivial behavior of nonlinear systems under the influence noise. It was first introduced by the Italian physicists Benzi et al. [13] in 1981 to explain the periodicity of earth's ice ages. The eccentricity of the orbit of the earth varies with a periodicity of about 10^5 years, but according to current theories the variation is not strong enough to cause a dramatic climate change. He supposes that the ice-covered and water-covered

earth correspond to the two local minima. The variation of eccentricity with the period 10^5 years is too weak to induce the transition from ice-covered to water-covered earth and vice-versa. By introducing a bistable potential, Benzi et al. [13] suggested that a co-operative effect between the weak periodic variation in the eccentricity (the signal) and the other random fluctuation might account for the strong periodicity observed. Thus, Benzi et al. show from the concept of SR that, in sharp contrast to the common perception of noise, a noise of suitable strength can be beneficial for a system. Motivated by their work, a first experimental verification of the stochastic resonance phenomenon has been done by Fauve and Heslot [14] in 1983, who studied the noise dependence of the spectral line of an ac-driven Schmitt trigger. The field then remained somewhat dormant until the modern age of stochastic resonance was ushered in by a key experiment in a bistable ring laser [15]. After, prominent dynamical theories in the adiabatic limit [16, 17, 18, 19] and in the full non-adiabatic regime [20, 21, 22] have been proposed.

The researchers of all domains and the engineers exploit this SR phenomenon nowadays as an instrument for their specific purposes. The interest of the SR problem comes from the large range of physical applications. SR has been developed to meet the needs in various engineering and research areas, such as aeronautic, astronomy, economy, mechanics, communication and civil engineering. SR has been and is a subject of interest. Much progress have been done in this field of study, leading to modern applications that can be found in several domains including Physics, Chemistry and Biology. In the near future, the SR is expected to lead to advanced technological applications. for example macro, nanoscale and micro oscillators and devices working in resonant modes as nonlinear mixers sensors and atomic scale imaging are found to give rise to higher efficiency and greatly improved performance. Biological systems use SR to their advantage [23]. This phenomenon has the potential to be utilized to control kinetically the pathways of a biochemical reaction [24] in Chemistry field.

Considerable progress have been made these last years in the analyse of occurrence of the SR in sinusoidal and nonsinusoidal systems. SR has been found to occur in diverse systems such as nanomechanical oscillators [25], tunnel diode [26], nanotube transistors

[27, 28], social systems [29], chemical systems [30], financial models [31], vegetation ecological systems [32], neuronal systems [33], periodic potential systems [34, 35] just to mention a few. Much researchers have extensively studied theoretically and experimentally this power phenomenon around the periodic systems like the monostable, bistable, multistable systems. Although all these works have been done around this topic, it will be judicious to take into account the substrate geometry. This is then in this context that this thesis is studied.

In this thesis, we specially use a wide class of potentials such as the nonsinusoidal Remoissenet-Peyrard (RP) potential, the double-well deformable potential (DWDP) and the asymmetric deformable potential (ASDP), all introduced by Remoissenet and Peyrard [36, 37] to study the SR in a system constituted of one particle and of N-coupled particles in the sinusoidal case of the RP. We focus our attention on the dependence of the system parameters like the shape of the potential, the friction coefficient, amplitude of the external force, the coupling and the chain size on the SR. The main novelty of this work resides in the fact that these kind of substrates have been never considered in the study of the possibility of occurrence of the SR.

To achieve these goals, we structure this thesis in three chapters.

In chapter one, we present the literature review on resonance in general and on stochastic resonance in particular. Other kind of resonances are also exhibited.

Second chapter is devoted to the methodology and the description of the mathematical tools and numerical methods used to solve the different equations. We present the Fourth-order Runge-kutta methods for solving Langevin equation and the quantities of interest.

Third chapter presents and discusses the main results obtained of our work.

The document ends with a general conclusion along with prospects. We summarize our results and give some future directions that could be investigated.

CHAPTER I

LITERATURE REVIEW ON STOCHASTIC RESONANCE AND PROBLEMS STATEMENTS

I.1 Introduction

The real challenge of the researchers nowadays is to provide some laws that can be used in the field of nano-mechanics and the construction of the particular oscillators. this is due to the fact that the general interest is to utilize the system in resonant mode. indeed The phenomenon where a maximum amplitude appears as a function of the frequency is called resonance [38, 39, 40, 41]. According to the parameter considered, it can get a specific name well-known in the literature. This Chapter provides an overview of the literature, a general information about resonance phenomena and a particular idea on the stochastic resonance phenomenon. To achieve it, firstly we present the resonance concept and some examples of resonance to better understanding of the results of this thesis. secondly, we give a brief generality on white noise. Thirdly, the stochastic resonance is presented point by point to allow a good perception of the studied phenomenon. Finally, we present the Josephson junction model which is one of the application of the Brownian motion and the problem statement of this thesis.

I.2 Resonance concept

The word resonance is usually applied in physics to cases in which a dynamical system, having periodic oscillations at some frequencies ω_i, when subject to a periodic forcing of frequencies near one of the ω_i, shows a marked response. In the recent studies, however, resonance has been utilized more broadly to describe situations where the adjustment of a parameter that is not always a frequency optimises the amplification or response of a system [42]. In the phenomenon of stochastic resonance [43], for instance, it is the noise intensity that is this parameter in question. Recent research has proven that many different types of external force can also induce resonances and that the latter can manifest in diverse forms, such as chaotic resonance [44, 46, 45], stochastic resonance [43, 47], coherence resonance [48, 49], ghost resonance [50], parametric resonance [42], vibrational resonance [51], antiresonance [52] and auto-resonance [42].

I.3 Examples of resonance

- **Chaotic resonance**, due to a perturbation of chaotic nature.
- **Coherence resonance**, induced by an external noise in the absence of any external periodic force.
- **Ghost resonance**, induced by a multi-frequency force at a frequency absent in the external force. The ghost resonance due to an external noise is the ghost stochastic resonance. This ghost resonance phenomenon can be used to explain the missing fundamental illusion in which a third lower pitched tone is often heard when two tones occur together [53].
- **Parametric resonance**, induced by a periodic variation of one or more of the parameter of the system. it produces generally in the systems whose the mathematical modelling gives a Mathieu equation.

- **Vibrational resonance (VR)**, firstly observed and shown numerically by Landa and McClintock [51] and confirmed theoretically by Gitterman [54] and by Blekhman and Landa [55, 56]. VR occurs in bi-harmonically driven non-linear systems when there is a large difference between the frequencies of the two driving forces, say, ω and Ω with $\Omega \gg \omega$. One of which is a fast oscillation at frequency much higher than that of the slower. In VR, the noise in the stochastic resonance case [57, 58, 59] is replaced by a high-frequency input signal, for appropriately chosen parameters, to an enhancement in the system's response to the slow signal.

- **Antiresonance**, in certain systems the amplitude of the response is found to be either zero or minimum at one or more frequencies or at certain values of a control parameter. When the adjusted parameter is the noise intensity, it is rather called stochastic antiresonance (SAR).

- **Autoresonance**, induced by an external force with time-dependent frequency.

- **Stochastic resonance**, induced by a weak noise at the frequency of the applied periodic force.

I.4 Generalities on noise

In common use, the word noise means any undesirable sound. In physics , noise is mostly unwanted random addition to a signal; it is called noise as a generalisation of the acoustic noise heard when listening to a weak radio transmission with significant electrical noise. Signal noise is heard as acoustic noise if the signal is converted into sound; it manifests as snow on a television or video image. High noise levels can block, distort, change or interfere with the meaning of a message in human, animal and electronic communication. In signal processing or computing noise can be considered random undesired data without meaning; that is, data that is not being used to transmit a signal, but is simply produced as an unwanted by-product of other activities. In biology, many different forms of cellular noise exist, where a measurement displays substantial

variance around its mean: for example, transcriptional noise describes the variability in gene activity between cells in a population [60]. In many cases, the special case of thermal noise arises, which sets a fundamental lower limit to what can be measured or signalled and is related to basic physical processes described by thermodynamics; in general, noise can refer to anything that interferes with what we want: it might be a single voice of someone sitting next to us in a movie, but the purest form of noise comes from a totally random source.

The earliest experience of noise in a physical system is the Brownian motion. This motion defined the random movement of particles in a fluid due to their collision with atoms or molecules. The random movement was totally due to the presence of the thermal fluctuations (noise). Noise can then be classified in two different ways. From their spectral properties, we distinguish the white and colored noises. By interesting on statistical properties, we have the uniform noises and Gaussian noises.

I.4.1 White noise

White noise is a signal whose samples are regarded as a sequence of serially uncorrelated random variables with zero mean and finite variance; a single realization of white noise is a random shock. Depending on the context, one may also require that the samples be independent and have identical probability distribution (in other words independent and identically distributed random variables are the simplest representation of white noise). White noise is a type of noise that is produced by combining signal of all different frequencies together. The adjective "white" is used to describe this type of noise because of the way white light works. White light is light that is made up of all the different colours (frequencies) of light combined together (a prism or a rainbow separates white light back into its component colors). In the same way, white noise is a combination of all of the different frequencies of a signal. Because white noise contains all frequencies, it is frequently used to mask other signal. In particular, if each sample has a normal distribution with zero mean, the signal is said to be additive white

Gaussian noise (AWGN).

I.4.2 Additive white Gaussian noise (AWGN)

Additive white Gaussian noise is a basic noise model used in information theory to mimic the effect of many random processes that occur in nature. The modifiers denote specific characteristics:

- Additive because it is added to any noise that might be intrinsic to the information system.
- White refers to the idea that it has uniform to power across the frequency band for the information system. It is an analogy to the color white which has uniform emissions at all frequencies in the visible spectrum.
- Gaussian because it has a normal distribution in the time domain with an average time domain value of zero.

Wideband noise comes from many natural noise, such as the thermal vibrations of atoms in conductors (referred to as thermal noise or Johnson-Nyquist noise), shot noise, black-body radiation from the earth and other warm objects, and from celestial sources such as the Sun. The central limit theorem of probability theory indicates that the summation of many random processes will tend to have distribution called Gaussian or Normal.

AWGN is often used as a channel model in which the only impairment to communication is a linear addition of wideband or white noise with a constant spectral density (expressed as watts per hertz of bandwidth) and a Gaussian distribution of amplitude. The model does not account for fading, frequency selectivity, interference, non-linearity or dispersion. However, it produces simple and tractable mathematical models which are useful for gaining insight into the underlying behaviour of a system before these other phenomena are considered.

I.4.3 spectral properties of the white noise

Assuming the environment to be an equilibrium heat bath with independent collisions, $\Gamma(t)$ is the Gaussian white noise of zero mean

$$\langle \Gamma(t) \rangle = 0 \tag{1}$$

Usually, the duration time τ_r of a collision is much smaller than the relaxation time $1/\gamma$ of the velocity of the small particle. We may therefore take the limit $\tau_r \to 0$ as a reasonable approximation.

By consequent, the autocorrelation function of a white noise is a function of the Dirac function. The white noise then satisfies fluctuation-dissipation relation,

$$\langle \Gamma(t)\Gamma(t') \rangle = 2D\delta(t - t') \tag{2}$$

Where t and $t^{'}$ are different times. Indeed, the fluctuation-dissipation theorem translates the fact that the energy dissipation and random fluctuations are not independent of each other since both of them have the same origin, namely the interaction of the particle with a huge number of macroscopic degrees of freedom of the environment. $D = \gamma k_B T$ represents the diffusion coefficient of the Brownian particle, γ is the damping parameter, k_B is the Boltzmann constant, and T is the temperature of the bath. The Dirac delta function appears because otherwise the average energy of the small particle cannot be finite as it should be according to the equipartition law

$$\frac{1}{2} m \langle v^2 \rangle = \frac{1}{2} K_B T \tag{3}$$

Of course white noise does not exist as physically realizable process; it is, however fundamental in mathematical, and indeed in a physical sense, in that it is an idealization of many processes that do occur.

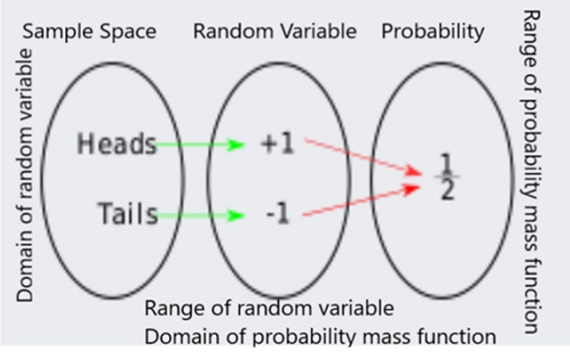

Figure 1: This graph shows how random variable is a function from all possible outcomes to numerical quantities and also how it is used for defining probability mass functions.

I.5 Random variables

In probability and statistics, a random variable, random quantity, aleatory variable, or stochastic variable is described informally as a variable whose values depend on outcomes of a random phenomenon [61]. The formal mathematical treatment of random variables is a topic in probability theory. In that context, a random variable is understood as a measurable function defined on a probability space whose outcomes are typically real numbers (see **Fig 1**).

A random variable's possible values might represent the possible outcomes of a yet-to-be-performed experiment, or the possible outcomes of a past experiment whose already-existing value is uncertain (for example, because of imprecise measurements or quantum uncertainty). They may also conceptually represent either the results of an objectively random process (such as rolling a die) or the subjective randomness that results from incomplete knowledge of a quantity. The meaning of the probabilities assigned to the potential values of a random variable is not part of probability theory itself but is instead related to philosophical arguments over the interpretation of probability. The mathematics works the same regardless of the particular interpretation in use.

As a function, a random variable is required to be measurable, which allows for probabilities to be assigned to sets of its potential values. It is common that the out-

comes depend on some physical variables that are not predictable. For example, when tossing a fair coin, the final outcome of heads or tails depends on the uncertain physical conditions which outcome will be observed is not certain. The coin could get caught in a crack in the floor, but such a possibility is excluded from consideration.

The domain of a random variable is a sample space, which is interpreted as the set of possible outcomes of a random phenomenon. For example, in the case of a coin toss, only two possible outcomes are considered, namely heads or tails.

A random variable has a probability distribution, which specifies the probability of its values. Random variables can be discrete, that is, taking any of a specified finite or countable list of values, endowed with a probability mass function characteristic of the random variable's probability distribution; or continuous, taking any numerical value in an interval or collection of intervals, via a probability density function that is characteristic of the random variable's probability distribution; or a mixture of both types.

Two random variables with the same probability distribution can still differ in terms of their associations with, or independence from, other random variables. The realizations of a random variable, that is, the results of randomly choosing values according to the variable's probability distribution function, are called random variates

I.6 Examples of the general effect of noise in some domains

- **In electronics**, noise is an unwanted disturbance in an electrical signal [62]. Noise generated by electronic devices varies greatly as it is produced by several different effects. Generally thermal noise is unavoidable, and generated by the random thermal motion of charge carriers (usually electrons), which happens regardless of any applied voltage. This thermal noise is approximately white, meaning that its power spectral density is nearly equal throughout the frequency spectrum. The amplitude of the signal has very nearly a Gaussian probability density function.

- **In communication**, noise is an error or undesired random disturbance of a useful information signal. The noise is a summation of unwanted or disturbing energy from natural and sometimes man-made sources. Noise is, however, typically distinguished from interference, for example in the signal-to-noise ratio (SNR), signal-to-interference ratio and signal-to-noise plus interference ratio measures. Noise is also typically distinguished from distortion, which is an unwanted systematic alteration of the signal waveform by the communication equipment, for example in signal-to-noise and distortion ratio and total harmonic distortion plus noise measures. A communication system affected by thermal noise is often modelled as an additive white Gaussian noise channel.

- **In biology**, noise permeates every level of the nervous system, from the perception of sensory signals to the generation of motor responses, and poses a fundamental problem for information processing [63, 64, 65].

- **In medicine**, noise health effects are the physical and psychological health consequences of regular exposure to consistent elevated sound levels. Elevated workplace or environmental noise can cause hearing impairment, tinnitus, hypertension, ischemic heart disease, annoyance, and sleep disturbance [66, 67]. Chronic noise exposure is associated with sleep disturbances and increased incidence of diabetes. Adverse cardiovascular effects occur from chronic exposure to noise due to sympathetic nervous system's inability to habituate [66].

Noise is commonly known to get a negative influence on physical systems, However, in 1981 it has been demonstrated that under the conditions such as

- a weak coherent signal

- an energetic activation barrier

noise can be beneficial for a physical system. Therefore noise-induced phenomena which are of great use in various context. One such noise-induced phenomenon

which has a wide range of application in various branches of science and engineering is stochastic resonance.

I.7 Stochastic resonance

I.7.1 Definition

Stochastic resonance is a cooperative phenomenon arising from the interplay between deterministic and random dynamics in a non-linear system wherein the coherent response to a deterministic monochromatic signal can be enhanced by the presence of an optimal amount of noise [68]. This phenomenon requires three ingredients: a weak coherent signal, a noise source and an energetic activation barrier. The mechanism of SR is relatively simple to explain. The optimal periodic response of a system to an external periodic drive as a function of the noise strength is referred as stochastic resonance. In other terms, it manifests by a synchronization activated hopping events between the potential minima and the weak periodic forcing. **Fig 2** shows the general scheme of a stochastic resonance phenomenon for the physical systems.

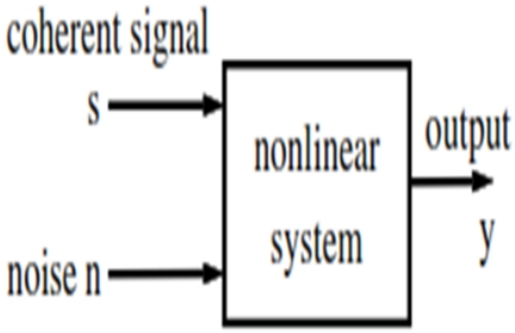

Figure 2: The general scheme of stochastic resonance.

Such a plot, **Fig 3** is a typical curve of output response versus input noise magnitude, for the systems capable of stochastic resonance.

In the domain of trapped particles, to the SR, although the periodic forcing is too weak to allow the periodic switching between the wells, the noise at a certain intensity

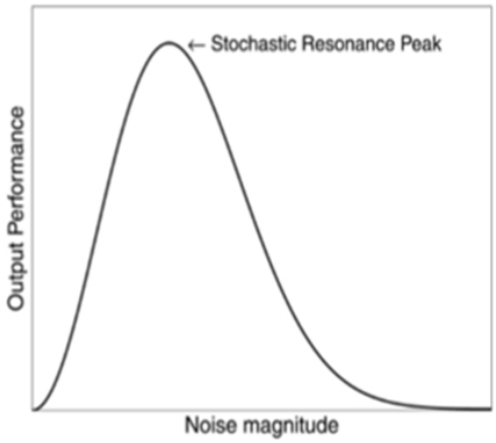

Figure 3: Typical curve of a manifestation of SR in the systems [69].

will permit the periodical inter-well transitions between wells, mainly with the period of the periodic external force. One then says that noise-induced has synchronized with the weak periodic forcing. The interest of the researchers to this phenomenon is mainly due to its origin, its goal and its vast application in many fields.

I.7.2 Origin, goal and consequence of the stochastic resonance phenomenon

Origin

The concept of stochastic resonance has been originally discovered by Benzi et al. and put forward in the review papers [13, 70, 71] wherein they treat the problem of the periodically recurrent ice ages. This good suggestion that stochastic resonance might rule the periodicity of the primary cycle of recurrent ice ages has been raised independently by C. Nicolis and G. Nicolis [72, 73, 74, 75]. A statistical analysis of continental ice volume variations over the last 10^5 years shows that the glaciation sequence gets an average periodicity of 10^5 years. This conclusion is intriguing because the only comparable astronomical time scale in earth dynamics known so far is the modulation period of its orbital eccentricity caused by planetary gravitational perturbations. The ensuing variations of the solar energy influx on the earth surface are exceedingly small. The question

climatologists debate is whether a geodynamical model can be devised, capable of enhancing the climate sensitivity to such a small external periodic forcing. Stochastic resonance provides a simple, although not conclusive answer to this question [76, 77, 78, 79]. In the model of Benzi et al., the global climate is modelled by a double-well potential, where one minimum represents a small temperature corresponding to an ice-covered earth and the other minimum represents a water-covered earth. The small modulation of the earth's orbital eccentricity is represented by a weak periodic forcing. Short-term climate fluctuations, such as the annual fluctuations in solar radiation, are modelled by Gaussian white noise.

Goal

Stochastic resonance is by now a well-established phenomenon. As a function of the studied field, it can have a particular aim. However, its main goal is to produce the large vibrations by adding of noise and allows to amplify feeble signals, and to treat a signal.

Consequence

SR can be an advantage for some systems as for instance the biological systems which utilize SR to their advantage [23]. It can also be an inconvenient for other systems such as the ecological vegetation growth systems [32] and civil engineering where the large vibrations caused at an appropriate noise intensity weakens the stability of the system.

Characterization of stochastic resonance

Having put forward the main physical ideas of SR, we define now the observables or statistical tools useful for the characterization of this phenomenon. These observables should be physically motivated, easily measurable, and/or be of technical relevance. To analyse the performance of the system in the presence of noise, several key quantities

in the literature are utilized such as the power spectral density (PSD) [80], the signal-to-noise ratio (SNR) [81], the residence-time distribution density of a particle in one of the potential wells [82], the response and the hysteresis loop area (HLA) [83].

- **Power spectral density (PSD)**

  By taking an ensemble average of the system response, it can be more convenient to obtain the relevant phase-averaged power spectral density $S(\omega)$ defined as

$$S(\omega) = \int_{-\infty}^{+\infty} e^{-i\omega\tau} \langle\langle f(t+\tau) f(t) \rangle\rangle d\tau. \tag{4}$$

  Where the inner brackets denote an ensemble average over the realizations of the noise and outer brackets indicate the average over the input initial phase. To calculate the power spectral density of a variable x, a set of 2^{10} data collected at a time interval of $(2\pi\omega)/10$ is used. The output of the fast Fourier transform (FFT) routine is the spectral density of the output signal. More accurate spectral densities are obtained by averaging over 25 different realizations of Gaussian random numbers.

- **Signal-to-noise ratio (SNR)**

  The most common measure used to characterize stochastic resonance is SNR. It is the ratio of the Fourier coefficient and the value of the noise at the frequency ω.

$$SNR = 10log_{10}(\frac{S(\omega)}{S_N(\omega)})dB \tag{5}$$

  The signal power $S = |X(\omega)|^2$ is the magnitude of the output power spectrum at the frequency ω.

- **Residence-time distribution density**

  An alternative quantity, which also clearly exhibits the stochastic resonance phenomenon is the probability distribution of normalized residence times. This is

obtained as follows. For a fixed noise intensity D, 10^5 residence times in a well are computed.

- **Response**

  The response is an appropriate method to characterize the signature of the SR. It corresponds to the output response $Q(\omega)$ and is generally calculate as follows

$$Q(\omega) = \frac{\sqrt{Q_{\sin}^2 + Q_{\cos}^2}}{A_0} \tag{6}$$

  $Q_{\sin}$ and $Q_{\cos}$ are the sine and cosine responses respectively. A_0 represents the amplitude of the periodic external force.

  The terms $Q_{\sin}$ and $Q_{\cos}$ are given by:

$$Q_{\sin} = \frac{2}{NT} \int_0^{NT} x(t) \sin(\omega t) dt \tag{7}$$

$$Q_{\cos} = \frac{2}{NT} \int_0^{NT} x(t) \cos(\omega t) dt \tag{8}$$

  Where $T = \frac{2\pi}{\omega}$ is the period and N is the number of periods.

- **Hysteresis loop area (HLA)**

  The input energy expended per period of the external force on the system by the field acts as a good quantifier of SR. This input energy is ultimately dissipated into the thermal bath. It is naturally a measure of the hysteresis loop area in position(x)-force(F) space. Although the input energy and hysteresis loop area are exactly the same in magnitude, the latter is an average quantity, where as input energy has a well-defined distribution. The input energy distribution provides useful information about stochastic resonance behaviour. An ensemble of details about the HLA will be put in evidence in the next chapter.

I.7.3 Application domains of the stochastic resonance

SR can be observed almost everywhere. For several decades, this intriguing phenomenon occurring in the systems pertaining has been an intense interest for the researchers of the domains.

Electronic

The one of first experimental verification of stochastic resonance was realized in an electronic circuit, a simple Schmitt trigger [14]. Since then, stochastic resonance has been observed in a variety of more or less complicated electronic devices, mostly constructed with the purpose of building flexible and inexpensive simulation tools. A rather peculiar electronic device that displays stochastic resonance is the tunnel diode, a semiconductor device with a bistable characteristic ($I - V$) curve. SR in a tunnel diode has also been observed for forcing frequencies as high as $10KHz$ [84, 85, 86]. recently, SR has been reported also in a non-bistable standard np semiconductor diode [87].

Optics

SR has been found in the optical systems such as ring laser [15] which consists of a ring interferometer formed by three or more mirrors and a laser medium inside the cavity. In two-mode ring lasers, the light can travel in a clockwise or counterclockwise direction. Bistability with respect to the direction has been discussed in large detail [88]. Random switching of the beam intensities, initiated by spontaneous emission in the laser medium and fluctuations in the pump mechanism, indicates bistable operation of the ring laser. To show stochastic resonance, the symmetry between the two modes has to be broken by applying a periodic modulation that favours one of the modes. The signal-to-noise ratio, shown in **Fig 4** reflects the manifestation of SR in the ring laser.

Sometimes due to weak signal the intensity of Raman spectrum and X-ray diffraction of some solutions corresponding to certain frequencies may not be clearly visible. They can be amplified by adding impurities as noise.

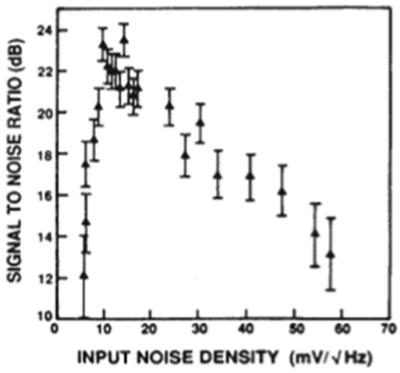

Figure 4: Picture illustrating the SNR, obtained from the time dependence of the intensity of one laser mode, shown as a function of the injected noise strength [15].

Stochastic resonance has theoretically been investigated in an optical bistable system, which consists of a unidirectional ring cavity and a photorefractive two-wave mixer Optics [89].

Biology

The expansion of stochastic resonance took a large leap forward when its potential relevance for neurophysiological processes had been accepted. Longtin, Bulsara, and Moss [90] observed that interspike interval histograms of periodically stimulated neurons exhibit a remarkable resemblance to residence-time distributions of periodically driven bistable systems [82, 91]. The relevant neurophysiological experiments described how stochastic resonance enters naturally into standard models for neuronal dynamics. In neurobiology, SR is used to detect the weak signals. By now, stochastic resonance is a well recognized paradigm in the biological and neurophysiological sciences, and several recent reviews on neurophysiological applications of stochastic resonance are available [92, 93, 94, 95]. The equation of movement governing the dynamics in these systems are the following,

$$\dot{x} = x - x^3 + \xi(t) + A_0 cos(\Omega t) \tag{9}$$

Eq (9) translates the interspike interval histograms of a sinusoidally stimulated au-

ditory nerve from an animal which have been compared with return-time distributions of the periodically driven quartic bistable potential.

A soft bistable potential lead to,

$$\dot{x} = x + btanh(x) + \xi(t) + A_0 cos(\Omega t) \tag{10}$$

Where $\xi(t)$ is Gaussian noise.

Economy

In Economy, bistable model of a financial market is frequently considered to model financial crashes and bubbles based on the Ising model with thermal-bath dynamics and long-range interactions, subject to a weak external information-carrying signal and noise. In the ordered phase, opposite stable orientations of magnetization correspond to the growing and declining market before and after the crash or bubble, and jumps of magnetization direction correspond to crashes and bubbles. It shows that the influence of an information-carrying signal, assumed to be too weak to induce magnetization jumps, can be enhanced by the external noise via the effect of stochastic resonance. It argues that in real stock markets the arrival of a piece of information, considers a posteriori to be the cause for a crash or bubble, can be enhanced in a similar way, thus leading to price return whose value is unexpectedly large in comparison with relatively weak importance of this piece of information .

Medecine

SR-based technics have been used to create a novel class of medical devices for enhancing sensory and motor functions such as vibrating insoles especially for the elderly, or patients with diabetic neuropathy or stroke [96]. Stochastic resonance has also been used as therapy method in Parkinson's disease. Indeed Stochastic whole body vibration may offer a supplementation to canonical physical treatments of Parkinson's disease motor symptoms [97].

Engineering

The one of sector of engineering where the SR mainly occurs, is in the Biomechanics. Domain like heart dynamics, blood streaming, muscle system functionality and vocal folds are followed. However predominantly problems of the human skeleton are tackled, see for instance [98, 99]. Here substantial attention is paid to SR which noise enhances the response of a non-linear system to weak signals in various biological sensory systems. At the same time it has been recognized that adding low magnitude periodic vibration greatly enhances bone formation in response to loading, which is definitely an excellent contribution of SR for the osteogenic processes.

Neuroscience

Stochastic resonance has been observed in the neural tissue of the sensory systems of several organisms. Computationally, neurons exhibit SR because of non-linearities in their processing. SR has yet to be fully explained in biological systems, but neural synchrony in the brain (specifically in the gamma wave frequency) has been suggested as a possible neural mechanism for SR by researchers who have investigated the perception of subconscious visual sensation. Single neurons in vitro including cerebellar Purkinje cells and squid giant axon could also demonstrate the inverse stochastic resonance, when spiking is inhibited by synaptic noise of a particular variance.

Neurobiology

A study conducted by Russell et al. involving the feeding behavior of paddlefish (see **Fig 5**) demonstrated that stochastic resonance can in fact influence animal behavior [100]. Paddlefish live in North American rivers, and feed on a variety of zooplankton, particularly Daphnia. Since the muddy turbidity of the waters in which they live inhibits the visual detection of their prey, paddlefish have developed a long, flattened rostrum extending from their mouth that is covered with passive electro-receptors. This rostrum is used to locate plankton such as Daphnia, which produce low frequency ex-

ternal fields. As is to be expected, more distant plankton are more difficult to locate. The researchers in this study hypothesized that the presence of background electrical noise at some optimal amplitude might allow paddlefish to locate and capture more distant prey as compared to zero-field controls via the mechanism of stochastic resonance [100].

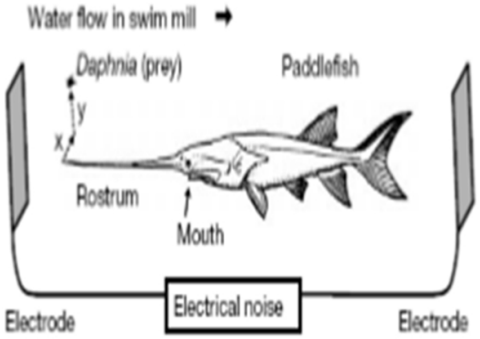

Figure 5: Paddlefish in the swim mill from the experimental setup of the Russell study [100]

Communication

Stochastic resonance is a non-linear effect wherein the noise turns out to be beneficial to the transmission or detection of an information-carrying signal (see **Fig 6**). When the intensity of the input image $s(l,m)$ is low relative to the threshold θ of the detector, i.e. when $\theta > 1$, then $s(l,m)$ (in the absence of noise) remains undetected as the output image $y(l,m)$ remains a dark image. Addition of the noise $\eta(l,m)$ will then allow a cooperation between the intensities of images $s(l,m)$ and $\eta(l,m)$ to overcome the detection threshold.

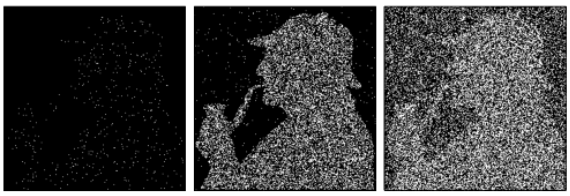

Figure 6: detection of an information-carrying signal from SR

The result of this cooperative effect can be visually appreciated on **Fig 6**, where an

optimal non-zero noise level maximizes the visual perception [101].

I.8 Artificial Brownian motors

I.8.1 Josephson Junction (JJ)

For several decades, there has been intense interest in the effect of noise on the dynamic characteristics of JJ. A theoretical description of thermal fluctuation in superconducting weak links has been developed via the phase or current, by analogy with the Brownian motion of a particle in a tilted periodic potential, and has been applied to both $d.c$ and $a.c$ Josephson effects and to the driven Josephson oscillator.

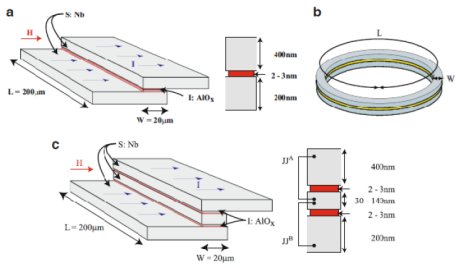

Figure 7: (a) Schematic drawings of a typical long Josephson junction (JJ) and its cross section. In this case, the JJ is made of bulk niobium superconductors (S) and aluminium oxide used as the dielectric barrier. Typical values of the junction's length (L), width (W) and thickness are indicated in the figure. The bias current (I) driving the JJ, and the magnetic field (H) applied at its edges, are designated too. (b) A long circular of JJ, (c) The same as in (a), but for a stack of two parallel magnetically coupled junctions.

The specific dynamics of tunnelling has been predicted by Josephson in the junction built as two bulk superconductors separated by a thin dielectric layer (oxide layer), across which Cooper pairs of superconducting electrons may tunnel keeping their coherence, i.e., the thickness of the dielectric barrier is much smaller than the correlation length of the superconducting state. A typical scheme of the long JJ is displayed in **Fig 7(a)**. The phase difference ϕ_{lr} ($\phi_{lr} = \phi_l - \phi_r$) between the wave functions for the left and right superconductors is given by the Josephson equation

$$\frac{d\phi(t)}{dt} = \frac{2eU(t)}{\hbar} \tag{11}$$

Here, $U(t)$ is the potential difference across the junction; e is the charge of the electron, and $\hbar = h/2\pi$, where h is Planck's constant. If the junction is small enough, it may be modelled (see **Fig 8(b)**) by a resistance R in parallel with a capacitance C, across which is connected a current generator I_{dc} (representing the bias current applied to the junction). At the other end of the junction (across the resistance R) is connected a phase-dependent current generator, $I_c sin\phi$, representing the Josephson super-current resulting from the Cooper pairs tunnelling through the junction. Since the junction operates at a temperature and a pressure above zero, there exists a white-noise current $\Gamma(t)$ superimposed on the bias current, which satisfies the conditions

$$\langle \Gamma \rangle = 0 \tag{12}$$

$$\langle \Gamma(t)\Gamma(t') \rangle = \frac{2K_B T}{R} \tag{13}$$

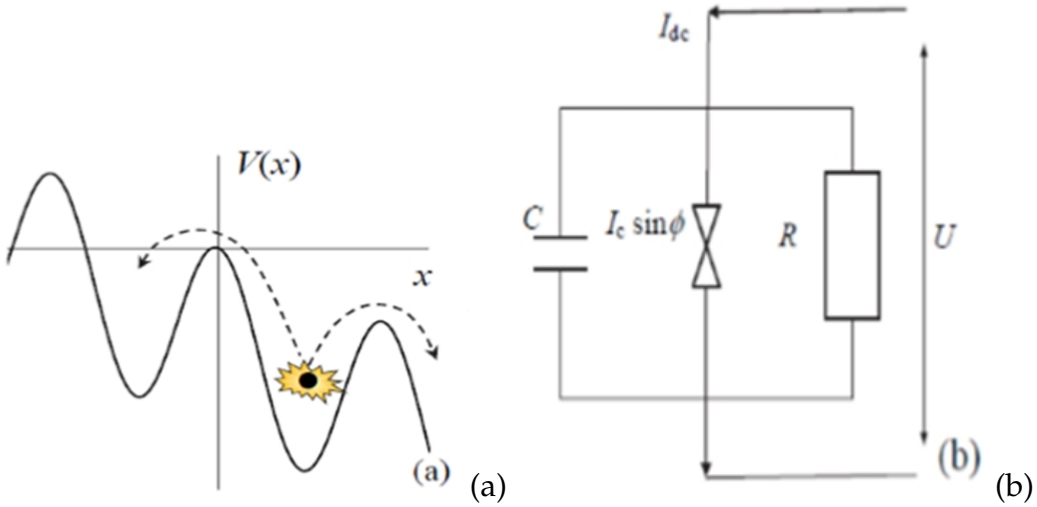

Figure 8: Particle in an effective potential (a) and his equivalent circuit of the Josephson junction (b).

where T is the temperature of the device, and K_B is the Boltzmann constant. The

meaning of the noise is simply that the current through the normal shunt resistor equals $V/R - \Gamma(t)$, where the thermal fluctuation noise current $\Gamma(t)$ is assumed independent on V . The current-balance equation for the junction is

$$C\frac{dU(t)}{dt} + \frac{U(t)}{R} + I_c sin\phi(t) = I_{dc} + \Gamma(t) \tag{14}$$

Substituting **Eq (11)** in **Eq (14)**, the Langevin equation for phase $\phi(t)$ is,

$$\frac{\hbar C}{2e}\frac{d^2\phi(t)}{dt^2} + \frac{\hbar}{2eR}\frac{d\phi(t)}{dt} + I_c sin\phi(t) = I_{dc} + \Gamma(t) \tag{15}$$

This is modelled in the Kirchhoff equation above (**Fig 8(b)**) by making an equivalent assumption that the current through the resistor is V/R, but the bias current is $I + \Gamma(t)$. So, we can now show the mechanical model of **Eq (15)** also called the Stewart-McCumber Model.

Josephson junction and its mechanical correspondence to the Brownian motion

A Josephson Junction is a quantum mechanical device, which is made of two superconducting electrodes separated by a barrier. The Josephson effect is an example of a macroscopic quantum phenomenon. It is named after the British physicist Brian David Josephson, who predicted in 1962 the mathematical relationships for the current and voltage across the weak link [102, 103] as shown in **Fig 9** [104], a Josephson tunnelling.

In Josephson junction, the quantities of physical interest are the current-voltage characteristics, the linear and non-linear junction impedance to an external high-frequency current, the Josephson radiation spectrum, and so on. Here, the junction is treated as a purely classical system, where the phase difference ϕ across the junction and the charge CU on the junction are considered as classical variables, which can be determined with arbitrary accuracy. However, the classical accuracy is inherently limited by Heisenberg's uncertainty principle, which, in this case, is $\Delta\phi\Delta N \geq 1$, where N is the number of Cooper pairs transferred across the junction.

The mechanical correspondence of **Fig 8(b)** is useful depicted by **Fig 8(a)** in term

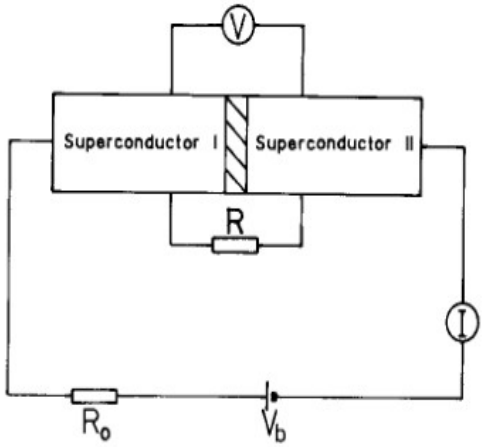

Figure 9: Josephson tunnelling junction

of Brownian particle of mass m_p in a spatial periodic potential $V(x)$ of period L and an barrier height ΔV, subjected to an external, unbiased external force and a Gaussian white noise. Multiplying the equation (15) by $\frac{\hbar}{2e}$, it becomes:

$$\frac{\hbar^2 C}{(2e)^2}\ddot{\phi}(t) + \frac{\hbar^2}{(2e)^2 R}\dot{\phi}(t) + \frac{I_c \hbar}{2e} sin\phi(t) - \frac{\hbar I_{dc}}{2e} = \frac{\hbar}{2e}\Gamma(t) \tag{16}$$

The mechanical analogy from the Stewart-McCumber dynamic **Eq (16)** can be written as

$$m_p\ddot{\phi}(t) = -\gamma\dot{\phi}(t) - \frac{I_c\hbar}{2e} sin\phi(t) + \frac{\hbar I_{dc}}{2e} + \frac{\hbar}{2e}\Gamma(t) \tag{17}$$

Where the effective potential phase particle mass is defined as $m_p = \dfrac{\hbar^2 C}{(2e)^2}$, so that the left term appears as mass times acceleration. Notice that the effective mass is proportional to the parallel capacitance of the junction C. We have also introduced the damping (friction) coefficient

$$\gamma = \frac{\hbar^2}{(2e)^2 R} \tag{18}$$

The definition displays that the damping is proportional to the normal conductance

of the shunt, $G = \frac{1}{R}$ and inversely proportional to normal resistance R. This means that a charge builds up on the electrodes causing some voltage and the electric field to occur. This voltage accelerates normal electrons, which then dissipate their kinetic energy into heat with a rate proportional to G.

Now for the analogy with classical mechanics, we introduce three effective forces, namely the friction force $F_d = -\gamma\dot{\phi}$, the phase difference force $F_\phi = -\frac{I_c\hbar}{2e}sin\phi$, and the bias current force $F_b = \frac{\hbar I_{dc}}{2e}$. Also, let us look at ϕ as though it is the position (spatial coordinate) of the effective phase particle. One will denote this position as x, and define it simply as $x = \phi$. In that case $F_d = -\gamma\dot{x}$, $F_\phi = -\frac{I_c\hbar}{2e}sinx$, and $\xi(t) = \frac{\hbar}{2e}\Gamma(t)$ is the Gaussian white noise coming from current representing the Johnson-Nyquist thermal current noise $\Gamma(t)$ in the shunt resistor R. Then, the dynamics equation of the Josephson junction is the Langevin equation

$$m_p\ddot{x} = F_d + F_\phi + \xi(t) = -\gamma\dot{x} - \frac{I_c\hbar}{2e}sinx + \frac{\hbar I_{dc}}{2e} + \frac{\hbar}{2e}\Gamma(t) \tag{19}$$

Fact that a classical particle and the JJ are both described by the same differential equation implies that the known classical-particle solution and methods solving the equation apply to JJ. It is usual in classical physics, the potential corresponding to the force F_ϕ is $U_\phi = E_j(1 - cosx)$, so that, as usual, $F_\phi = -\frac{dU_\phi}{dx}$. Here $E_j = \frac{I_c\hbar}{2e}$ is called the Josephson energy. The bias potential energy is $U_b = \frac{I_{dc}\hbar x}{2e}$, so that $F_b = -\frac{dU_b}{dx}$. The total energy, which is, in fact, the Gibbs free energy of the current-biased junction is

$$U_{wb} = U_\phi + U_b = E_j[(1 - cosx) - ix] \tag{20}$$

where $i = I/I_c$ is the normalised bias current which defines the tilt. The potential energy U_{wb} is frequently called the titled washboard potential because it resembles to a hand-washing board.

Using these notations the equation of motion of the Stewart-McCumber model becomes

$$m_p\ddot{x} = -\gamma\dot{x} - \frac{dU_{wb}}{dx} + \xi(t) \tag{21}$$

Eq (21) is the same as the Langevin equation for a single particle moving in a substrate potential.

I.8.2 Superionic conductors

Brownian particles have also been studied in detail in connection with superionic conductors. Superionic conductors, represent a class of solid materials that shows an unusually high ionic conductivity of an order of magnitude as usually found for molten salts [105, 106]. They consist of species of high mobile particles considered to be Brownian particles moving on a periodic structure with diffusion coefficients comparable to those found in liquids [107]. Their structure is characterized by a strong disorder in the sublattice of conductivity ions. All the ions of one sublattice are in this highly mobile state. There is another species of ions which cannot diffuse. They form a framework which is usually called the rigid sublattice. The activation energy required for the mobile ions to diffuse is far lower than that found in ordinary ionic solids. As an example, we consider silver iodide ($\alpha - AgI$) for illustration (see **Fig 10**).

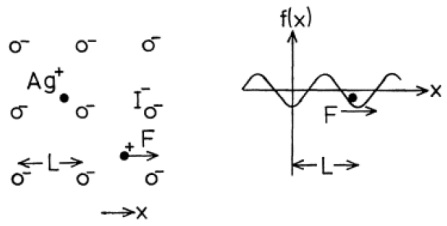

Figure 10: Highly movable Ag^+ ions in the nearly fixed iodide lattice and the corresponding potential in one dimension [104]

Here, the lattice consists of iodide (I^-) ions, while the silver ions (Ag^+) are highly mobile (**Fig 10**). In $\alpha - AgI$ at 3000 Celcius, the diffusion coefficient for Ag^+ ions is close to $2.10^{-5}cm^2/s$. The one of the I^- ions is negligible. In this context, the motion of ions considered as non-interacting Brownian particles is treated as a stochastic motion

in a medium with periodic lattice structure. These materials show high ionic conductivity and have led to very important advances in designing new devices based on the motion of ions through periodic structures. This may help to improve components in electrochemical energy storage and conversion devices such as batteries, fuel cells and electrochemical membranes, which are critical in the societal shift to renewable energy. In a number of these materials,the conduction process is confined to lower dimensionality; examples include β-alumina ($d = 2$), potassium hollandite ($d = 1$), etc. If an external field F is applied to a one-dimensional model, neglecting interaction of different Ag^+ ions, then, the equation of motion divided by the mass m in the periodic potential $mf(x)$ [108] is

$$m\ddot{x} + \gamma\dot{x} + f'(x) = F + \xi(t) \tag{22}$$

I.9 Problem statement of the thesis

I.9.1 Deformable potential as realistic potential for Brownian particles and lattices

The vast majority of works on Brownian motion is done in the systems based on the standard sinusoidal periodic potential and, concentrated on the behavior of the directed transport as a function of parameters of the system, such as temperature, energy barrier, or some other control variable. However, these systems with periodic structure, although interesting, describe realistic systems only with certain approximations. To obtain a physically more realistic periodic substrate for several complex systems, the effects of physical parameters such as temperature and pressure should be considered. Under such constraints, some physical systems such as Josephson junctions, incommensurate systems, charge-density wave condensates, superionic conductors or crystals with dislocations may undergo changes such as shape distortion, variation of crystalline structures, or conformational changes. Hence, it appears necessary to take

into account the deformable character of the medium in Brownian particles field. Indeed, deformable models have been considered both from mathematical and physical points of view. From a mathematical point of view, the foundations of deformable models represent a confluence of geometry, physics, and approximation theory. Geometry serves to represent object shape, physics imposes constraints on how the shape may vary over space and time, and optimal approximation theory provides the formal underpinnings of mechanisms for fitting the models to measured data. From a physical point of view, deformable models are viewed as elastic bodies that respond naturally to applied forces and constraints. In fact, the term deformable models stems primarily from the use of elasticity theory at the physical level, generally with a Lagrangian dynamics setting.

I.9.2 Statement of the problem

Having review the majority of works on SR, we noticed that these works have been based on the occurrence of SR phenomenon in the systems with sinusoidal periodic potential. However, the question of the occurrence of SR in periodic deformable substrate potentials introduced by Remoissenet and Peyrard has not been resolved. These kinds of potential which have already been introduced for the study of the soliton, stick-slip movement, diffusion phenomena, and anomalous transport, take into account some particular situations in physics such as high temperature and pressure which could modify the substrate leading to the deformation of a non-linear crystal-lattice, shape distortion, variation of crystalline structures, geometric configuration, and dislocation in solids. Therefore, it will be important to consider the deformable character of the medium for the study of SR in the physical systems. The dependence of SR phenomenon on the parameters of system such as potential shape, chain size, coupling or some other control parameter will be analysed in this thesis.

I.10 Conclusion

In this chapter, we have provided and explained the concept of stochastic resonance. SR is a powerful phenomenon that has changed our ideas on noise. We have presented some applications of SR and how this phenomenon manifests in the systems. The problems that we will have to solve in the thesis have been well-established. The following chapter will be devoted to the mathematical model formulation and numerical simulations methods used to solve the problems of the thesis.

CHAPTER II

METHODOLOGY: MODELS AND NUMERICAL METHODS

II.1 Introduction

The previous chapter has clearly presented the phenomenon of SR under many axis. Thus, from a phenomenological point of view, the problem is interesting because it is enough simple to understand and to analyse. In this chapter, we introduce the mathematical formalism for our investigation the presentation of the analytical, numerical and stochastic methods that will be used to solve the problems addressed by this thesis.

II.2 Langevin equation

The Langevin equation is a stochastic differential equation describing the dynamics of a particle that is subjected to friction and stochastic forcing. This equation initiated for the first time in 1908 by Paul Langevin presents in a global way the mathematical equations modelling the stochastic systems. The general Langevin equation with Gaussian white noise terms is given by the following expression:

$$\frac{dx}{dt} = f(x) + G(x)\xi(t) \tag{23}$$

Where $x = (x_1, x_2, ..., x_n)$ and $\xi = (\xi_1, \xi_2, ..., \xi_n)$. $f(x)$ is the deterministic part, $x(t)$ and $\xi(t)$ are the position of the particle and Gaussian white noises or Langevin stochastic force respectively. G is a square matrix which depend on x when the white noise is a multiplicative noise while for an additive noise G is constant.

II.3 Model of a particle in the on-site Remoissenet-Peyrard potential

In order to study the SR phenomenon in this system, we consider a Brownian particle of mass m with spatial position $x(t)$ (see **Fig 11**) subjected to an external periodic force $F(t) = F_0 + A_0 cos(\omega t)$ of frequency ω ($\omega = 2\pi/\tau$, with τ which represents the period of the external force) and the thermal fluctuations. We model these fluctuations as a time dependent-random force $\xi(t)$, whose statistical properties can be mimicked by a Gaussian white noise: $\langle \xi(t) \rangle = 0$ and $\langle \xi(t)\xi(t') \rangle = 2\gamma T \delta(t - t')$ where the medium temperature T is in units of the Boltzmann constant k_B. At the same time the substrate potential exerts on the moving particle a frictional force f_d proportional to the particle's velocity; $f_d = -\gamma v$, where γ is the friction coefficient. We assume that the Brownian particle moves in a force field with deformable Remoissenet-Peyrard (RP) potential energy $U_{RP}(x, r)$, already introduced some years ago in the contexts of the solitons [109] and recently in the context of [110] . The RP potential is given by the following expression,

$$U_{RP}(x, r) = U_0 (1 - r)^2 \frac{1 - \cos x}{(1 + r^2 + 2r \cos x)}. \tag{24}$$

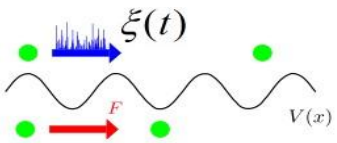

Figure 11: Particles moving in symmetric periodic structures in the presence of an external force F and the stochastic force $\xi(t)$

This potential is symmetric and 2π-periodic in x, the shape of the potential is defined by the parameter r with $-1 < r < 1$. U_0 is a constant which measures the amplitude of the potential. The illustration of corrugation potential is given in **Fig 11**. When $r < 0$, the non-sinusoidal RP potential has the shape of sharp wells separated by flat wide barriers (see **Fig 12(a)**) for $r = -0.6$). While for $r > 0$ it has the flat bottoms separated by thin

barriers (see **Fig 12(c)**) for $r = 0.6$), while for At $r = 0$, the RP potential reduces to the well-known Sine-Gordon potential as displayed in **Fig 12(b)**.

Therefore, relatively to the equations (15), (21) and (22), the dynamic equation of this particle can be described by the following Newton-Langevin equation,

$$m\frac{d^2x}{dt^2} = -\gamma\frac{dx}{dt} - \frac{\partial V\left(x,r,t\right)}{\partial x} + \xi\left(t\right). \tag{25}$$

where

$$V\left(x,r,t\right) = U_{RP}\left(x,r\right) - xF\left(t\right) \tag{26}$$

is the effective potential of the system. In **Eq (25)**, the inertial effects related to the mass of the particle are described by the term on the left hand side where the over-dot indicates differentiation with respect of time t.

II.3.1 Evolution of the effective and determination of the energy barrier

The solution for a local minimum where the particle resides x_a and a transition point x_b can be determined from $\frac{\partial V}{\partial x} = 0$. Other variables can be obtained from these positions such as the energy barrier $\Delta V = V(x_b) - V(x_a)$, the frequencies ω_a and ω_b which represent the angular frequency of the potential in the potential minimum x_a and the angular frequency at the top of the barrier located at x_b, respectively. The barrier between any two consecutive wells of the effective potential V disappears ($\Delta V = 0$) when the magnitude of the external field exceeds the critical force F_c. At that time switching between the potential wells are possible. A critical point x_c where the barrier vanishes and the critical force F_c can be obtained by solving equations $\frac{\partial V}{\partial x} = 0$ and $\frac{\partial^2 V}{\partial x^2} = 0$. After a few mathematical calculations, the critical force can be deduced as:

$$F_c = \frac{U_0\left(1-r^2\right)^2\sin x_c}{\left(1+r^2+2r\cos x_c\right)^2}, \tag{27}$$

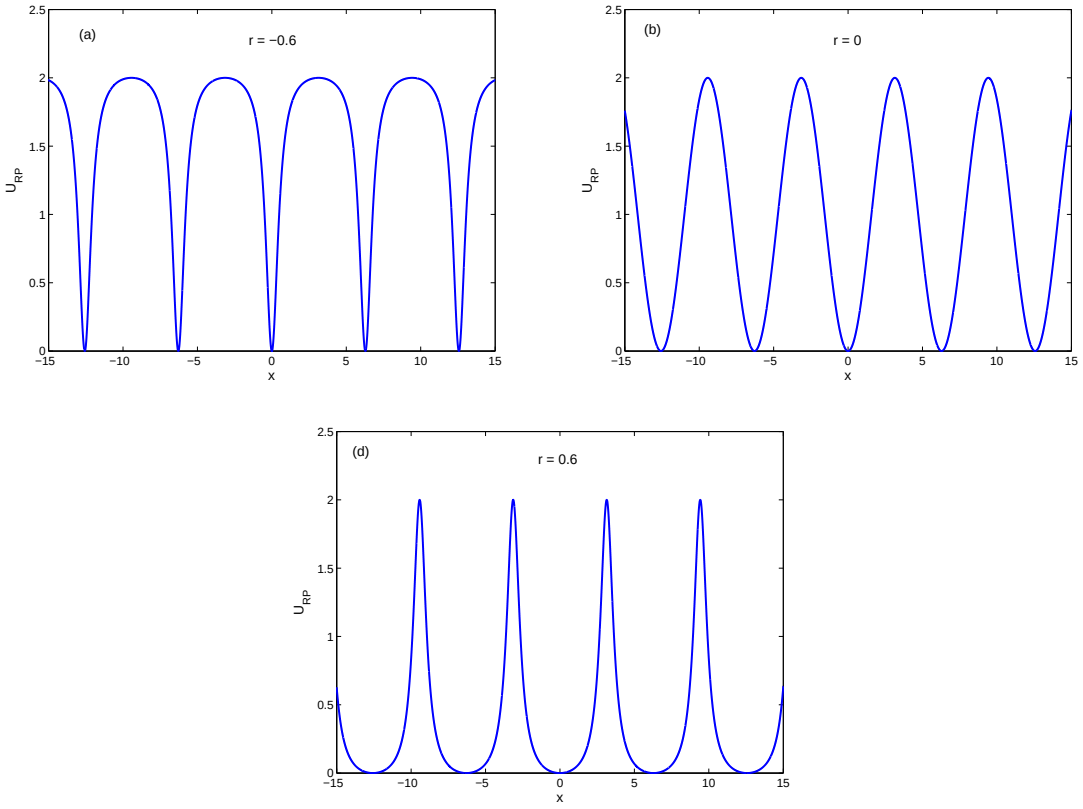

Figure 12: Illustration of the RP potential $U_{RP}(x, r)$ for different values of r indicated on the figure, with $U_0 = 1$. The shape potential depends on the parameter r. When $r = 0$ (b), we have a sinusoidal profile of potential.

with, $x_c = \pm \arccos\left(\frac{1+r^2-\sqrt{r^4+34r^2+1}}{4r}\right)$ is the instability point.

Assuming that when x_a and x_b converge to critical point (x_c, F_c) the switching events occur around the critical point (x_c, F_c), so $V_{xx}(x_b, F)$ and $V_{xx}(x_a, F)$ can be obtained by Taylor expansion around the critical point,

$$V_{xx}\left(x_b, F\right) = V_{xx}\left(x_c, F_c\right) + V_{xxx}\left(x_b - x_c\right) + V_{xxF}\left(F - F_c\right) + 0\left(\delta x^2\right). \tag{28}$$

However, $V_{xx}\left(x_c, F_c\right) = 0$ and $V_{xxF} = 0$ thus,

$$V_{xx}\left(x_b, F\right) = \left(U_{RP}\right)_{xxx}\left(x_b - x_c\right), \tag{29}$$

and

$$V_{xx}\left(x_a, F\right) = \left(U_{RP}\right)_{xxx}\left(x_a - x_c\right), \tag{30}$$

here $_{xx}$ indicates the second derivative with respect to x and $V_{xxx} = (U_{RP})_{xxx}$. The energy barrier is defined as,

$$\Delta V = V(x_b, F) - V(x_a, F), \tag{31}$$

therefore for the determination of ΔV, it is important to make a Taylor expansion around (x_c, F_c) as illustrated by Dong et al. [111]:

$$\begin{aligned} V\left(x, F\right) = V\left(x_c, F_c\right) + \frac{\partial V}{\partial x}\left(x - x_c\right) + \frac{\partial V}{\partial F}\left(F - F_c\right) + \frac{\partial^2 V}{\partial x \partial F}\left(x - x_c\right)\left(F - F_c\right) + \\ \frac{1}{2}\frac{\partial^2 V}{\partial x^2}\left(x - x_c\right)^2 + \frac{1}{2}\frac{\partial^2 V}{\partial F^2}\left(F - F_c\right)^2 + \frac{1}{2}\frac{\partial^3 V}{\partial x^2 \partial F}\left(x - x_c\right)^2\left(F - F_c\right) + \\ \frac{1}{2}\frac{\partial^3 V}{\partial x \partial F^2}\left(x - x_c\right)\left(F - F_c\right)^2 + \frac{1}{6}\frac{\partial^3 V}{\partial x^3}\left(x - x_c\right)^3 + \frac{1}{6}\frac{\partial^3 V}{\partial F^3}\left(F - F_c\right)^3 + \\ 0\left(\delta x^4\right) \end{aligned} \tag{32}$$

At the critical point (x_c, F_c), $V_x = V_{xx} = V_{FF} = V_{xxF} = V_{xFF} = V_{FFF} = 0$, thus:

$$V\left(x_b,F\right)=V\left(x_c,F_c\right)+\frac{\partial V}{\partial F}\left(F-F_c\right)+\frac{1}{6}\frac{\partial^3 V}{\partial x^3}\left(x_b-x_c\right)^3 \tag{33}$$

and

$$V\left(x_a,F\right)=V\left(x_c,F_c\right)+\frac{\partial V}{\partial F}\left(F-F_c\right)+\frac{1}{6}\frac{\partial^3 V}{\partial x^3}\left(x_a-x_c\right)^3. \tag{34}$$

By substituting the equations **(33)** and **(34)** into the relation **(31)**, the expression of the energy barrier is given as,

$$\Delta V=(x_b-x_a)(F_c-F)+\frac{1}{6}\left(U_{RP}\right)_{xxx}\left[\left(x_b-x_c\right)^3-\left(x_a-x_c\right)^3\right]. \tag{35}$$

Researching now the equilibrium points from $\dfrac{\partial V(x,F)}{\partial x}=0$, with $V(x,F)$ given by the relation **(32)** we obtain,

$$F_c-F=-\frac{1}{2}\left(U_{RP}\right)_{xxx}\left(x-x_c\right)^2. \tag{36}$$

This, we permit then to have the equilibrium points as:

$$x_b-x_c=\sqrt{\frac{2}{-\left(U_{RP}\right)_{xxx}}}\left(F_c-F\right)^{\frac{1}{2}}, \tag{37}$$

and

$$x_a-x_c=-\sqrt{\frac{2}{-\left(U_{RP}\right)_{xxx}}}\left(F_c-F\right)^{\frac{1}{2}}, \tag{38}$$

thus,

$$\Delta V=\frac{4\sqrt{2}}{3}\left(-\left(U_{RP}\right)_{xxx}\right)^{-\frac{1}{2}}\left(F_c-F\right)^{\frac{3}{2}}. \tag{39}$$

Before to do the investigations on SR phenomenon in the Remoissenet-Peyrard substrate potential, we must make short that the signal amplitude of the external force $F(t)$ is small enough that, in the absence of any fluctuation force, it is insufficient to force a

particle to move one well to another ($F(t) < F_c$) at all time. So let us first analyse the effective potential given by **Eq (26)**.

Figure 13 illustrates the evolution of the effective potential V as a function of the positions x for $U_0 = 1$. Here, the potentials clearly show the presence of an initial minimum (stable particle position) and an initial maximum (unstable particle position). When one takes the initial value of external force F from 0.05 to critical force $F_c = 1.15$ corresponding to the shape potential $r = 0.2$, we can see that the energy barrier ΔV decreases and finally vanishes as F equals to F_c.

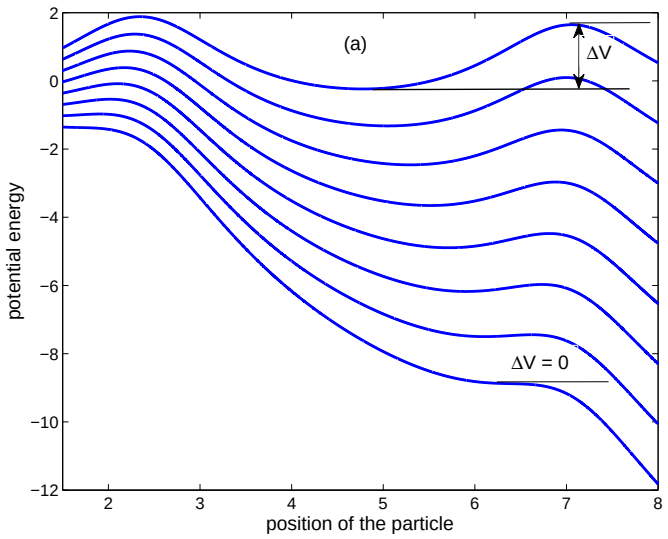

Figure 13: Schematic illustration of the evolution of the effective potential, showing the decreasing of the energy barrier. From top to bottom each curve corresponds to a change in F of 0.22 step starting from 0.05, for $r = 0.2$.

Fig 14 shows the energy barrier (**Eq. (38)**) obtained analytically as a function of external force F taken over a large range for several values of shape potential r. For each value of shape potential, we have the critical force F_c given by **Eq. (26)**, thus for $r = \pm 0.2$; $F_c = 1.15$, $r = \pm 0.4$; $F_c = 1.62$, $r = \pm 0.5$; $F_c = 2.02$ and $r = \pm 0.6$; $F_c = 2.65$. One can observe a decreasing of the energy barrier with increasing of the external force until it vanishes when F is equal to F_c.

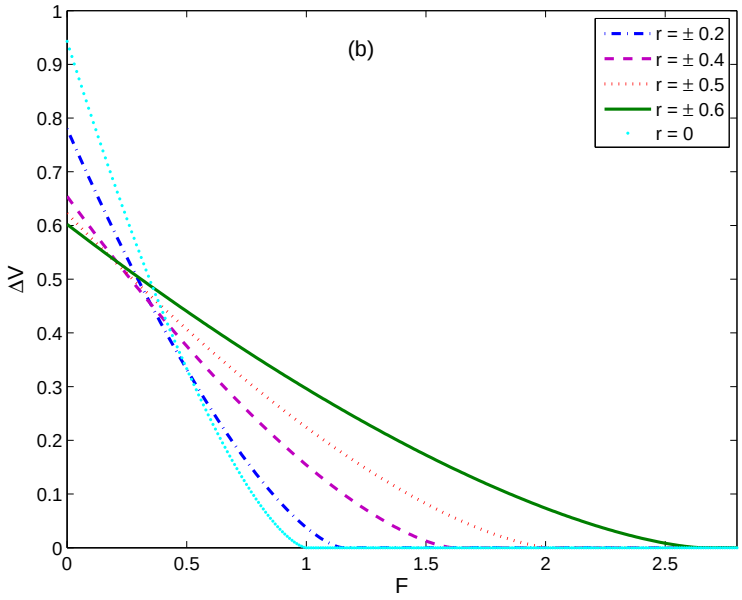

Figure 14: Illustration of energy barrier of the effective potential as a function of external force F, for some shape potential.

II.4 Model of a particle in the on-site asymmetric well potential and double-well deformable potential

In connection with SR phenomenon and to gain a good dependence of SR on shape parameter r, let us now consider a Brownian particle of mass m with spatial position $x(t)$, subjected to an external periodic force $F(t) = F_0 + A_0 cos(\omega t)$ of frequency ω ($\omega = 2\pi/\tau$, with τ which represents the period of the external force)and the thermal fluctuations. We model these fluctuations as a time dependent-random force $\xi(t)$, whose statistical properties can be mimicked by a Gaussian white noise: $\langle \xi(t) \rangle = 0$ and $\langle \xi(t)\xi(t') \rangle = 2\gamma T\delta(t - t')$ where the medium temperature T is in units of the Boltzmann constant k_B. We model these fluctuation as a time dependent-random force $\xi(t)$, whose statistical properties can be mimicked by a Gaussian white noise: $\langle \xi(t) \rangle = 0$ and $\langle \xi(t)\xi(t') \rangle = 2\gamma T\delta(t - t')$ where the medium temperature T is in units of the Boltzmann constant k_B. At the same time the substrate potential exerts on the moving particle a

frictional force f_d proportional to the particle's velocity; $f_d = -\gamma v$, where γ is the friction coefficient. We now assume that the Brownian particle moves in a force field with asymmetric deformable potential (ASDP) energy on the one part, and on the other hand with double-well deformable potential (DWDP) energy introduced by Remoissenet and Peyrard. The general expression of these potentials is given as,

$$U\left(x,r\right) = A\left(r\right)\frac{1+e\cos x}{\left[1+r^2+2r\cos\left(x/m\right)\right]^p} \tag{40}$$

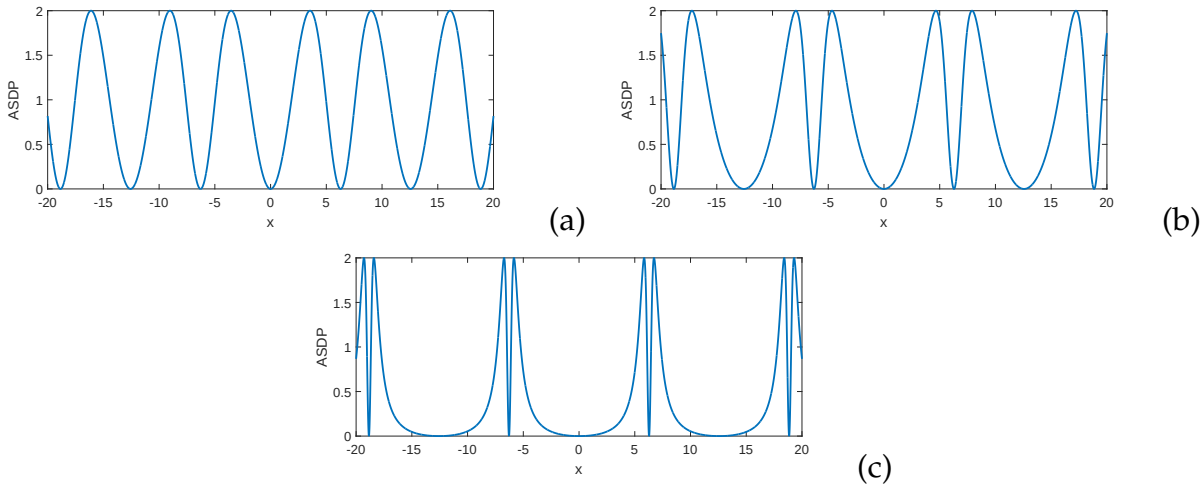

Figure 15: Illustration of the asymmetric deformable potential (ASDP) for the values of $r = 0.1$ (a), $r = 0.4$ (b) and $r = 0.8$ (c) with $U_0 = 1$. The shape potential depends on the parameter r.

- **ASDP** is obtained for $A(r) = U_0(1-r^2)^2$, $m = p = 2$, $e = -1$ and $0 < r < 1$, illustrated in **Fig 15** for various values of r. This potential presents two successive wells which are not same with, respectively, a flat and sharp bottom.

- **DWDP** is obtained for $A(r) = U_0(1-r)^4$, $m = p = 2$, $e = 1$ and $0 < r < 1$, plotted in **Fig 16** for various values of r. Inside one well, there is the sub-wells, what can support the intra-well dynamics of the particle.

To model the dynamics of these systems, we utilize the Newton-Langevin equation. Therefore, the Langevin equation corresponding of these both systems is given by:

$$m\frac{d^2x}{dt^2} = -\gamma\frac{dx}{dt} - \frac{\partial U\left(x,r\right)}{\partial x} + F_0 + A_0 cos(\omega t) + \xi\left(t\right). \tag{41}$$

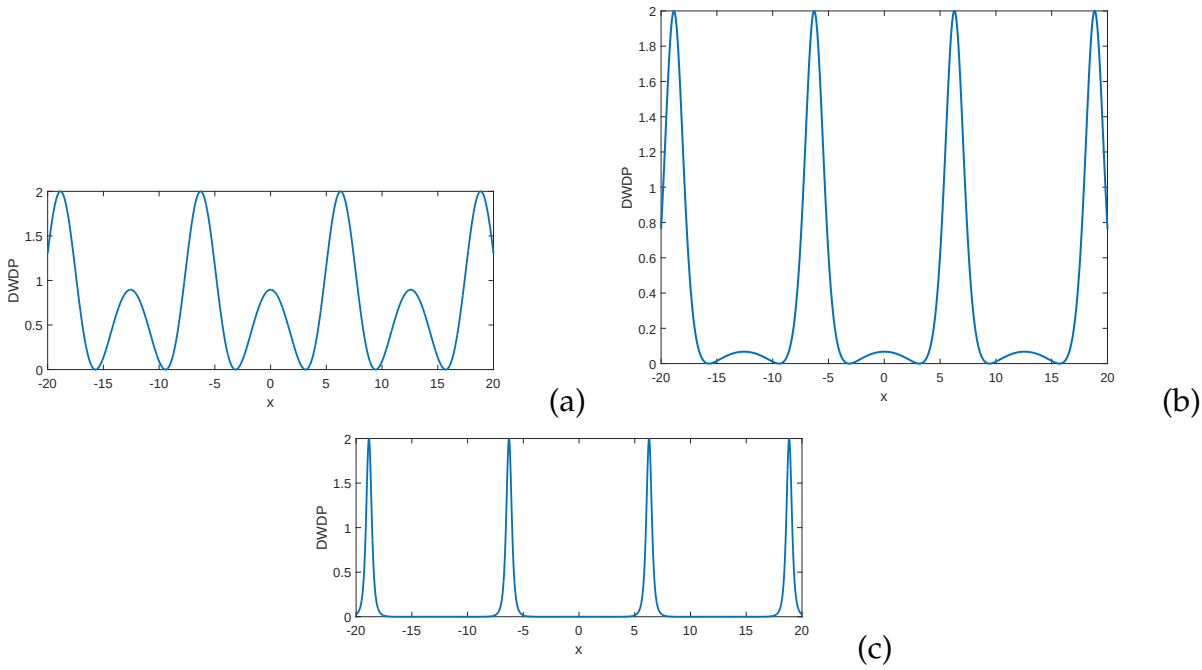

Figure 16: Illustration of the double-well deformable potential (DWDP) for the values of $r = 0.1$ (a), $r = 0.4$ (b) and $r = 0.8$ (c) with $U_0 = 1$. The shape potential depends on the parameter r.

II.5 Model of N-coupled particles in a particular case of the RP potential

Researches on the discrete Sine-Gordon lattice have been a surge of interest recently since it can be used to model many physical system, such as dislocations, magnetic and ferromagnetic domain walls, spin and charge-density wave, and arrays of Josephson junction [112, 113]. The coupling mechanism of the discrete Sine-Gordon chain is generally nonlinear (anharmonic). For a chain of atoms or molecules, the coupling law may be the Lenard-Jones, Toda or Morse [114]. For a DNA chain, the coupling of the helices and base pairs are complicated rotator interactions. In the discussions of antiferroelec-

tric liquid crystals, the coupling mechanism of dipoles and layers is also the sinusoidal form [115]. The non-convex coupling cases are more interesting than the convex cases.

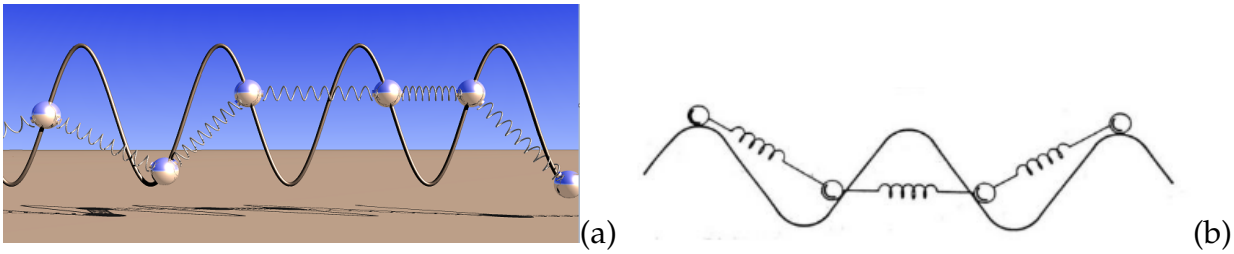

(a) (b)

Figure 17: Models of N particles coupled sinusoidally by nonlinear spring in a particular case of RP.

Noise can enhance a system's internal coherence (stochastic resonance) or damage it (stochastic anti-resonance). In order to study the SR, SAR, also to analyse the influence of coupling, chain size, and briefly the frequency on SR, we consider N Brownian particles sinusoidally coupled as illustrated in **Fig 17(a)** and **17(b)**, moving unidirectionally in a force field with potential energy $U(x) = 1 - u_0 sin(x)$. Each particle has a mass m_i ($i = 1, 2, ..., N$) and is also subjected to an external periodic force $F(t) = F_0 cos(\omega t)$ of frequency ω. Indeed, each particle moving through the fluid is acted on by frequent and uncorrelated momentum impulse arising from the thermal motion of the fluid. We model these fluctuation as a time dependent-random force $\xi_i(t)$, whose statistical properties can be mimicked by a Gaussian white noise: $\langle \xi_i(t) \rangle = 0$ and $\langle \xi_i(t)\xi_i(t') \rangle = 2\lambda T\delta(t - t')$ where the medium temperature T is in units of the Boltzmann constant k_B. Let $x_i(t)$ be the coordinates of these particles. At the same time the fluid exerts on the moving of each particle a frictional force f_d proportional to the particle's velocity; $f_d = -\lambda v_i$, where λ is the friction coefficient. In this system first and last particles are not connected each other, thus for the first particle, the interaction force between the nearest neighbours is defined as

$$F_{int_1} = k\left(1 + \varepsilon \sin\left(x_1 - x_2\right)\right)\left(x_1 - x_2\right) \tag{42}$$

the interaction force between the nearest neighbours for the intermediate particles

($i = 2, ..., N-1$) is given as

$$F_{int_i} = k\left(1 + \varepsilon \sin\left(x_i - x_{i-1}\right)\right)\left(x_i - x_{i-1}\right) + k\left(1 + \varepsilon \sin\left(x_i - x_{i+1}\right)\right)\left(x_i - x_{i+1}\right) \tag{43}$$

the interaction force between the nearest neighbours for the last particle is given as,

$$F_{int_N} = k\left(1 + \varepsilon \sin\left(x_N - x_{N-1}\right)\right)\left(x_N - x_{N-1}\right) \tag{44}$$

Using the fundamental relation of dynamics, the equations of motion of the N particles can be described by the following system of the Langevin equations,

$$\begin{cases} m_1\ddot{x}_1 + \lambda\dot{x}_1 - u_0\cos\left(x_1\right) + k\left(1 + \varepsilon\sin\left(x_1 - x_2\right)\right)\left(x_1 - x_2\right) = F_0\cos\left(\omega t\right) + \xi_1\left(t\right) \\ i = 2, 3, ..., N-1 \\ m_i\ddot{x}_i + \lambda\dot{x}_i - u_0\cos\left(x_i\right) + k\left(1 + \varepsilon\sin\left(x_i - x_{i-1}\right)\right)\left(x_i - x_{i-1}\right) \\ +k\left(1 + \varepsilon\sin\left(x_i - x_{i+1}\right)\right)\left(x_i - x_{i+1}\right) = F_0\cos\left(\omega t\right) + \xi_i\left(t\right) \\ m_N\ddot{x}_N + \lambda\dot{x}_N - u_0\cos\left(x_N\right) + k\left(1 + \varepsilon\sin\left(x_N - x_{N-1}\right)\right)\left(x_N - x_{N-1}\right) = F_0\cos\left(\omega t\right) + \xi_N\left(t\right) \end{cases} \tag{45}$$

The coupling strength is represented by the parameters k which is the linear part and ε the non-linear part, if $\varepsilon = 0$, one finds the usual linear coupling. The interaction force resulting from local interaction between adjacent particles in coupled chain derived from the interaction part of the inner energies. Similar interaction can be observed in a PT (parity-time) symmetry model [116] where the polarization angle of the motion in the top chain of the double Frenkel-Kontorova (FK) chains determines the relative strength of the couplings. A sinusoidal coupling has also been considered extensively in terms of the so-called sine-lattices [117, 118, 119, 120], which represent, e.g., base-rotator models of the DNA double helix [121]. Sinusoidal coupling has also been considered for Josephson junction array [122]

II.6 Numerical method for stochastic differential equations

As the analytical methods cannot be used, we frequently deal with the numerical methods. Generally put forward in Physics in order to resolve the differential equations modelling the dynamics of the complex systems. These methods have also allowed to obtain a better understanding of the Physical problems or phenomena. The one of these methods is the fourth order Runge-kutta for stochastic differential equation which is the most common method to make a numerical integration.

II.6.1 Fourth order Runge-kutta (RK4) for stochastic equation: Kasdin algorithm

To solve the stochastic differential equations, we introduce an implementation of the fourth-order Runge-Kutta (RK4) algorithm developed by Kasdin [123]. This method, probably easy to implement is known for its performance. By implementing this method, we must first separate the one variable equation with second order derivatives into two variable equations with first order derivatives.

$$\dot{X} = F(X,t) + \xi(t) \tag{46}$$

Where X and $F(X,t)$ are the vectors.

$$\begin{cases} \dot{x} = v \\ \dot{v} = -\dfrac{\gamma}{m} - \dfrac{1}{m}\dfrac{\partial V(x,r,t)}{\partial x} + \dfrac{\xi(t)}{m} \end{cases} \tag{47}$$

where $\dot{x} = v$ and $\dot{v} = \ddot{x}$ are used to reduce the derivative order of the equation. Now, we can use vectors X, $F(X,t)$, and $\xi(t)$ with two elements each to describe the variables of the equation sets.

Assuming that the value of $X_k = \begin{pmatrix} x \\ v \end{pmatrix}$ is known at time step t_k, through fourth-step calculation, the value of X_{k+1} at time t_{k+1} is given by the relation

$$X_{k+1} = X_k + \alpha_1 K_1 + ... + \alpha_n K_n \tag{48}$$

where the K_j coefficients are

$$K_1 = hF\left(X_k, t_k\right) + h(Dq_1)^{1/2} \begin{pmatrix} 0 \\ \\ r_1 \end{pmatrix}, \tag{49}$$

$$K_j = hF\left(X_k + \sum_{i=1}^{j-1} \alpha_{ji} K_i, t_k + hc_j\right) + h(Dq_j)^{1/2} \begin{pmatrix} 0 \\ \\ r_j \end{pmatrix}, \tag{50}$$

with h the time step, $D = \frac{2mk_BT}{h}$, $j = 1...n$. For $n = 4$ we obtain the fourth order algorithm, and r is sampled by standard Gaussian distribution with zero mean value and a variance of 1. The coefficients a_{ji}, α_j and q_j are constant coefficients whose the values are given in table 1, and $c_j = \sum_{i}^{j-1} a_{ji}$.

Table 1: Fourth-order, time-varying RK coefficients [123].

coefficients	value
α_1	0.25001352164789
α_2	0.67428574806272
α_3	- 0.00831795169360
α_4	0.08401868181222
a_{21}	0.66667754298442
a_{31}	0.63493935027993
a_{32}	0.00342761715422
a_{41}	- 2.32428921184321
a_{42}	2.69723745129487
a_{43}	0.29093673271592
q_1	3.99956364361748
q_2	1.64524970733585
q_3	1.59330355118722
q_4	0.26330006501868

II.6.2 Production of random number sequences: Box-Muller transformation

For a stochastic equation, we need to generate Gaussian random variables. this is frequently realized in the simulation described above from a transformation created in 1958 by Georges Edward Pelham Box and Mervin Edgar Muller [124]. This transformation states that if y_1 and y_2 are two independent random variables uniformly distributed between 0 and 1, then the variables:

$$z_1 = \sqrt{-2\ln(y_1)}cos(2\pi y_2) \tag{51}$$

$$z_2 = \sqrt{-2\ln(y_1)}sin(2\pi y_2) \tag{52}$$

are the Gaussian random variables, each one having a zero mean and a variance equal to unity.

II.6.3 Computation of Hysteresis loop area and input energy distribution

In order to examine the SR in our different models, we use the hysteresis loop area (HLA) which is a powerful indicator of stochastic resonance in the systems. HLA is equivalent to the input energy lost by the system to the environment per period to external force $F(t)$. As the system is underdamped, the energy is continually dissipated to the environment to which the system is in contact at given temperature. The required energy is supplied by the external field. Following the stochastic energetics formulation of Sekimoto [125], The energy absorbed by the particle per period of the external field is termed as input energy or work done by the field and is calculated as:

$$W\left(t_0, t_0 + \frac{2\pi}{\omega}\right) = -\int_{F(t_0)}^{F\left(t_0+\frac{2\pi}{\omega}\right)} xdF \tag{53}$$

Using the expression of the external force, the input energy becomes,

$$W\left(t_0, t_0+\frac{2\pi}{\omega}\right)=\int_{t_0}^{t_0+\frac{2\pi}{\omega}} x\left(t\right)\omega A_0\sin\left(\omega t\right)dt=A \tag{54}$$

where A is the magnitude of the HLA corresponding to the particle. The input energy per period, $\overline{W}$, averaged over an entire trajectory is

$$\overline{W}=\frac{1}{N_1}\sum_{n=0}^{n=N_1} W\left(\frac{2\pi n}{\omega}, \frac{2\pi\left(n+1\right)}{\omega}\right) \tag{55}$$

The number of periods N_1 of the driving force $F(t)$ has taken equal to 10^5 in all the simulation.

Since $x(t)$ is a stochastic variable it is unreasonable to expect a sensible hysteresis loop over a period of the field. Moreover, when averaged over the entire duration of a trajectory, a well defined hysteresis loop $\bar{x}(F(t_i))$ and its area is obtained:

$$\bar{x}\left(F\left(t_i\right)\right)=\frac{1}{N_1}\sum_{n=0}^{n=N_1} x\left(F\left(n\tau+t_i\right)\right), \tag{56}$$

for all $[0\leq t_i<\tau]$.

At the lowest temperature $\overline{W}$ depends very strongly on the initial conditions $(x(0), v(0))$. However it is always sensible to ensemble average $\overline{W}$ over all possible initial positions and obtain the average input energy per period $\langle\overline{W}\rangle$.

In the model of N-coupled particles, the input energy of each particle will be calculated as

$$W_i\left(t_0, t_0+\frac{2\pi}{\omega}\right)=\int_{t_0}^{t_0+\frac{2\pi}{\omega}} x_i\left(t\right)\omega F_0\sin\left(\omega t\right)dt=A_i \tag{57}$$

The distribution can carry important information about the system and mainly the stochastic resonance. The values of W are different depending on whether during the particular period of $F(t)$, input energy has then a well-defined distribution. One can compute the input energy distribution over ensembles with different initial position $x(0)$.

II.7 Fourth-order Runge-Kutta method for ordinary differential equations

Fourth-order Runge-Kutta (RK4) is a numerical method introduced to solve the differential equations. Let an initial value problem be specified as follows:

$$\dot{y} = f(t, y) \tag{58}$$

$$y(t_0) = y_0 \tag{59}$$

Here y is an unknown function of time t, which we would like to approximate; we are told that $\dot{y}$, the rate at which y changes, is a function of t and of y itself. At the initial time t_0 the corresponding y value is y_0. The function *f* and the initial conditions t_0, y_0 are given.

Now pick a step-size $h > 0$ and define

$$y_{n+1} = y_n + \frac{1}{6}(k_1 + 2k_2 + 2k_3 + k_4) \tag{60}$$

$$t_{n+1} = t_n + h \tag{61}$$

for $n = 0, 1, 2, 3, ...$, using

$$\begin{aligned} k_1 &= hf(t_n, y_n), \\ k_2 &= hf(t_n + \frac{h}{2}, y_n + \frac{k_1}{2}), \\ k_3 &= hf(t_n + \frac{h}{2}, y_n + \frac{k_2}{2}), \\ k_4 &= hf(t_n + \frac{h}{2}, y_n + k_3). \end{aligned} \tag{62}$$

Here y_{n+1} is RK4 approximation of $y(t_{n+1})$, and th next value y_{n+1} is determined by the present value y_n plus the weighted average of four increments, where each increment

is the product of the size of the interval, h, and an estimated slope specified by function f on the right-hand side of the differential equation.

The RK4 method is a fourth-order method, meaning that the local truncation error is on the order of $0(h^5)$, while the total accumulated error is on the order of $0(h^4)$.

II.8 Investigation of the Chaos

This section is devoted to discussing the variation of the largest Lyapunov exponent (LLE). The negative sign of the LLE indicates that the phenomenon of chaos occurs. To calculate it, we consider a small deviation from the stochastic process $x(t)$ is noted by δx, which satisfies the equation $\delta \dot{x} = J(x)\delta x$, where $J(x)$ is the Jacobian matrix. Thus, the largest Lyapunov exponent can be calculated as follows,

$$\lambda_{max} = \lim_{t\to\infty} \frac{1}{t} log\left(\parallel \delta x \parallel\right). \tag{63}$$

II.9 Conclusion

This chapter has presented the mathematical formalisms whose we needed for analytical and numerical investigations. The models and the explicit form of the substrates have been exhibited. In the goal to get the solid results and do the good analysis, the RK4 for stochastic process (Kasdin algorithm) has clearly been described. The quantities of our interest have also been presented, even the way to calculate them. Having all these tools, the next chapter will then be focused on the different results and their discussions.

CHAPTER III

RESULTS AND DISCUSSION

III.1 Introduction

In this chapter, we apply the numerical and analytical methods presented in the previous chapter to answer the different questions around our thesis. To reach our aim, we organize this chapter as follows: In the first we study the phenomenon of SR in the Remoissenet-Peyrard potential. In section 2, we use the asymmetric and double-well deformable potentials to investigate input energy, SR, input energy distribution and probably the chaos. Section is devoted to the analysis of the SR phenomenon in the N-coupled particles system and finally in the last section we conclude the chapter.

III.2 Stochastic resonance in the periodic Remoissenet-Peyrard potential

In order to understand the dynamical processes of the present system, **Eq (25)** has been integrated numerically from the Kasdin algorithm over a time long enough of $N_1 + 1$ periods τ with time step $h = 0.01$. Initial velocity $\dot{x}(0) = 0$ for all cases and the initial position $x(0) = x(t = 0)$ are chosen at 99 equispaced points $x_i, i = 1, 2, ..., 99$, between 0 and 2π. The drive frequency $\omega = \frac{2\pi}{\tau}$ ($\tau = 8$) is chosen to be close to the natural frequency at the bottom of the wells of the potential.

III.2.1 Potential shape and friction coefficient dependence of the stochastic resonance

The set of numerical results for several shape of the potential, which describes SR is depicted in **Fig 18** by numerically calculating **Eqs (41)** and **(55)**. These figures illustrate the variation of the average input energy $\langle \overline{W} \rangle$ as a function of temperature for the values of $\gamma = 0.2$, $\gamma = 0.3$, $\gamma = 0.5$ and for six shapes of the potential namely, $r = -0.4$ (**Fig 18(a)**), $r = -0.2$ (**Fig 18(b)**), $r = 0$ (**Fig 18(c)**), $r = 0.2$ (**Fig 18(d)**), $r = 0.4$ (**Fig 18(e)**) and $r = 0.6$ (**Fig 18(f)**). These curves increase until reaching a maximum and decrease gradually as the temperature increases, thus showing a signature feature of SR. For these three values of γ each curve displays typical maximum average of the input energy. We note that for all these values of r the phenomenon of stochastic resonance is exhibited through the peaks. We observe from **Fig 18(a)** that the peaks of resonance are less defined and the maximum value of the average input energy $\langle \overline{W} \rangle_{max}$ increases as γ increases. We can also see that the same value of the average input energy is reached despite the differences in the damping coefficient γ at lower temperature. The temperature T_{SR} of occurrence of stochastic resonance also increases with γ. The same behaviour is observed in **Fig 18(b)** with the shape potential $r = -0.2$, but in this case the peaks of resonance are well-defined. When the shape parameter r increases, the peaks become more pronounced and quite broad as reflected by **Fig 18(c)** and **18(d)** for $r = 0$ and $r = 0.2$. The temperature T_{SR} increases with γ like the case of $r = -0.4$ but contrary on **Fig 18(a)**, the maximum of the average input energy $\langle \overline{W} \rangle_{max}$ decreases rapidly when γ increases. Let us mention that, when the temperature T is too small ($T << T_{SR}$), the switching events become very rare; thus the inter-well transitions are hardly visible. However, beyond $T = T_{SR}$ ($T >> T_{SR}$), the inter-well dynamics become more frequent. Single maxima are reached at different value of the temperature. There is, however, a remarkable difference between the nature of motion of the particle at the temperature T_{SR} of maximum of the average input energy $\langle \overline{W} \rangle_{max}$ for different values of the shape parameter r.

In order to gain a good appreciation of the effect of the shape parameter and the

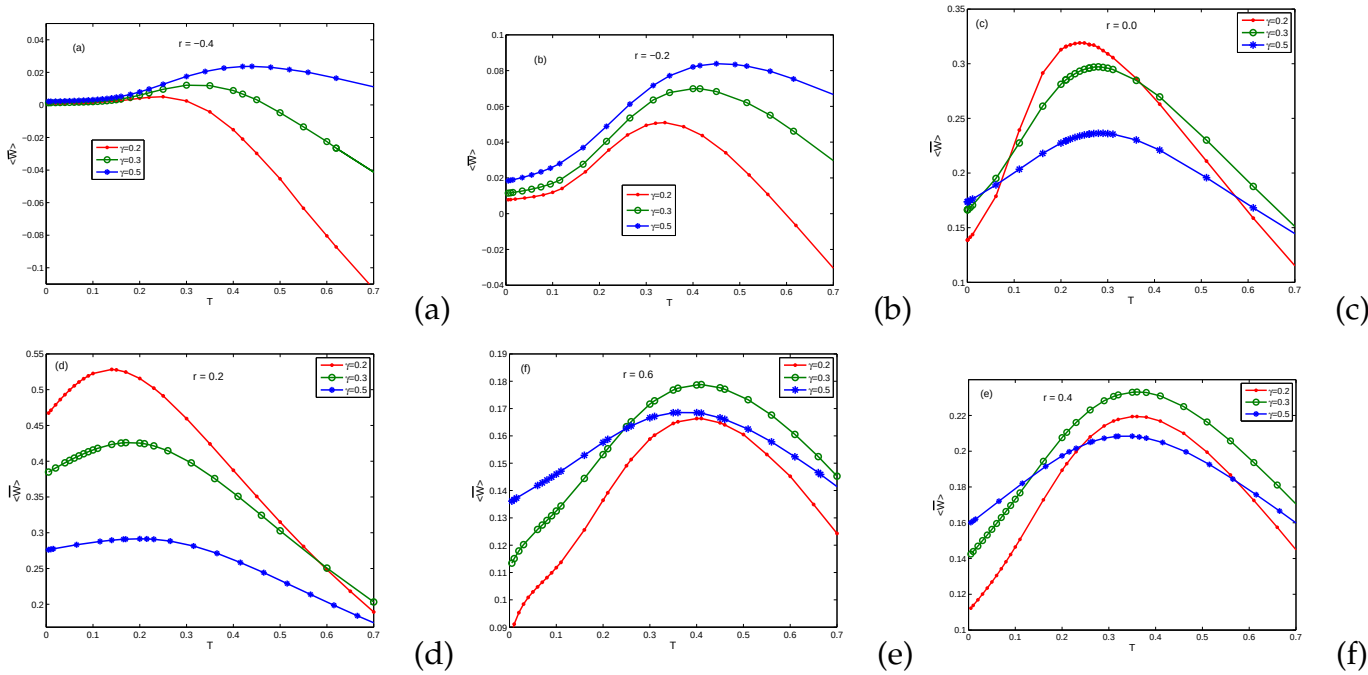

Figure 18: Plot of $\langle \overline{W} \rangle$ as a function of T, for values of $\gamma = 0.2$, $\gamma = 0.3$ and $\gamma = 0.5$ for $r = -0.4$ (a), $r = -0.2$ (b), $r = 0$ (c), $r = 0.2$ (d), $r = 0.4$ (e), and $r = 0.6$ (f). Other parameters are $m = 1$, $U_0 = 1$, $A_0 = 0.2$ and $F_0 = 0.1$.

friction coefficient, other calculations are done for a large range of parameters γ and r. The effect of the different shape potential on the SR as well as of the damping coefficient is depicted in **Fig 19**. Therefore, for a given value of the shape parameter r, there is a range of the parameter γ where the phenomenon of SR does not occur. For low values of the shape parameter r $(r < -0.6)$, SR does not occur for all parameter γ. This may be due to the suitable choice of the other parameters of the system, m, U_0, A_0, F_0 and in particular to the judicious choice of the period τ of the external periodic force. The position of the average input energy $\langle \overline{W} \rangle$ peaks also depends of the parameter r as well as of the parameter γ. This dependence is shown in **Fig 19(a)** where the T_{SR} is represented as a function of the parameter γ for several shape parameters. As one can see from **Fig 19(b)**, when γ is high, the value of $\langle \overline{W} \rangle_{max}$ converges towards 0.1. It is also noted from **Fig 19(b)** the reduced of SR peak when the parameter γ increases, however for small value of γ, one can also notice a small increasing of SR peak when γ is less than 0.2 in certain range of the parameter r. A high value of $\langle \overline{W} \rangle_{max}$ is obtained for low

values of γ and when r goes to 0.2.

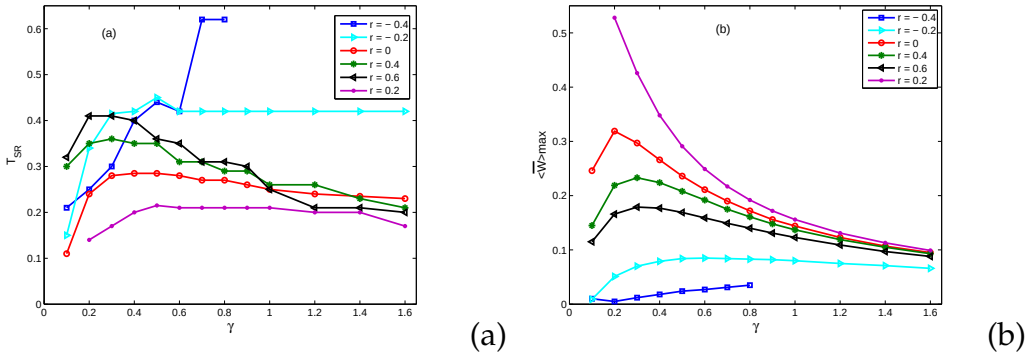

(a) (b)

Figure 19: Variation of T_{SR} as a function of γ (a) and the variation of $\langle \overline{W} \rangle_{max}$ as a function of γ (b).

For further investigation, the average input energy $\langle \overline{W} \rangle$ as a function of the shape parameter r is simulated using some resonance temperature T_{SR}. This shows more clearly the effects on $\langle \overline{W} \rangle$ by varying the shapes of the potential. **Figure 20** shows that the highest value of the average input energy can be obtained for $r = 0.11$ with $\gamma = 0.2$. One can see that the $\langle \overline{W} \rangle$ shows a maximum as a function of the shape potential r, these maxima are obtained around $r = 0.13$. It is very clear from **Fig 20** that the average input energy $\langle \overline{W} \rangle$ for the parameter $\gamma = 0.2$ is generally higher than the other values of the parameter γ. When the shape parameter r is lower than -0.2 ($r < -0.2$) or higher than 0.4 ($r > 0.4$), the values of the input energy $\langle \overline{W} \rangle$ are generally closed together.

III.3 Stochastic resonance in a periodic asymmetric and double-well deformable substrate potential

In this section, we use the initial velocities $\dot{x}(0) = 0$ for all cases and the initial positions $x(0)$ are chosen between 0 and 4π. The frequency $\omega = \frac{2\pi}{\tau}$ with $\tau = 8$ is taken to be close to the natural frequency at the bottom of the wells of each potential. **Eq (41)** is integrated over a time long enough of $N_1 + 1$ periods.

In order to deduce information on microscopic properties of the ASDP and DWDP

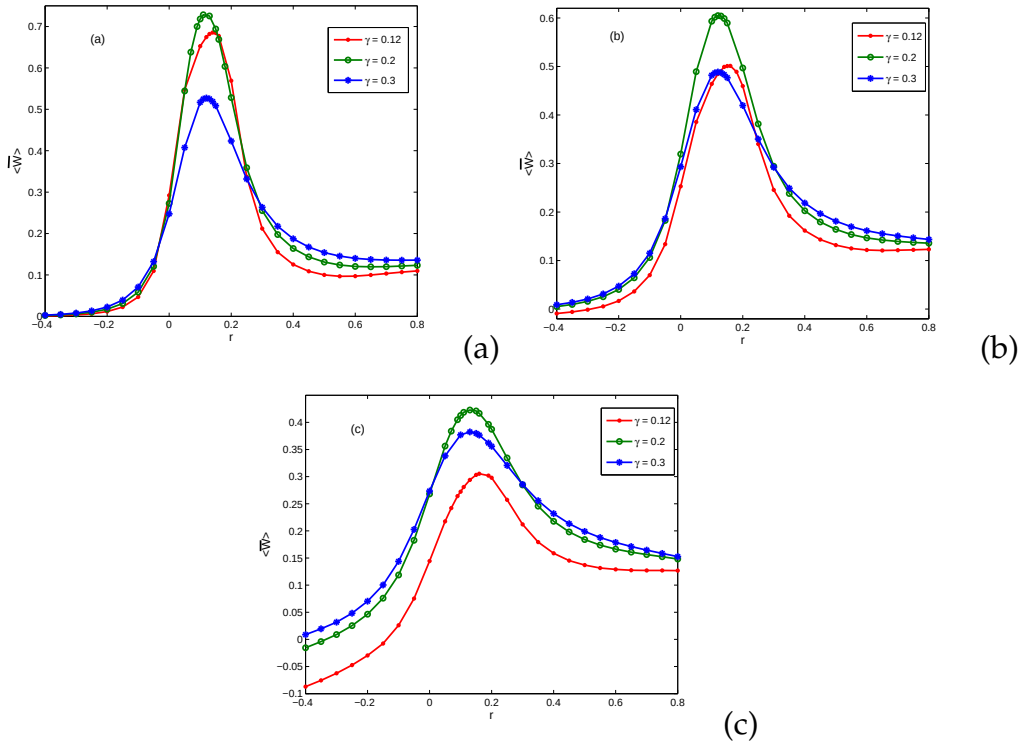

Figure 20: Plot of the variation of $\langle \overline{W} \rangle$ as a function of shape potential r for $T = 0.14$ (a), $T = 0.24$ (b) and $T = 0.4$ (c). Other parameters are $m = 1$, $U_0 = 1$, $A_0 = 0.2$ and $F_0 = 0.1$.

systems from the observed dynamics of the particle, we focus our attention on the occurrence of the phenomena of the SR. System can achieve each dynamics by taking various values of the system parameters F_0, γ, A_0 and ω. In the following, we present the results of our numerical calculations and analyze how the particle trajectories in the ASDP and DWDP systems from mean residence time, and hence the input energy and the input energy distribution, are affected by the shape parameter r. We examine the occurrence of SR in the ASDP and DWDP models.

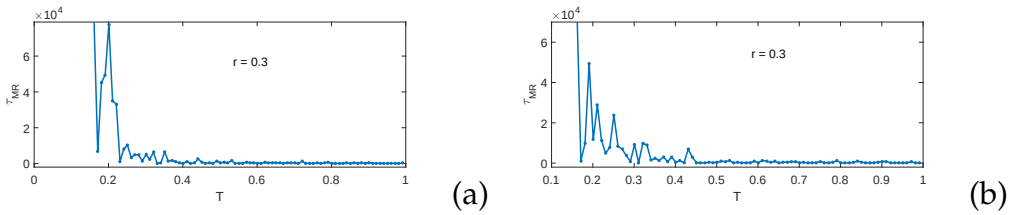

Figure 21: Mean residence time τ_{MR} of the particle in the initial well for ASDP system (a) and double well for DWDP system (b) as a function of T when $r = 0.3$. Other parameters are $m = 1$, $U_0 = 1$, $\gamma = 0.2$, $A_0 = 0.2$ and $F_0 = 0.1$.

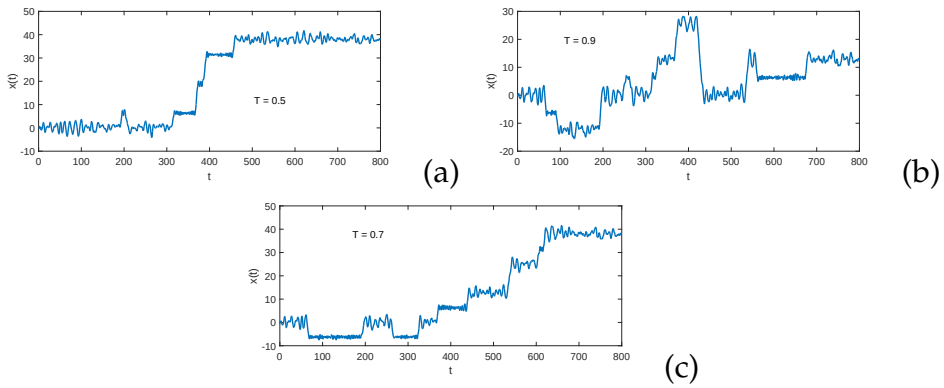

Figure 22: Trajectories $x(t)$ versus time t for ASDP model and for $r = 0.3$ at various values of the temperature. Other parameters are $m = 1$, $U_0 = 1$, $\gamma = 0.2$ and $F_0 = 0.1$.

One of the objectives is to deduce information on the properties of the system to understand how the particle stays in a well before switching to another well; this refers to mean residence time τ_{MR}. For a weak amplitude of the external force and in the absence of noise, the motion of the particle is confined to a well or an equilibrium state. That is, before the noise induced dynamics (or even the external force), the residence time of the system in each well is infinite (τ_{MR} is much larger than the period). **Figs 21(a)** and **21(b)** illustrate numerically computed τ_{MR} on each well for at set of $n * \tau$ transitions ($n = 5000$) as a function of the temperature T when $x(0) = 0$, $r = 0.3$ and $A_0 = 0.2$. At the weak values of T, there is no switching and so τ_{MR} is infinite and the number of times that the particle jumped from initial well to another well is zero in both the systems. At appropriate optimum noise intensity a periodic switching between the wells take place. This noise-induced phenomenon is called SR [68, 70, 71]. In each of these two potentials, far before resonance $\tau_{MR} >> n/2$.

At the resonance where HLA becomes maximum $\tau_{MR} = n/2$. $\tau_{MR} << n/2$ for far after resonance. one can remark that τ_{MR} is non-monotonical, this is clearly explained by the behavior of the trajectories $x(t)$ in **Fig 22**, plotted for various temperatures. Where in some case, although the particle go out of the initial well, it can return in this well with the time. By considering the temperature $T = 0$, we calculate τ_{MR} for different values of the amplitude of the external force A_0. **Fig 23** represents the mean residence

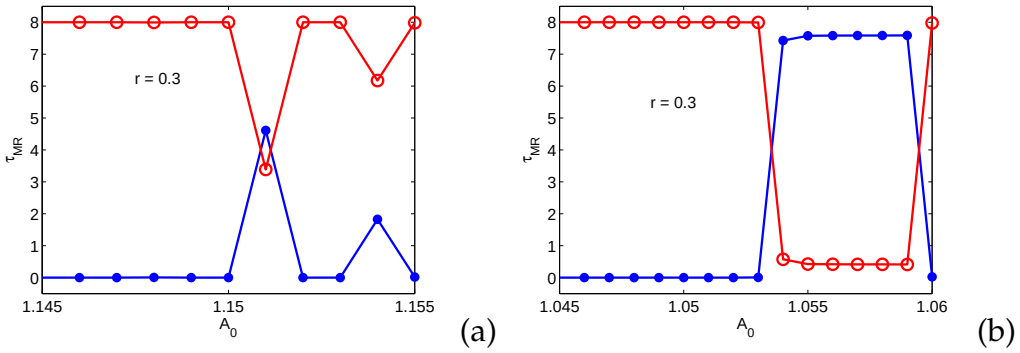

Figure 23: Mean residence time in the initial well (blue circle line) while the red dot line is the mean residence time of the particle out of the initial well as a function of amplitude of external force A_0 in the absence of noise for $r = 0.3$ and for the both models: (a) ASDP , (b) DWDP (initial double well). Other parameters are $m = 1$, $U_0 = 1$, $\gamma = 0.2$ and $F_0 = 0.1$.

time of the particle on each well (circle line) and the mean residence time out of the initial well (dot line) computed for one period of the external force as a function of A_0 for $r = 0.3$. we observe that when $A_0 < A_{0s}$, A_{0s} being the value of A_0 at which switching starts, the mean residence time of the particle out of the initial well (dot line) is null whereas the mean residence time in the initial well is equal to τ. This means that the probability to find the particle in initial well is equal to 1. We then note that the normalized residence time (τ_{MR}/τ) is equal to 1, this means no switching occurs and the trajectories are intrawell in nature. One can note that the value of A_0 for which switching between wells begin strongly depends of the shape parameter as shown in **Fig 24** plotted for ASDP system.

III.3.1 Input energy and input energy distribution

Input energy

By using the relations **(54)** and **(55)**, we compute the input energy $\overline{W}$ which at the lowest temperature depends very strongly on the initial conditions $(x(0), v(0))$. We can thus present an investigation of the variation of the input energy profile averaged over a trajectory as a function of the initial positions $x(0)$ in the ASDP and DWDP models for

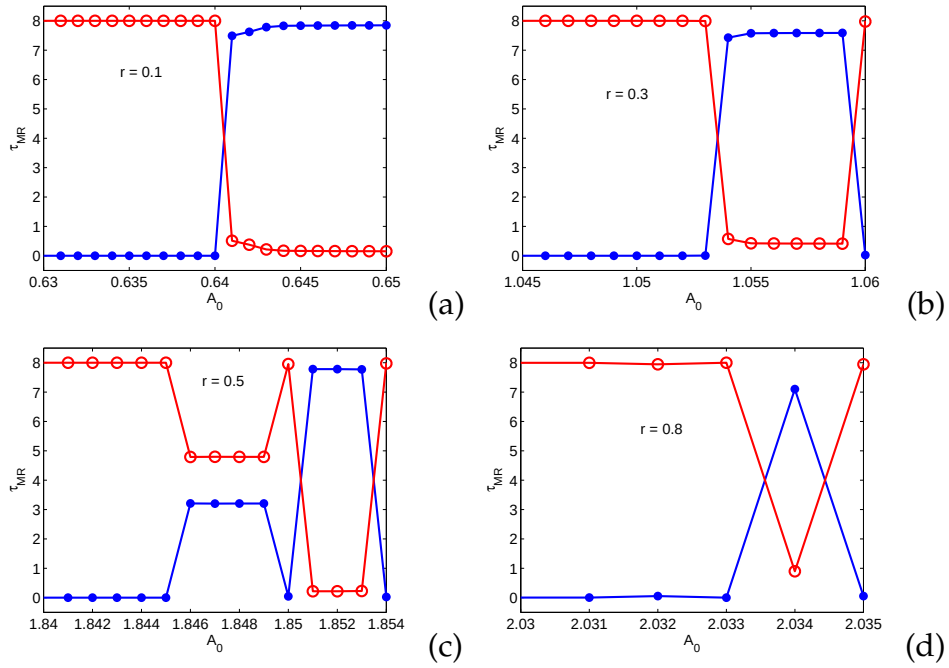

Figure 24: Mean residence time in the initial well (blue circle line) while the red dot line is the mean residence time of the particle out of the initial well as a function of amplitude of external force A_0 in the absence of noise for $r = 0.1$ (a), $r = 0.3$ (b), $r = 0.5$ (c) and $r = 0.8$ (d) in the ASDP model. Other parameters are $m = 1$, $U_0 = 1$, $\gamma = 0.2$ and $F_0 = 0.1$.

several shape parameters and for a temperature $T = 0.001$. As a function of the shape of the potential, $\overline{W}$ can display two or one narrow band. In the case of ASDP system, we observe that the curves of $\overline{W}$ are confined to two narrow bands when $r < 0.5$, and gradually increasing r, $\overline{W}$ makes a transition towards only one narrow band as shown in **Fig 25**. However, the input energy $\overline{W}$ clearly displays two bands for $r < 0.3$ and one band for $r > 0.3$ in the DWDP model as illustrated by **Fig 26**. In fact, for a shape of potential given a band of $\overline{W}$ corresponds to a state of energy in which the particle can be found. It has been shown in **ref** [35] that the two narrow bands observed on $\overline{W}$ curves correspond to the existence of two dynamical states distinctly identified by the phase difference between the external force and the trajectory $x(t)$.

Table 2 shows a summary of the values of $\overline{W}$ bands for the ASDP and DWDP systems when r is varied. The behavior of $\overline{W}$ is then controlled by the parameter r. Of course, for both the systems, it is important to point that for the values of r where two bands

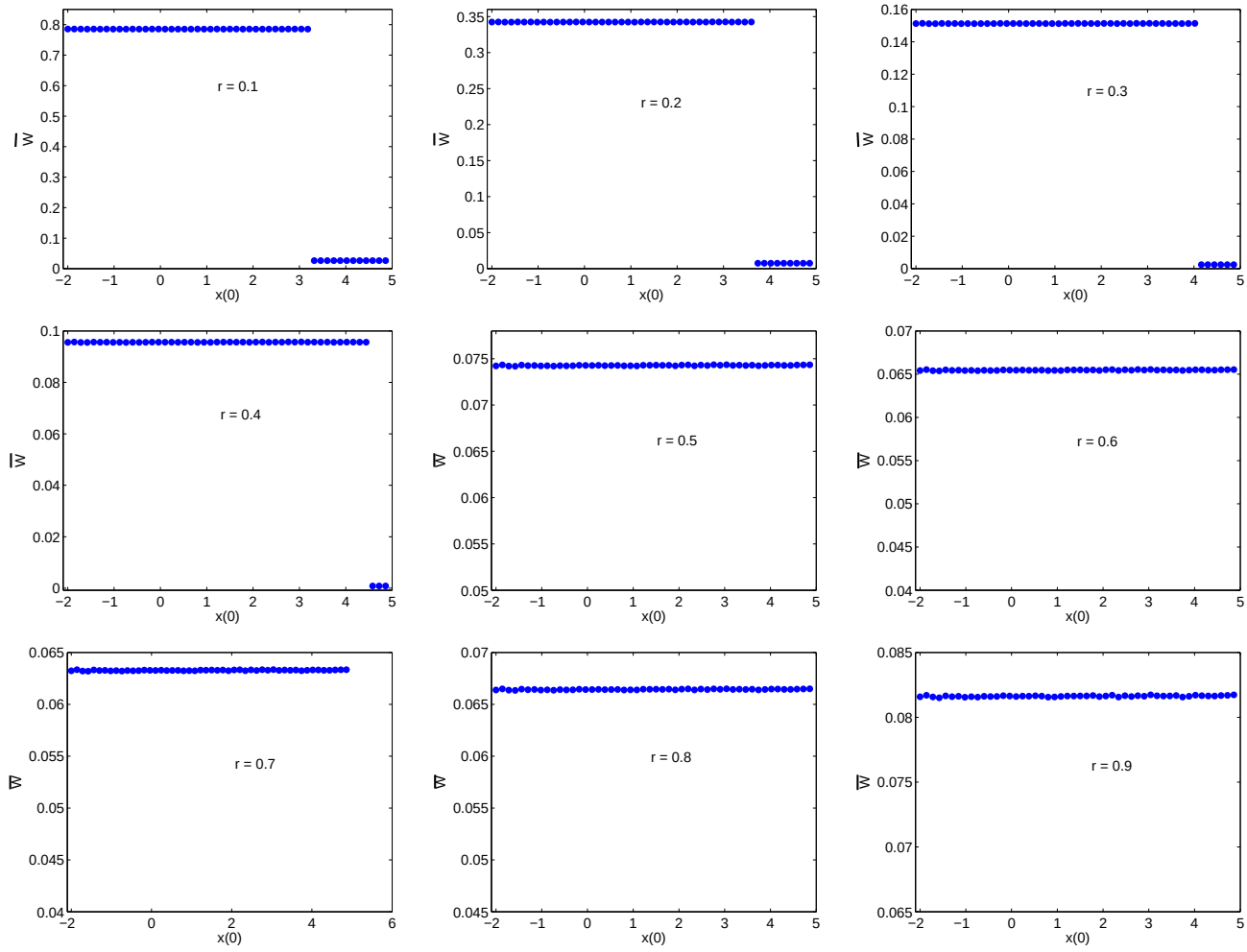

Figure 25: Variation of the input energy $\overline{W}$ with initial positions $x(0)$ at a temperature $T = 0.01$ for ASDP system and for various values of shape parameters r. Other parameters are $m = 1$, $U_0 = 1$, $\gamma = 0.2$, $A_0 = 0.2$ and $F_0 = 0.1$.

appear, the upper band gradually diminishes, then disappears and joins the lower band as r is increased. Thereby, one can say that some states have made a transition to another states. The shape parameter influence is then similar to the action of temperature in thermodynamic equilibrium systems and leads to the effective reducing of the depths of potential well. Although considering a entire space period of these systems where both the wells are included, the behavior of $\overline{W}$ is not affected. In order to know how this input energy is distributed in each system, in the following we examine the behavior of input energy distribution.

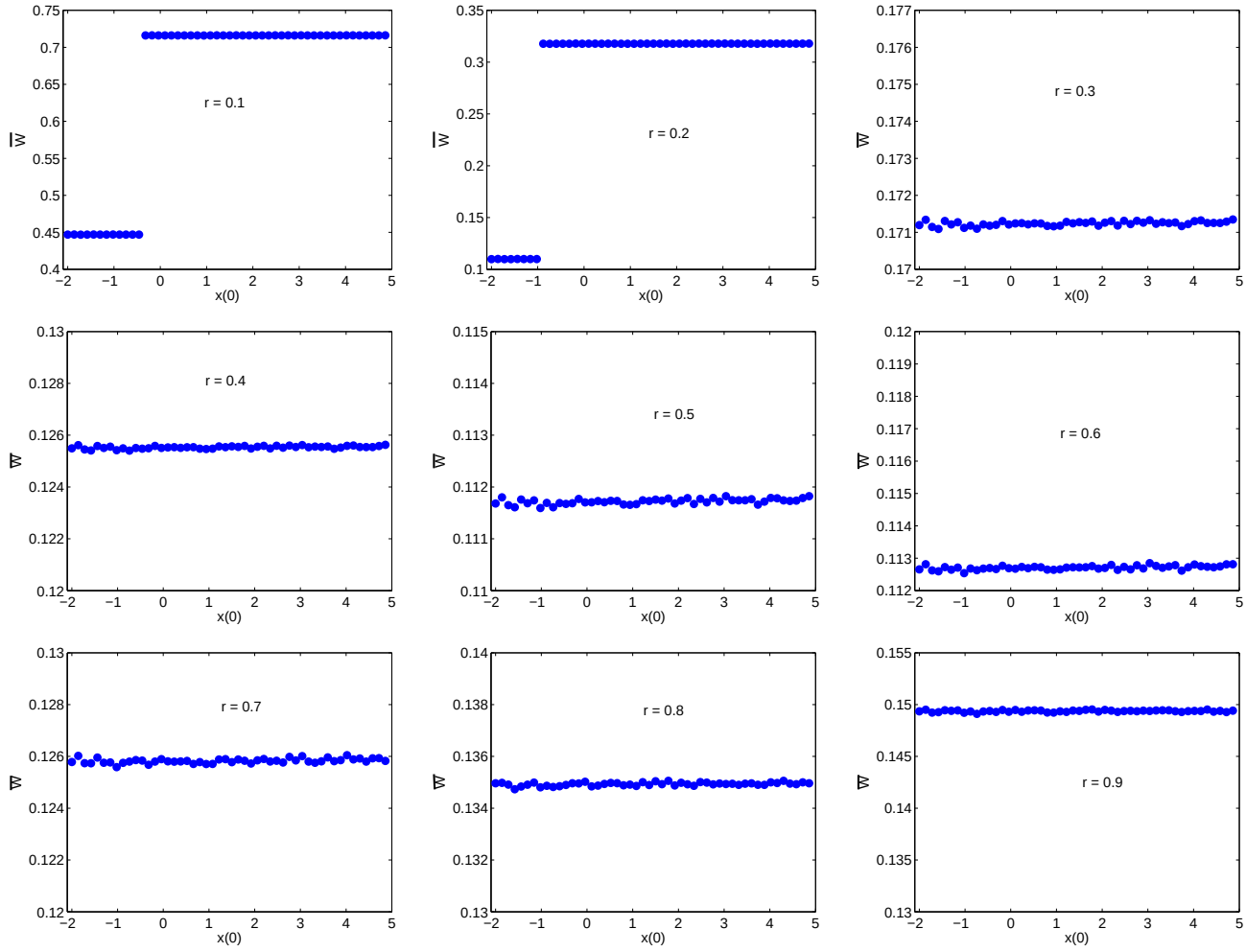

Figure 26: Variation of the input energy $\overline{W}$ with initial positions $x(0)$ at a temperature $T = 0.01$ for DWDP system and for various values of shape parameters r. Other parameters are $m = 1$, $U_0 = 1$, $\gamma = 0.2$, $A_0 = 0.2$ and $F_0 = 0.1$.

Input energy distribution

The distribution can carry important information about the system and mainly the stochastic resonance. The values of W are different depending on whether during the particular period of $F(t)$, input energy has then a well-defined distribution. One can compute the input energy distribution over ensembles with different initial position $x(0)$. In **Fig 27**, the distribution of W is exhibited for various shape parameters r at a temperature $T = 0.001$ for ASDP system. As we can see the peaks of $P(W)$ are quite sharp. The nature of $P(W)$ depends of the value of r, thus $P(W)$ displays a bimodal distribution when $r < 0.5$. The height of the first peak decreases with r, this peak gradually

Table 2: Values of $\overline{W}$ band of the ASDP and DWDP systems for various values of r.

r	ASDP	DWDP
0.1	0.026 ; 0.785	0.446 ; 0.716
0.2	0.007 ; 0.342	0.109 ; 0.317
0.3	0.002 ; 0.151	0.171
0.4	0.0008 ; 0.095	0.125
0.5	0.074	0.111
0.6	0.065	0.112
0.7	0.063	0.125
0.8	0.066	0.134
0.9	0.081	0.149

disappears yet to lose completely from $r = 0.5$. Therefore, for $r > 0.4$ the input energy distribution $P(W)$ changes from two peaks to only one and their width increases with r. All these peaks are exactly centred at the values of $\overline{W}$ bands. The apparition of $P(W)$ peaks then obeys at the behavior of $\overline{W}$. For DWDP system, two peaks are observed when $r < 0.3$, $P(W)$ peaks also obey at the behavior of $\overline{W}$. Nevertheless, for $r > 0.6$, it is interesting to note that, although $\overline{W}$ is consisted of only one band, $P(W)$ has a bimodal nature.

Thereby there is no longer any relationship between $P(W)$ and $\overline{W}$. That can be due to weird nature of the hysteresis loops. $P(W)$ is uni-modal for the other values of r as illustrated in **Fig 27**. When $r > 0.6$, In both the models, the height of the peaks non-monotonically depends of r. These distributions can also provide many informations about the number of state having a well-defined input energy. Notice the intrusion of W into the negative value. The increase of negative region of $P(W)$ goes hand in hand with increasing r. In both the systems the position of peaks varies along with the changing of the shape of the potential that is because the shape parameter affects the values of the input energy.

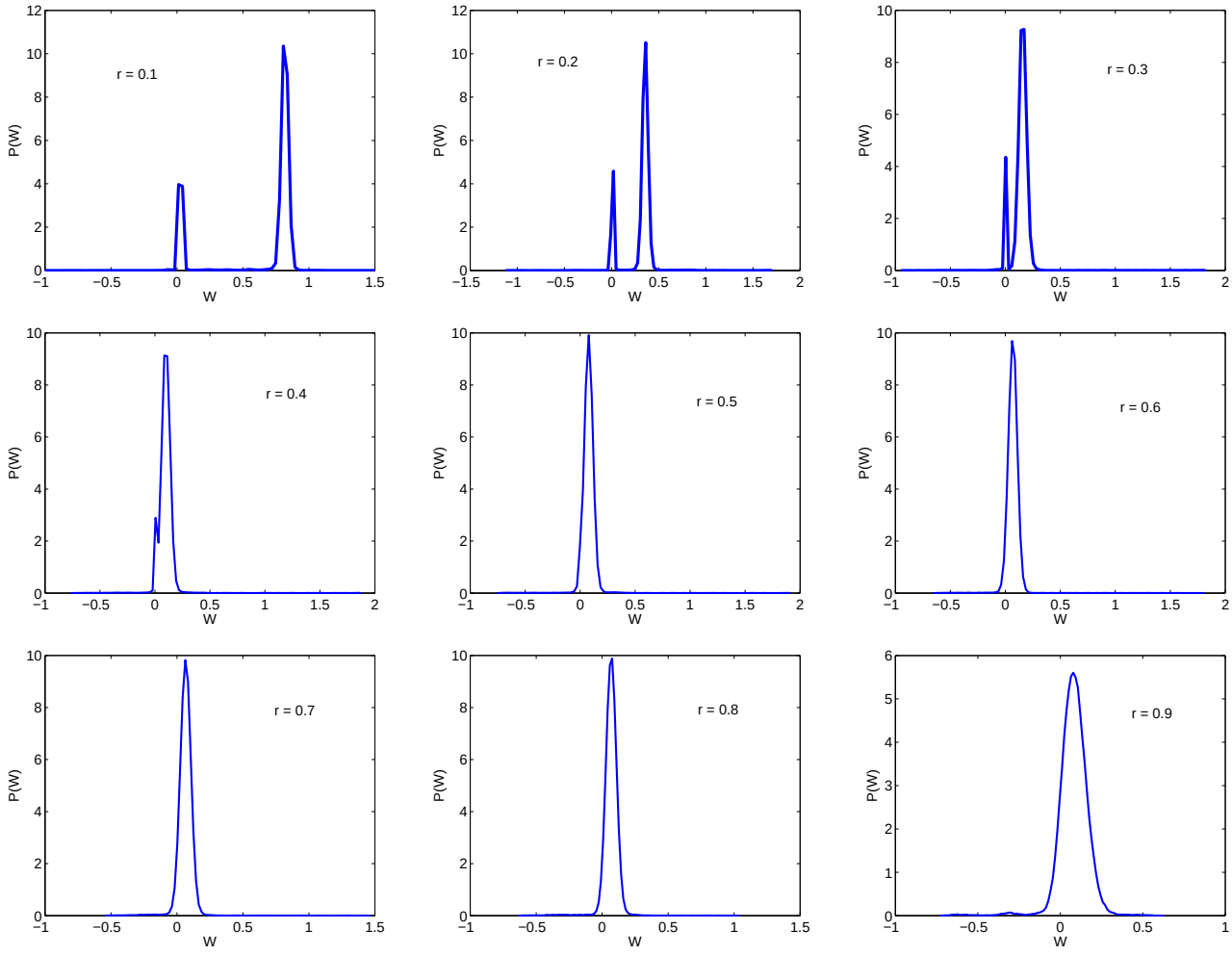

Figure 27: Input energy distribution $P(W)$ at a temperature $T = 0.01$ for ASDP model and for various values of shape parameters r. Other parameters are $m = 1$, $U_0 = 1$, $\gamma = 0.2$, $A_0 = 0.2$ and $F_0 = 0.1$.

III.4 Hysteresis loop area: Stochastic resonance

In order to characterize the SR phenomenon, we use the hysteresis loop whose the area will allow to quantify it. Hysteresis loop closely resemble an ellipse. The hysteresis loops are different for various trajectories depending on the duration of the dynamics and shape of the potential. By numerically calculating **Eqs (41)** and **(55)**, one obtains the average input energy $\langle \overline{W} \rangle$ which is computed by averaging $\overline{W}$ over ensemble with different initial positions. For several values of the shape parameters we plot in **Fig 29** the variation of the average input energy $\langle \overline{W} \rangle$ as a function of the temperature for

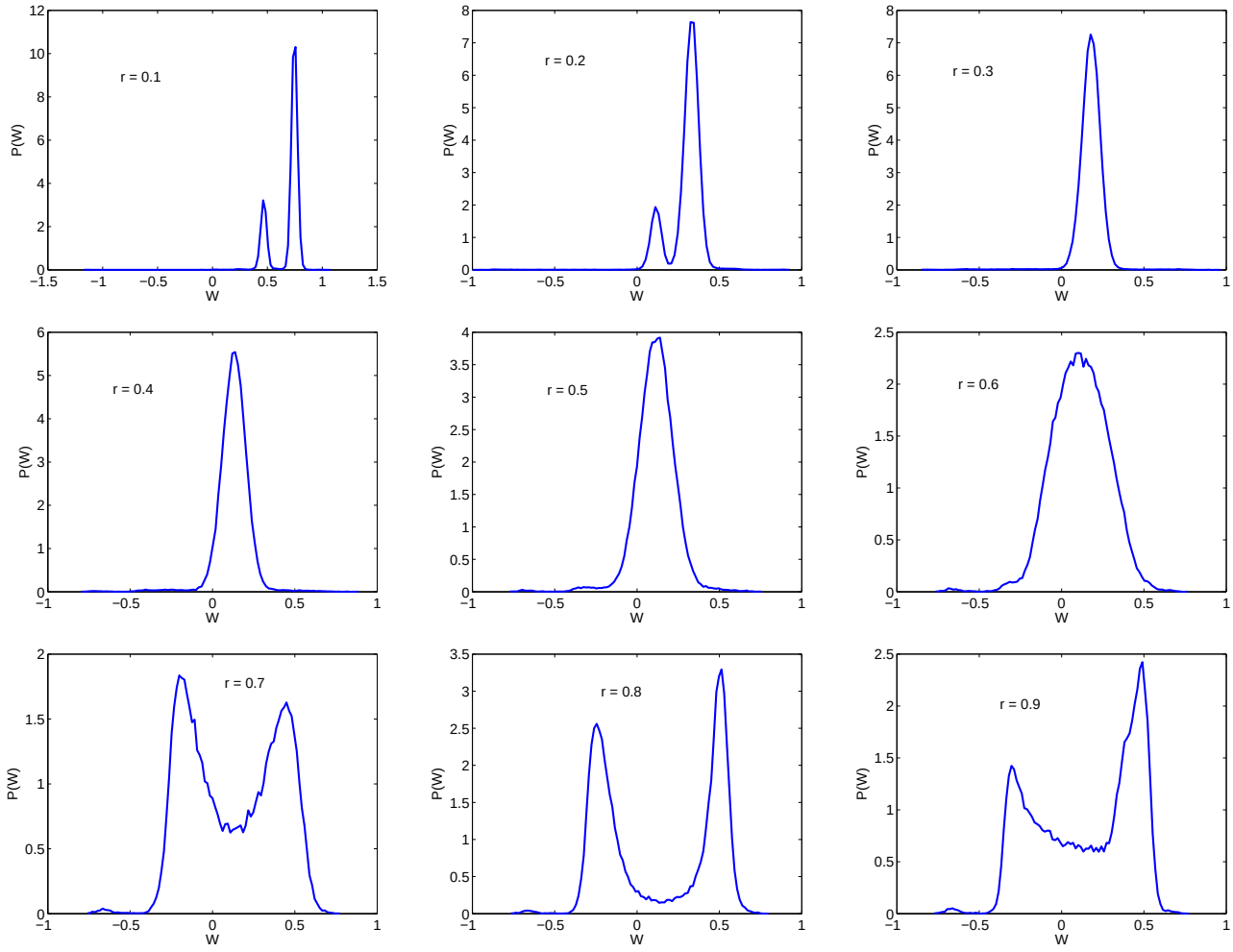

Figure 28: Input energy distribution $P(W)$ at a temperature $T = 0.01$ for DWDP model and for various values of shape parameters r. Other parameters are $m = 1$, $U_0 = 1$, $\gamma = 0.2$, $A_0 = 0.2$ and $F_0 = 0.1$.

ASDP case. The curves of $\langle \overline{W} \rangle$ initially increase, reach a maximum, decrease until attain a minimum, increase again until an other maximum and then gradually decrease with T. $\langle \overline{W} \rangle$ then displays two maxima whose the energy of the first is higher. In the literature, it is known that one maximum characterizes the phenomenon of SR, thus two maxima cannot be only a simple SR but rather a double SR. The cooperative effect of noise and external force does then show up. Due to finite tilting force F_0 the ASDP system illustrates two resonant temperatures for a wide range of shape parameter r. The first peak appears at the weak temperature namely at the limit of the deterministic. It has nothing to do with usual mechanical resonance, but it just associated to the

intra-well dynamics, where less favourable conditions for transitions between wells are realized. Thus the temperature of occurrence of this first peak is not enough to allow to the particle to across the potential barrier. So, this peak corresponds to a frequency resonance where the particle oscillates periodically around its initial position. Second peak arising at higher temperature, relates to the classical SR phenomenon which is due to the mechanism of synchronization of the periodic external force with the activated inter-well dynamics.

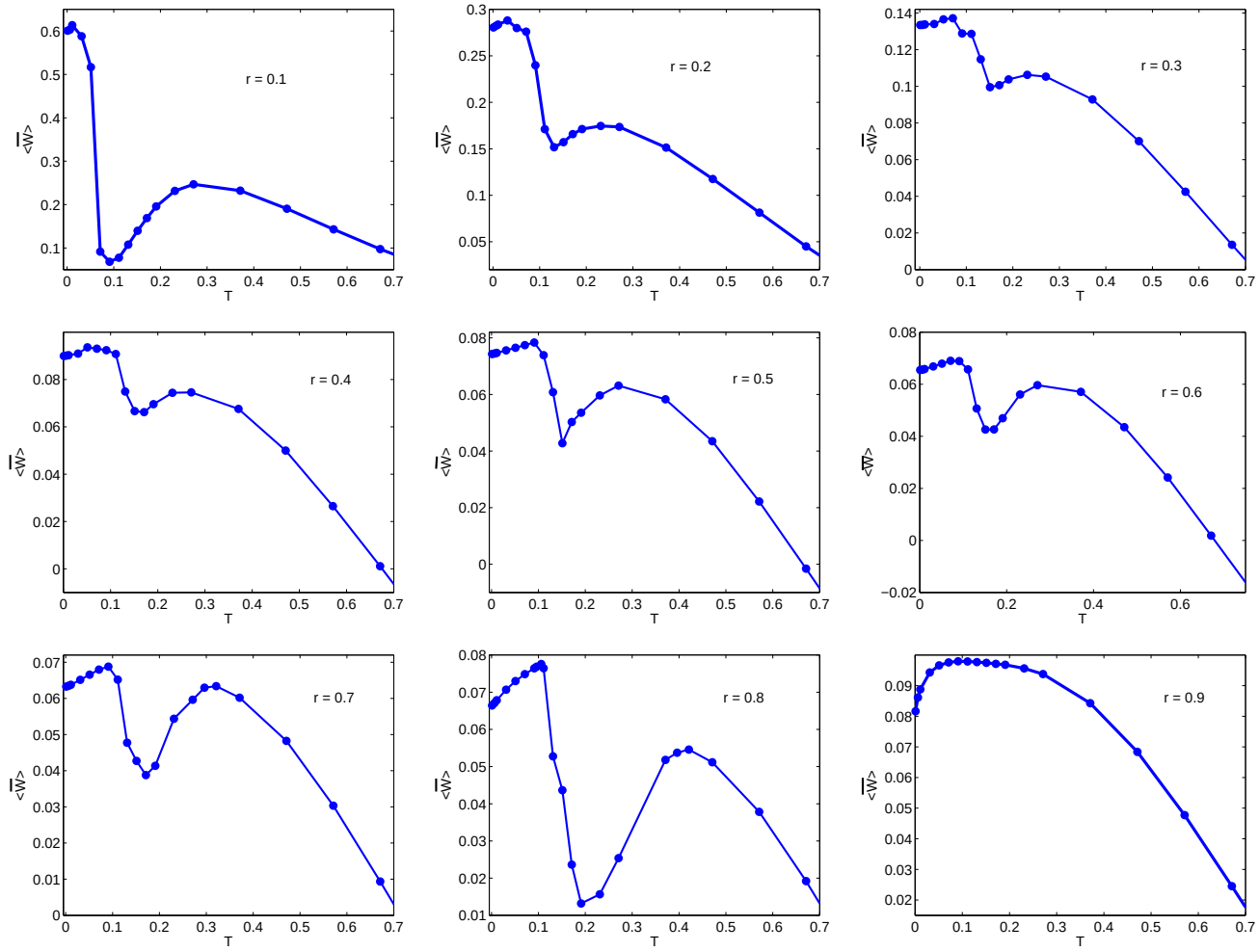

Figure 29: Variation of $\langle \overline{W} \rangle$ as a function of T for ASDP system and for various values of shape parameters r. Other parameters are $m = 1$, $U_0 = 1$, $\gamma = 0.2$, $A_0 = 0.2$ and $F_0 = 0.1$.

However, for $r = 0.9$, $\langle \overline{W} \rangle$ not exhibits two peaks of resonance but only one. In the DWDP case the behaviour of $\langle \overline{W} \rangle$ is quite different from the one obtained for the ASDP model. As displayed in **Fig 30**, $\langle \overline{W} \rangle$ exhibits a maximum as T is increased. The

phenomenon of SR then occurs in this system for any value of r excepted for $r = 0.3$ where the curve of $\langle\overline{W}\rangle$ is monotonic. This no-appearance of SR phenomenon for $r = 0.3$ is certainly due to the choice of the parameter's systems. To confirm that, let us take $\gamma = 0.12$ in the case of $r = 0.3$, where SR did not occur. The system clearly defines a peak of resonance, SR then takes place as depicted in **Fig 31(a)**. in this model, SR appears at lower temperatures than the ASDP system. The average input energy as well as temperature of occurrence of the SR strongly depend of r. each of both the systems gets the particular properties under the effects of noise and external force.

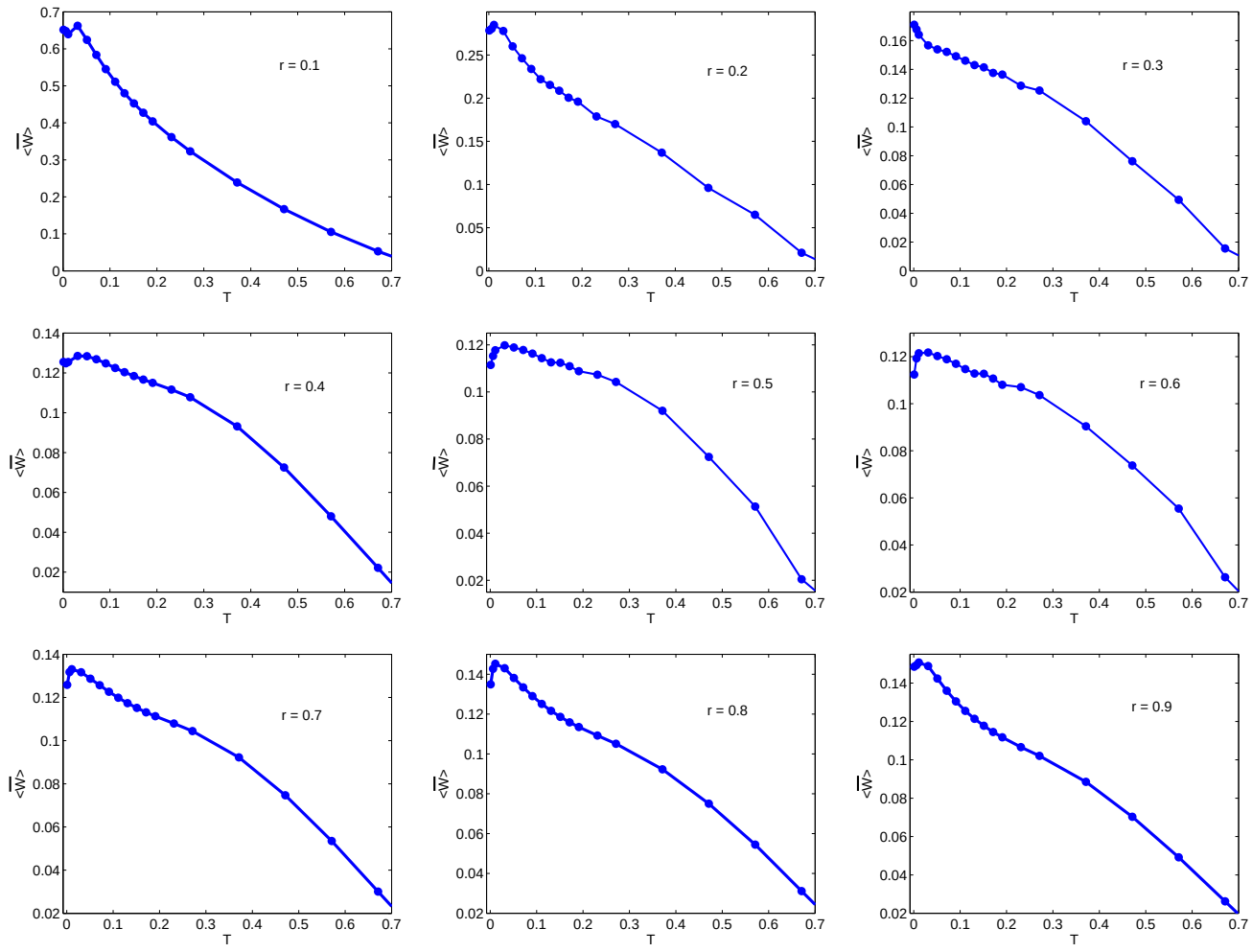

Figure 30: Variation of $\langle\overline{W}\rangle$ as a function of T for DWDP system and for various values of shape parameters r. Other parameters are $m = 1$, $U_0 = 1$, $\gamma = 0.2$, $A_0 = 0.2$ and $F_0 = 0.1$

Moreover, it is necessary to point that in this kind of system, there is generally com-

petition between the phenomena such as the Chaos and the stochastic resonance for example. What is the case for the DWDP system, for which we study the system's state from the Lyapunov exponent (**Eq 62**) which is a good indicator of Chaos in dynamical system. For $r = 0.9$, one plots in **Fig 31(b)** the Lyapunov exponent λ as a function of the amplitude of the external force A_0. Dashed line separates the domain where the Chaos is present ($\lambda > 0$) and the other hand where it is absent ($\lambda < 0$). Taking the values of $A_0 = 0.15$, 0.22 and 0.3, mainly where the Chaos is present in the system, we investigate the variation of $\langle \overline{W} \rangle$ with T in **Fig 32**. Remark that SR appears for $A_0 = 0.22$ and doesn't occur for the two others values. Thus, the Chaos is responsible of the destruction of the SR phenomenon in the system when $A_0 = 0.15$ and $A_0 = 0.3$. Nevertheless it is not enough sufficient to prohibit the SR when $A_0 = 0.22$.

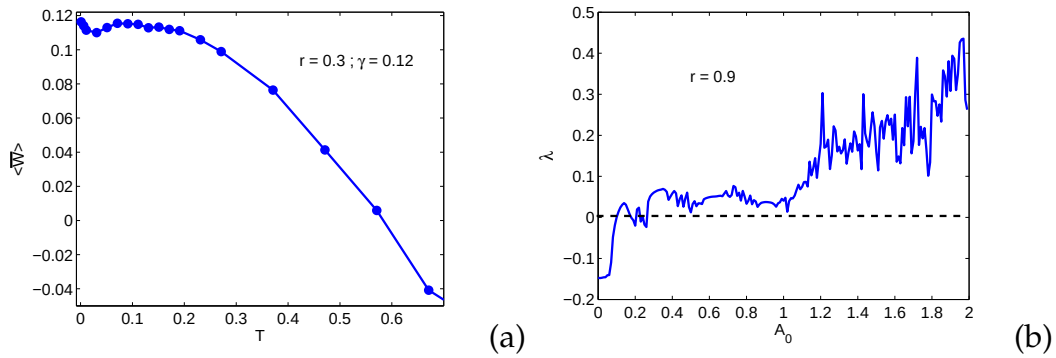

Figure 31: Variation of $\langle \overline{W} \rangle$ as a function of T in the DWDP system for $r = 0.3$ and $\gamma = 0.12$ (a). Evolution of Lyapunov exponent λ with A_0 for $r = 0.9$ and $\gamma = 0.2$ (b). Other parameters are $m = 1$, $U_0 = 1$, $A_0 = 0.2$ and $F_0 = 0.1$.

III.5 Stochastic resonance and stochastic antiresonance in a unidirectionally N-coupled particles in a particular case of the RP potential

First, let us mention that the common tilted sinusoidal potential can be deduced from **Eq (24)** trough a continuous deformation when the parameter r goes to zero (see

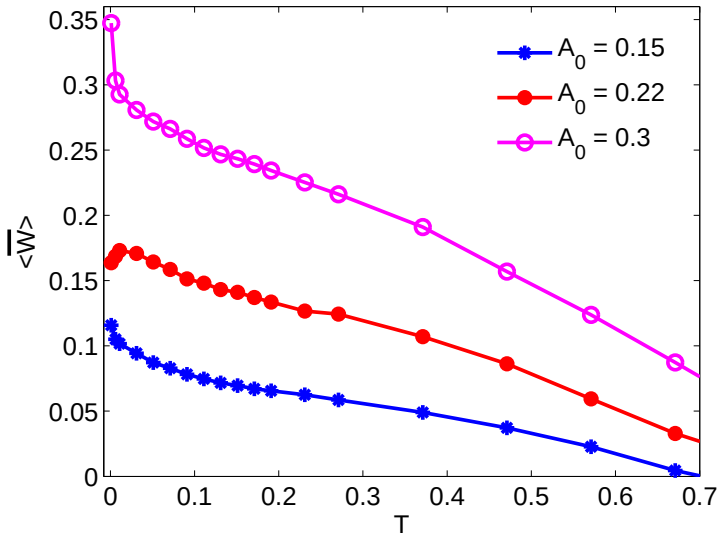

Figure 32: plot of $\langle \overline{W} \rangle$ with T in the DWDP model for $r = 0.9$ and for the values of A_0 indicated on the figure. Other parameters are $m = 1$, $U_0 = 1$, $\gamma = 0.2$ and $F_0 = 0.1$.

Fig 12(b)). We would like to point that $1-cosx$ and $1-sinx$ present a difference in phase which does not affect the dynamics of the system. So $U(x) = 1 - u_0 sin(x)$ is a particular case of the RP potential. In this section, we focus our attention on the occurrence of the phenomena of the stochastic resonance and the stochastic antiresonance (SAR) in the main objective to deduce information on microscopic properties of the system from the observed dynamics of the particles. For convenience reason we use dimensionless variables, where identical mass $m_i = m = 1$ and $u_0 = 1$. The system is initialised with the particles placed at the uniform separation and their initial velocities are null $\dot{x}_i(0) = 0$. The equations **(45)** are integrated over a time long enough of $N_1 + 1$ periods.

III.5.1 Effect of the coupling strength k

Let us first consider that the coupling is linear $\varepsilon = 0$. In order to evaluate the constructive role of noise, we plot in **Fig 33** the average input energy $\langle \overline{W}_1 \rangle$ of the first particle for various values of k and for $N = 50$. Throughout **Fig 33(a)** plotted for a frequency $\omega = 0.785$, one observes that initially the curves of $\langle \overline{W}_1 \rangle$ increase with increasing T, reach a maximum then decrease until attain a minimum and then again increase grad-

ually with T. This maximum displays a signature feature of the phenomenon of SR whereas the minimum shows the SAR phenomenon. For an other frequency $\omega = 1$ as illustrated in **Figs 33(b)** and **33(c)** SR disappears. **Fig 33(c)** is for $\varepsilon = 0.1$ indicating that even for weak non-linear coupling ε, the SR phenomenon does not occur for $\omega = 1$. The judicious choice of the frequency is thus very important for the appearance of the SR. The system is then able to oscillate coherently with subthreshold periodic input signals in a wide frequency range. We therefore seek to find values of parameters k and ε such that the system is able to oscillate coherently with sub-threshold periodic input signals in a wide frequency range. In order to achieve our goal, we choose a frequency ω ($\omega = 1$) for which there is no SR without the non-linear coupling and see how the inclusion of the non-linear coupling brings SR in the system. For that let us take $\varepsilon = 0.5$.

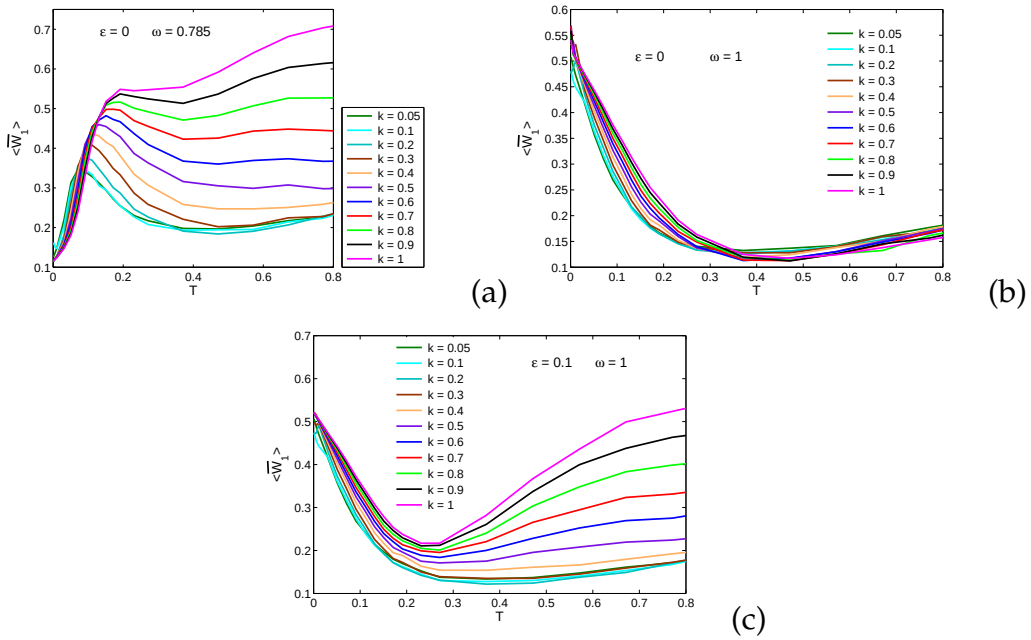

Figure 33: Variation of $\langle \overline{W}_1 \rangle$ as a function of T for various values of k from 0.05 to 1 when $\varepsilon = 0$ and $\omega = 0.785$ (a); $\varepsilon = 0$ and $\omega = 1$ (b); $\varepsilon = 0.1$ and $\omega = 1$ (c). Other parameters are $F_0 = 0.2$, $N = 50$ and $\lambda = 0.2$.

Fig 34 depicts the evolution of $\langle \overline{W}_1 \rangle$ as a function of the temperature T when $\varepsilon = 0.5$ and for different values of the parameter k. In **Fig 34(a)** plotted for $k = 0.05$, 0.1, 0.2, 0.3 and 0.31, the curves of $\langle \overline{W}_1 \rangle$ only present a minimum when T is increased for the values of $k \leq 0.3$. However, for $k = 0.31$ $\langle \overline{W}_1 \rangle$ also exhibits a maximum. Therefore

for k between 0 and 0.3 denoted by k_{SAR} the phenomenon of stochastic antiresonance only occurs. For the values of $k = 0.32$, 0.4, 0.5, 0.55, 0.59, 0.6 and 0.62 represented here on **Fig 34(b)**, first $\langle \overline{W}_1 \rangle$ curves start to decrease with increasing T, reach a minimum then increase until attain a maximum when $k \in]0.3, 0.6[$, however when $k = 0.6$ and 0.62 $\langle \overline{W}_1 \rangle$ only displays a maximum. This demonstrates that there is a range of k noted k_{SAR+SR} for which SAR and SR appear. One then notes that when k increases from the value 0.32, it is observed that SAR disappears gradually while only the SR takes place. It is also interesting to point that the phenomenon of SR gradually disappears and does not occur for a certain range of k as shown in **Fig 34(c)**. We can then more clearly notice that the average input energies of occurrence of the SAR ($\langle \overline{W}_1 \rangle_{SAR}$) as well as SR ($\langle \overline{W}_1 \rangle_{SR}$) increase whereas the temperature of occurrence of SAR ($T_{1_{SAR}}$) as well as that of the SR ($T_{1_{SR}}$) decrease as k is increased. In **Fig 34(d)** and **34(e)** are presented the hysteresis loop in the plane $(x_1 - F)$ for the temperatures $T = 0.001$ (**Fig 34(d)**), $T = 0.2$ (**Fig 34(e)**) and for several fixed values of k. The hysteresis loop size of the system increases with k, this is in agreement with the results observed in the calculations of the areas of these hysteresis loops.

For a more comprehensive description of the effect of k, we present the dependence of $\langle \overline{W}_1 \rangle$ on both T and k in **Fig 35(a)**. As one can see the increasing of k until a certain range can reduce the constructive effect of the noise. What explains the fact that there exists the values of k which destabilise systematically the occurrence of SR and SAR. This may be due to the apparition of a new phenomenon in the system for this range of k which will come to destroy the SR and SAR phenomena. We observe from **Fig 35(a)** that the position of the $\langle \overline{W}_1 \rangle$ peaks and the minima of $\langle \overline{W}_1 \rangle$ crucially depend on the parameter k. These dependences are exhibited in **Fig 35(b)** in which $T_{1_{SR}}$ and $T_{1_{SAR}}$ are displayed as a function of the parameter k. We can also observed the evolution of $\langle \overline{W}_1 \rangle_{SR}$ and $\langle \overline{W}_1 \rangle_{SAR}$ when k is increased as presented in **Fig 35(c)**. Where it is noted that the increasing of the parameter k amplifies the maximum and the minimum of $\langle \overline{W}_1 \rangle$. Furthermore, $T_{1_{SR}}$ and $T_{1_{SAR}}$ as well as $\langle \overline{W}_1 \rangle_{SR}$ and $\langle \overline{W}_1 \rangle_{SAR}$ are found to depend non-linearly on k.

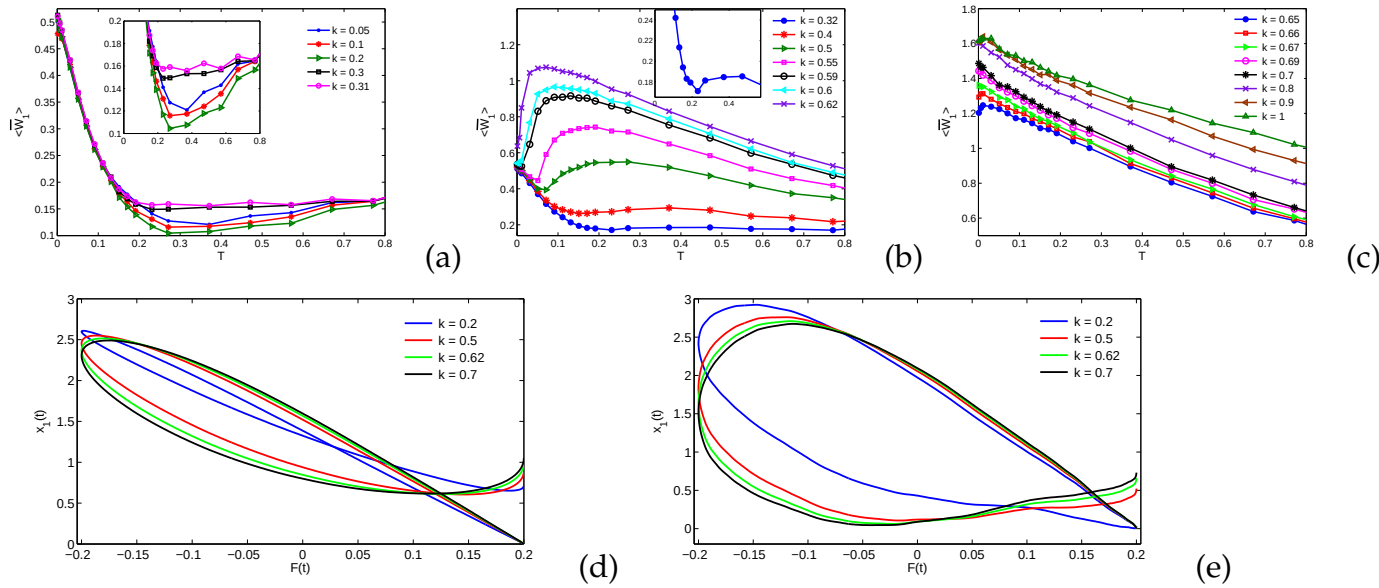

Figure 34: Variation of $\langle \overline{W}_1 \rangle$ as a function of T for several fixed values of k and for $\varepsilon = 0.5$. Hysteresis loop in the plane (x_1, F) for four values of k indicated on figure and for $T = 0.001$ (**fig 32(d)**), $T = 0.2$ (**fig 34(e)**). Other parameters are $\omega = 1$, $F_0 = 0.2$, $N = 50$ and $\lambda = 0.2$.

We numerically computed the response of the last particle denoted as $\langle \overline{W}_N \rangle$ for the particular values of k indicated in **Fig 36(a)**. In this figure $\langle \overline{W}_N \rangle$ illustrates different kind of dependence on the parameter k. We see that $\langle \overline{W}_N \rangle$ only displays SAR when $k = 0.2$ whereas for $k = 0.62$ only SR is exhibited, however for $k = 0.5$ both SR and SAR occur but for $k = 0.7$ none of the two phenomena is not occurred. For several values of k we plot in **Fig 36(b)** the temperatures $T_{N_{SR}}$ and $T_{N_{SAR}}$ then in **Fig 36(c)** $\langle \overline{W}_N \rangle_{SR}$ and $\langle \overline{W}_N \rangle_{SAR}$. Observe that $\langle \overline{W}_N \rangle_{SR}$ and $\langle \overline{W}_N \rangle_{SAR}$ behave almost the same way than $\langle \overline{W}_1 \rangle_{SR}$ and $\langle \overline{W}_1 \rangle_{SAR}$. That is not the case with the temperatures at which SR and SAR occur. To understand the general behaviour of the system, we examine the mean value $\langle \overline{W}_m \rangle$ of the average input energies of all particles as a function of T for the values of k used in **Fig 37**.

Throughout **Fig 37(a)**, one notices that for each value of the linear parameter k the phenomena of SR and SAR occur but with the amplitudes very lower than the one's obtained with the first and last particle. Point out that although SR and SAR does not occur for the first and last particle when $k = 0.7$, we notice that they occur through

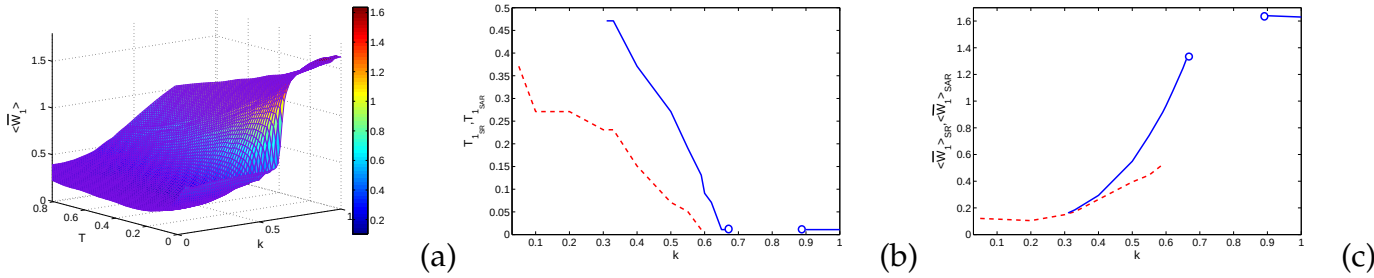

Figure 35: Dependence of $\langle \overline{W}_1 \rangle$ on the parameter k and temperature T (a), plot of the variation of $T_{1_{SR}}$ and $T_{1_{SAR}}$ as a function of k (b) and variation of $\langle \overline{W}_1 \rangle_{SR}$ and $\langle \overline{W}_1 \rangle_{SAR}$ as a function of k (c). Other parameters are $\omega = 1$, $\varepsilon = 0.5$, $F_0 = 0.2$, $N = 50$ and $\lambda = 0.2$.

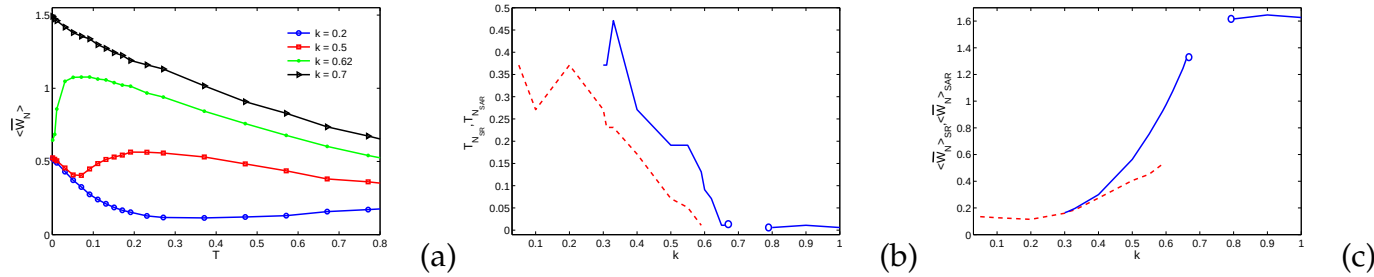

Figure 36: $\langle \overline{W}_N \rangle$ as a function of T for the values of $k = 0.2$, 0.5, 0.62 and 0.7 (a), plot of the variation of $T_{N_{SR}}$ and $T_{N_{SAR}}$ as a function of k (b) and variation of $\langle \overline{W}_N \rangle_{SR}$ and $\langle \overline{W}_N \rangle_{SAR}$ as a function of k (c). The parameters are the same as for **Fig 33**.

the system. The efficiency η which is the ratio of the dissipated power associated with the directed motion of the particles against friction, and the input power from the time-periodic forcing is investigated as in **ref** [10]. We plot in **Fig 37(b)** the variation of η as a function of the temperature T for the same values of k used in **Fig 37(a)**. As one can see, η exhibits the peaks and the minima as the case of the mean value $\langle \overline{W}_m \rangle$. We also note a similarity on the position on these peaks and these minima.

III.5.2 Effect of the chain size N

Having established the interdependence between coupling and phenomena of SR and SAR. In this section we turn our attention on the effect of the chain size for a value of $k = 0.58$ where SR and SAR phenomena are observed. In order to explore the significant influence of the number of particles N on the average input energy $\langle \overline{W}_1 \rangle$ of the first

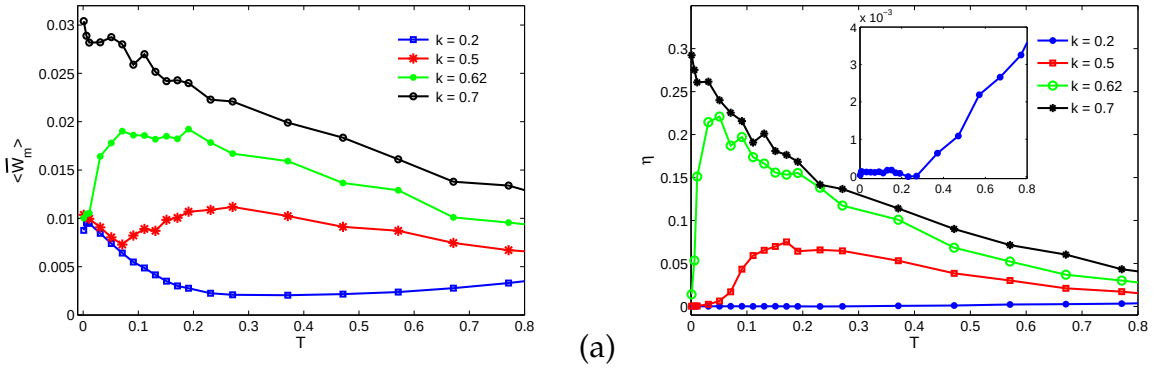

Figure 37: plot of the mean $\langle \overline{W}_m \rangle$ (a) and the efficiency η (b) as a function of T for the values of k indicated on the figure. The parameters are the same as for **Fig. 33**.

particle, one plots in **Fig 38** the variation of $\langle \overline{W}_1 \rangle$ as a function of the temperature T for several sizes of the chain. **Fig 38(a)** illustrates a typical curve for a given value of N, in each of the cases, it can be seen that there is two extrema for which $\langle \overline{W}_1 \rangle$ takes its minimum value and the other where $\langle \overline{W}_1 \rangle$ is maximal. This shows that the output of the system has a non-trivial dependence on its size. Then note that when T increases $\langle \overline{W}_1 \rangle$ exhibits a resonant and anti-resonant behavior. This demonstrates that the first particle displays the SR and SAR phenomena. For too large N, the curves of $\langle \overline{W}_1 \rangle$ are closed together. Thereby point that the depth of the minimum of $\langle \overline{W}_1 \rangle$ decreases and moves towards its value at $T = 0$ when N is increased, however the maximum of $\langle \overline{W}_1 \rangle$ increases with N until reaches the saturation. Also remark that The temperature $T_{1_{SAR}}$ at which SAR occurs, decreases very weakly when N is increased whereas $T_{1_{SR}}$ decreases more rapidly.

In order to gain a good appreciation of the effect of the number of particles N, we depict the dependence of $\langle \overline{W}_1 \rangle$ on the number of particles N and the temperature T in **Fig 38(b)**. The position of the minima and peaks of energy $\langle \overline{W}_1 \rangle$ depend of N. This dependence is shown in **Fig 39(a)** where T_{SR} and T_{SAR} are represented as a function of N. The amplitudes of these minima and these peaks also strongly depend of N as illustrated in **Fig 39(b)**.

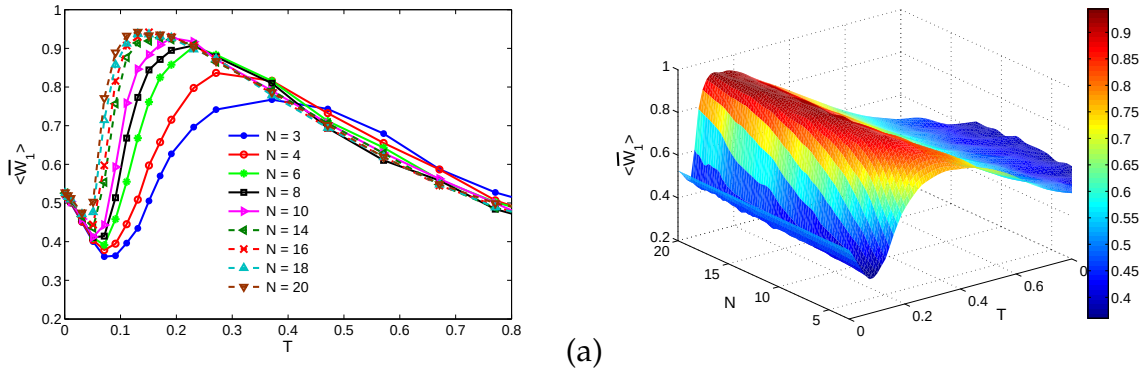

Figure 38: plot of $\langle \overline{W}_1 \rangle$ as a function of T for several values of N (a) and Dependence of $\langle \overline{W}_1 \rangle$ on the number of particle N and temperature T (b). Other parameters are $\omega = 1$, $\varepsilon = 0.5$, $F_0 = 0.2$, $k = 0.58$ and $\lambda = 0.2$.

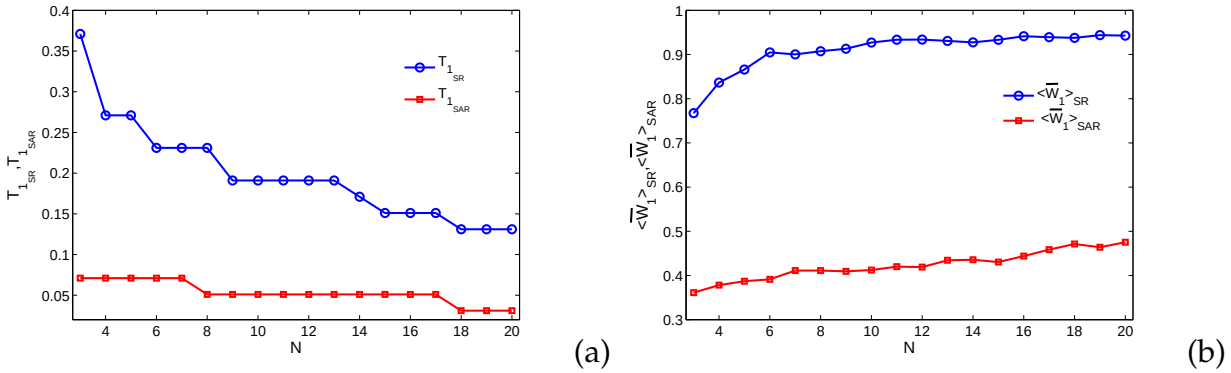

Figure 39: Variation of $T_{1_{SR}}$ and $T_{1_{SAR}}$ (a) and $\langle \overline{W}_1 \rangle_{SR}$ and $\langle \overline{W}_1 \rangle_{SAR}$ (b) as a function of N. Other parameters are $\omega = 1$, $\varepsilon = 0.5$, $F_0 = 0.2$, $k = 0.58$ and $\lambda = 0.2$.

III.6 Conclusion

In this chapter, we have presented and discussed the numerical and analytical results obtained in this work. We have clearly studied the phenomenon of SR in the models described in the previous chapter. From our results, one notes that it's very important to consider the deformable substrate in the physical studies of the systems because the shape parameter play a significant role on the dynamical systems. So, the main goal of the study was to explore the occurrence of SR phenomenon in a deformable potential. We have found that the phenomenon of SR occurs in the deformable substrate and shown that this phenomenon is strongly affected by the potential shape, chain size N as

well as coupling. Stochastic antiresonance has also been identified and analysed in our different results. The better summary of the obtained results is presented in the general conclusion.

General Conclusion

Main results

In this work, we have studied the dynamics of the particles in the deformable media which are media more realistic in order to explore the phenomenon of stochastic resonance. This phenomenon, very frequent, is nowadays the basis of many advanced technological. Our study has been made under three aspects: the case of a particle driven in the nonsinusoidal Remoissenet-Peyrard substrate potential, the case of the N-coupled particles in a sinusoidal substrate potential, and case of a particle in asymmetric and double-well deformable substrate potential. The main focus concerned the influence of the system parameters such as potential shape, coupling and chain size on stochastic resonance. In the goal to get the solutions to the problems of the thesis, first we started by giving a literature review on the concept of resonance in general and on stochastic resonance in particular in chapter I. The quantities which characterize this phenomenon and its physical definition have also been given. We have presented in chapter II, the Langevin equations of the different aspects cited above and the numerical methods that we have used to solve the open problems exhibited in chapter I. The corrugation deformable substrate potentials and the quantities of our interest such as Hysteresis loop area and input energy have clearly been presented. Chapter III was devoted to the main novel results that have been found in this thesis. These results were in general obtained from the numerical simulations.

When the particle moves in the nonsinusoidal Remoissenet-Peyrard substrate potential, the occurrence of the stochastic resonance has been shown in the system through an investigation of the hysteresis loop area. We have calculated the energy barrier and

proven that it exists a critical force F_c at which the energy barrier vanishes. We have also shown that the variation of the potential shape affects significantly and not trivially the heigh of the potential barrier as well as the occurrence of SR. So, SR is evident in some range of the shape parameter of the potential ($r > -0.6$), but cannot be observed in the other range ($r < -0.6$). For $r > -0.6$, the occurrence of the SR depends on the value of the damping coefficient γ. We have been pointed out that the position of the average input energy peaks crucially depend on the potential shape. Even the maximum of the average input energy generally decreases when the friction coefficient is increased.

In the asymmetric and double-well deformable substrate potentials study, we have first analysed the dynamics of both the systems. At lowest temperature, we have been shown that input energy depends of the initial conditions. What has allowed to find that for each of these two substrates $\overline{W}$ can be confined to two bands and only one as a function of r and $P(W)$ can have a bimodal or unimodal nature. We have found that for ASDP model, $\overline{W}$ displays two narrow bands when $r < 0.5$, and only one band when $r \geq 5$. The distribution $P(W)$ of this input energy has a bimodal distribution when $r < 0.5$ and a unimodal distribution when $r \geq 0.5$. The apparition of $P(W)$ peaks then obeys at the behavior of $\overline{W}$. However, in the case of DWDP, $\overline{W}$ clearly presents two bands for $r < 0.3$ and one band for $r > 0.3$. $P(W)$ gets a bimodal nature although $\overline{W}$ displays only one band when $r > 0.6$. Thereby, there is no longer any relationship between $P(W)$ and $\overline{W}$ in case of DWDP. After analysis, we have shown that each system presents the SR phenomenon, we have noticed the presence of a double SR in the ASDP model for each value of r excepted for $r = 0.9$. SR also occurs in the DWDP, mainly at lowest temperature. The presence of Chaos has also been investigated in DWDP, where we show that the Chaos affects the SR phenomenon. in fact Chaos can prohibit the appearance of SR in the system. We have thus proven that input energy, input energy distribution as well as SR are strongly affected by the shape potential.

For N-coupled particles in a periodic sinusoidal substrate potential, We have found that each particle displays a particular behaviour and shown the dependence of the coupling parameter as well as the system size on SR and SAR is analysed. We have

shown that the variation of the coupling parameter as well as the number of particles affect the occurrence of the SR and the SAR in the system namely the first and the last particle. Dealing first with the first particle, we have shown that for a certain frequency ω the increasing of the coupling can bring SR. Also found that there is a range of coupling parameter where only SAR is observed, where both SAR and SR occur, where only SR is observed and where neither SAR nor SR does not appear, same to the case of the last particle. However, the mean value $\langle \overline{W}_m \rangle$ of the average input energies of each particle shows typical SR and SAR but with the very weak amplitudes. One has also been shown that the increasing of the chain induces the increasing of the average input energy of the first particle and demonstrated that there exists an optimal value of the number of particles N for which the average input energy of the first particle reaches the saturation. SR can be obtained in a periodic potential even for a system of complex particles.

Open problems and future directions

Many interesting results have thus been obtained in the present thesis. However numerous points related to this developing topic remain unsolved, and then may be subject to future investigations.

- investigate the stochastic resonance in a deformable substrate potential with fractional derivative.
- In reality, the particle moves in two dimensions, this means that the particle usually takes a $2D$ trajectory instead of a straight line path. So, we could extend the study of stochastic resonance in a $2D$ deformable substrate potential.
- Study the interdependence between stochastic resonance and chaos

in a future work.

Bibliography

[1] U. Parlitz, Int. J. Bifurcat. Chaos 3 (1993) 703.

[2] U. E. Vincent, A. N. Njah, O. Akinlade, A. R. T. Solarin, Chaos 14 (2004) 1018.

[3] Z. Zhang, X. Wag, M. C. Cross, Phys. Rev. E 65 (2002) 056211.

[4] A. P. Munuzuri, V. Perez-Munuzuri, M. Gumez-Gestena, L.O. Chua L O, V. Perez-Villar, Int. J. Bifurcat. Chaos 5 (1995) 17.

[5] A. Kenfack, Chaos Solitons Fractals 5 205 (2003).

[6] J. Kozlowski, U. Parlitz, W. Lauterborn, Phys. Rev. E 51 (1995) 1861.

[7] U. E. Vincent, A. Kenfack, Phys. Scr. 77 (2008) 045005.

[8] T. Hikihara, K. Torri, Y. Ueda, Phys. Lett. A 281 (2001) 155.

[9] T. L. M. Djomo Mbong, M. Siewe Siewe, C. Tchawoua, Commun Nonlinear Sci Numer Simulat 22 (2015) 228.

[10] L. Machura, M. Kostur, P. Talkner, J. Łuczka, F. Marchesoni, P. Hänggi Phys. Rev. E 70 (2004) 061105.

[11] A. M. Fopossi Mbemmo, G. Djuidjé Kenmoé and T. C. Kofané, Physica A 496 (2018) 1.

[12] Y. J. Wadop Ngouongo, G. Djuidjé Kenmoé and T. C. Kofané, Physica A 472 (2017) 25.

[13] R. Benzi, A. Sutera, A. Vulpiani, J. Phys. A 14 (1981) 453.

[14] S. Fauve, F. Heslot, Phys. Lett. A 97 (1983) 5.

[15] B. McNamara, K. Wiesenfeld, R. Roy, Phys. Rev. Lett. 60 (1988) 2626.

[16] L. Gammaitoni, F. Marchesoni, E. Menichella-Saetta, S. Santucci, Phys. Rev. Lett. 62 (1989) 349.

[17] B. McNamara, K. Wiesenfeld, Phys. Rev. A 39 (1989) 4854.

[18] C. Presilla, F. Marchesoni, L. Gammaitoni, Phys. Rev. A 40 (1989) 2105.

[19] G. Hu, G. Nicolis, C. Nicolis, Phys. Rev. A 42 (1990) 2030.

[20] P. Jung, P. Hänggi, Europhys. Lett. 8 (1989) 505.

[21] P. Jung, P. Hänggi, Phys. Rev. A 41 (1990) 2977.

[22] P. Jung, P. Hänggi, Phys. Rev. A 44 (1991) 8032.

[23] K. Wiesenfeld, F. Moss, Nature (London) 373 (1995) 33.

[24] P. K. Ghosh, B. C. Bag, D. S. Ray, Phys. Rev. E 75 (2007) 032101.

[25] R. L. Badzey, P. Mohanty, Nature 437 (2005) 995.

[26] R. N. Mantigna, B. Spargnola, Phys. Rev. E 49 (1994) 1792

[27] I. Y. Lee, X. I. Liu, B. Kosko, C. W. Zhou, Nano Lett 3 (2003) 1683.

[28] I. Lee, X. Liu, C. Zhou, B. Kosko, IEEE Trans. Nanotechnol 5 (2006) 613.

[29] R. Wallace, D. Wallace, H. Andrews, Environ. Plan. A 29 (1997) 525.

[30] Y. Gong, B. Xu, H. Han, X. Ma, Physica A 387 (2008) 407.

[31] X. M. Mao, K. Sun, Q. Ouyang, Chin. Phys. 11 (2002) 1106.

[32] Q. Han, T. Yang, C. Zeng, H. Wang, Z. Liu, Y. Fu, C. Zhang, D. Tian, Physica A 408 (2014) 96

[33] H. Zhanga, T. Yang, Y. Xu, W. Xu, Eur. Phys. J. B 88 (2015) 125.

[34] M. I. Dykman, D. G. Luchinsky, R. Mannella, P. V. E. McClintock, N. D. Stein, N. G. Stocks, J. Stat. Phys. 70 (1993) 463.

[35] S. Saika, A. M. Jayannavar, M. C. Mahato, Phys. Rev. E 83 (2011) 061121.

[36] M. Peyrard, M. Remoissenet, Phys. Rev. B 26 (1982) 2886.

[37] M. Remoissenet, Phys. Rev. B 29 (1984) 6.

[38] G. Galileo, Galileo first introduced the notion of resonance (resonanza), in Dialogues Concerning Two New Sciences, translated by H. Crew and A. De Salvio (Dover, New York, 1954), pp 9799.

[39] N. Minorsky, Nonlinear Oscillations (Van Nostrand, New York, 1962).

[40] A. H. Nayfeh, D. T. Mook, Nonlinear Oscillations (Wiley, New York, 1979).

[41] D. W. Jordan, P. Smith, Nonlinear Ordinary Differential Equations (Oxford University Press, Oxford, 2007).

[42] S. Rajasekar, M. A. F. Sanjuan, Nonlinear Resonances, Springer Series in Synergetics (Springer, Switzerland, 2016).

[43] M. I. Dykman, D. G. Luchinsky, R. Mannella, P. V. E. McClintock, N. D. Stein, N. G. Stocks, Nuovo Cimento D 17 661 (1995).

[44] L. Y. Chew, C. Ting, C. H. Lai, Phys. Rev. E 72 (2005) 036222.

[45] I. T. Tokuda, Cheol E. Han, Kazuyuki Aihara, Mitsuo Kawato, Nicolas Schweighofer, Neur. Net. 23 (2010) 836.

[46] S. Nobukawa, H. Nishimura, T. Yamanishi, Sci. Rep 7 (2017) 1331.

[47] J. Casado-Pascual, J. Gomez-Ordonez, M. Morillo, Chaos 15 (2005) 26115.

[48] Arkady S. Pikovsky Jurgen Kurths, Phys. Rev. Lett. 78 (1997) 775.

[49] O. V. Ushakov, H. J. Wunsche, F. Henneberger, I. A. Khovanov, L. Schimansky-Geier, M. A. Zaks, Phys. Rev. Lett 95 (2005) 123903.

[50] S. Rajamani, S. Rajasekar, M. A. F. Sanjuan, Comm. Nonlin. Sc. Num. Sim. 19 (2014) 4003.

[51] P. S. Landa, P. V. E. McClintock, J. Phys. A: Math. Gen. 33 (2000) L433.

[52] Jothimurugan, K. Thamilmaran, S. Rajasekar, M. A. F. Sanjuan, Nonlin. Dyn. 83 (2016) 1803.

[53] D. R. Chialvo, Chaos 13 (2003) 1226.

[54] M. Gitterman, J. Phys. A: Math. Gen. 34 (2001) L355.

[55] I. I Blekhman, Vibrational Mechanics (World Scientic,Singapore, 2000).

[56] I. I Blekhman, P. S Landa, Intern. J. Non-Lin. Mech. 39 (2004) 421.

[57] Ruoshi Yuan, Xinan Wang, Yian Ma, Bo Yuan, Ping Ao, Phys. Rev. E 87 (2013) 062109.

[58] S. Saikia, A. M. Jayannavar, Mangal C Mahato, Phys. Rev. E 83 (2011) 061121.

[59] Jing Li, Chaos 21 (2011) 043115.

[60] A. Raj, A. Van Oudenaarden, Nature 135 (2008) 26.

[61] J. Blitzstein, J. Hwang, Introduction to probability CRC Press (2014) ISBN 9781466575592.

[62] C. D Motchenbacher, J. D. Connelly (1993) Low-noise electronic system design Wiley Interscience ISBN 0-417-57742-1

[63] C. E. Shannon, Bell Syst Tech J 27 (1948) 373.

[64] J. Von Neumann, Automata Studies 34 (1956) 43.

[65] A. Aldo Faisal, L. P. J. Selen, D. M. Wolpert, Nat Rev Neurosci 9 (2008) 292.

[66] T. Munzel, F. P. Schmidt, S. Steven, J. Herzog, A. Daiber, M. Sorensen, J. American Coll. Card 71 (2018) 688.

[67] E. Kerns, E. A. Masterson, C. L. Thermann, G. M. Calvert, American J. Ind. Med 61 (2018) 477.

[68] L. Gammaitoni, P. Hanggi, P. Jung, F. Marchesoni, Rev. Mod. Phys 70 (1998) 223.

[69] M. D. McDonnell, D. Abbott, Computational Biology 5 (2009) 5.

[70] R. Benzi, G. Parisi, A. Sutera, A. Vulpiani, Tellus 34 (1982) 10.

[71] R. Benzi, A. Sutera, G. Parisi, and A. Vulpiani, SIAM (Soc. Ind. Appl. Math.) J. Appl. Math 43 (1983) 565.

[72] C. Nicolis, Sol. Phys. 74 (1981) 473.

[73] C. Nicolis, J. Stat. Phys. 70 (1993) 3.

[74] C. Nicolis, Tellus 34 (1982) 1.

[75] C. Nicolis, G. Nicolis, Tellus 33 (1981) 225.

[76] G. Matteucci, Climate Dynamics 3 (1989) 179.

[77] G. Matteucci, Climate Dynamics 6 (1991) 67.

[78] J. Imbrie, A. C. Mix, D. G. Martinson, Nature (London) 363 (1993) 531.

[79] I. J. Winograd, T. B. Coplen, J. M. Landwehr, A. C. Riggs, K. R. Ludwig, B. J. Szabo, P. T. Kolesar, K. M. Revesz, Science 258 (1992) 225.

[80] B. Lindner and L. Schimansky, Phys. Rev. E 61 (2000) 6103.

[81] I. Gudyma, A. Maksymov, Phys. Rev. E 90 (2014) 052135.

[82] L. Gammaitoni, F. Marchesoni, S. Santucci, Phys. Rev. Lett 74 (1995) 1052.

[83] M. C. Mahato, S. R. Shenoy, Phys. Rev. E 50 (1994) 2503.

[84] R. N. Mantegna, B. Spagnolo, Phys. Rev. E 49 (1994) R1792.

[85] R. N. Mantegna, B. Spagnolo, Nuovo Cimento D 17 (1995) 873.

[86] R. N. Mantegna, B. Spagnolo, Phys. Rev. Lett. 76 (1996) 563.

[87] P. Jung, K. Wiesenfeld, Nature (London) 385 (1997) 291.

[88] L. Mandel, R. Roy, S. Singh, in Optical Bistability, edited by C. M. Bowden, M. Ciftan, and H. R. Robl (Plenum, New York), (1981) p. 127.

[89] C. Guangzhan, L. Hongjun, L. Xuefeng, N. Huang, S. Qibing, Optics Express 22 (2014) 4.

[90] A. Longtin, A. Bulsara, F. Moss, Phys. Rev. Lett 67 (1991) 656.

[91] T. Zhou, F. Moss, Phys. Rev. A 41 (1990) 4255.

[92] F. Moss, in Contemporary Problems in Statistical Physics, edited by G. H. Weiss (SIAM, Philadelphia), (1994) 205.

[93] F. Moss, D. Pierson, D. OGorman, Int. J. Bifurcation Chaos Appl. Sci. Eng 4 (1994) 1383.

[94] F. Moss, K. Wiesenfeld, Sci. Am. 273 (1995) 50.

[95] F. Moss, K. Wiesenfeld, Spektrum der Wissenschaft 273 (1995) 92.

[96] E. Sejdic, L. A. Lipsitz, "Necessity of noise in physiology and medicine", Computer Methods and Programs in Biomedicine 111 (2013) 459.

[97] O. Kaut, N. Allert, C. Coch, S. Paus, A. Grezeska, M. Minnerop, U. Wullner, NeuroRehabilitation 28 (2011) 1.

[98] S. M. Tanaka, I. Alam, E. H. Turner, FASEB Journal 3 (2002)

[99] S. M. Tanaka, J. Li, R. L. Duncan, D. B. Burr, C. H. Turner, J. B. Min. Research 16 (2001) S481.

[100] L. Wilkens, D. Russell, F. Moss, Nature 402 (1999) 291

[101] C. Blondeau, M. Planat, ed., Lecture Notes in Physics 550 (2000) 137

[102] B. D. Josephson, Rev. Mod. Phys 46 (1974) 251254.

[103] B. D. Josephson, Physics Letters 1 (1962) 251.

[104] H. Risken, The Fokker-Planck equation and methods of solution and applications, 2nd edn. (Springer, Berlin, 1989).

[105] M. B. Salamon, ed., "Physics of Superionic Conductors" (Springer, Berlin, 1979)

[106] K. Funke, in Advances in Solid State Physics, 20, J. Treusch, ed. (Vieweg, Braunschweig, 1980)

[107] A. Asaklil, Y. Boughaleb, M. Mazroui, M. Chhib, L. El Arroum, Diffusion of Brownian particles: dependence on the structure of the periodic potentials, Solid State Ionics 159 (2003) 331343.

[108] P. Fulde, L. Pietronero,W. R. Schneider, S. Strassler, Problem of Brownian motion in a periodic potential, Phys. Rev. Lett. 35 (1975) 1776.

[109] Y. S. Kivshar, M. Salerno, Phys. Rev. E 49 (1994) 3543.

[110] G. Djuidje Kenmoe, E. Djiha Tchaptchet, T. C. Kofané, Tibol Lett 55 (2014) 533.

[111] Y. Dong, D. Perez, H. Gao, A. Martini, J. Phys: Condens. Matter 24 (2012) 265001.

[112] M. Remoissenet, Wave solitons, concepts and experiments (Springer-Verlag, Berlin, 1994).

[113] S. Watanabe, H. Zant, S. Strogatz, T. Orlando, Physica D 97 (1996) 429.

[114] I. Markov, A. Trayamov, J. Phys. C 21 (1988) 2475.

[115] S. Takeno, S. Homma, J. Phys. Soc. Jpn 59 (1990) 1890.

[116] J. Cuevas-Maraver, B. A. Malomed, P. G. Kevrekidis, Symmetry 8 doi:10.3390/sym8060039 (2016) 39.

[117] S. Takeno, S. Homma, J. Phys. Soc. Jpn 55 (1986) 65.

[118] S. Takeno, S. Homma, J. Phys Soc. Jpn 55 (1986) 2547.

[119] S. Takeno, S. Homma, J. Phys. Soc. Jpn 56 (1986) 3480.

[120] S. Takeno, S. Homma, J. Phys. Soc. Jpn 60 (1991) 1931.

[121] S. Takeno, S. Homma, Prog. Theor. Phys 70 (1983) 308.

[122] S. Ryu, W. Yu, D. Stroud, Phys Rev E 53 (1996) 2190.

[123] N. Kasdin, J. Guid. Control Dyn. 18 (1995) 114.

[124] J.C Breton. Cours Processus Gaussiens. Universit de La Rochelle, M2 (2006). https://perso.univ-rennes1.fr/jean-christophe.breton/Fichiers/gauss M2.pdf

[125] K. Sekimoto, J. Phys. Soc. Jpn. 66 (1997) 1234.

[126] W. L. Reenbohn, S. S. Pohlong, Mangal C. Mahato, Phys. Rev. E 85 (2012) 031144.

[127] W. L. Reenbohn, Mangal C. Mahato, Phys. Rev. E 88 (2013) 032143.

List of Publications

1- G. Djuidjé Kenmoé, Y. J. Wadop Ngouongo and T. C. Kofané, *"Effect of the potential shape on the stochastic resonance processes"*, J. stat. Phys **161** (2015) 475.

2- Y. J. Wadop Ngouongo, G. Djuidjé Kenmoé and T. C. Kofané, *"Effect of coupling on stochastic resonance and stochastic antiresonance processes in a unidirectionally N-coupled systems in periodic sinusoidal potential"*, Physica A **472** (2017) 25.

3- Y. J. Wadop Ngouongo, G. Djuidjé Kenmoé and T. C. Kofané. *"Dynamics of a particle periodically driven in the deformable potentials: stochastic resonance"*, Physica A **527** (2019) 121321.

Other publications

4- Y. J. Wadop Ngouongo, M. Djolieu Funaye, G. Djuidjé Kenmoé and T. C. Kofané, *"Stochastic resonance in deformable potential with time-delayed feedback"*, Phil. Trans. R. Soc. A **379** (2020) 20200234.

5- A. F. Moyo Tala, Y. J. Wadop Ngouongo, G. Djuidjé Kenmoé and T. C.

Kofané. *"Ghost stochastic resonance in asymmetric Duffing oscillator"*, Physica A **582** (2021) 126247.

J Stat Phys
DOI 10.1007/s10955-015-1333-7

Effect of the Potential Shape on the Stochastic Resonance Processes

G. Djuidjé Kenmoé[1,2] · **Y. J. Wadop Ngouongo**[1] · **T. C. Kofané**[1,2]

Received: 13 January 2015 / Accepted: 17 July 2015

Abstract The stochastic resonance (SR) induced by periodic signal and white noises in a periodic nonsinusoidal potential is investigated. This phenomenon is studied as a function of the friction coefficient as well as the shape of the potential. It is done through an investigation of the hysteresis loop area which is equivalent to the input energy lost by the system to the environment per period of the external force. SR is evident in some range of the shape parameter of the potential, but cannot be observed in the other range. Specially, variation of the shape potential affects significantly and not trivially the heigh of the potential barrier in the Kramers rate as well as the occurrence of SR. The finding results show crucial dependence of the temperature of occurrence of SR on the shape of the potential. It is noted that the maximum of the input energy generally decreases when the friction coefficient is increased.

Keywords Stochastic resonance · Hysteresis loop area · Noise · Nonsinusoidal periodic potential

1 Introduction

A particle trapped in a potential well constitutes a model useful for understanding of variety of phenomena. It has been established that the presence of noise source in nonlinear dynamical systems can induce completely new regimes that cannot be realized without noise [1,2].

✉ G. Djuidjé Kenmoé
kdjuidje@yahoo.fr

Y. J. Wadop Ngouongo
yannickwadop@yahoo.fr

T. C. Kofané
tckofane@yahoo.com

[1] Department of Physics, Laboratory of Mechanics, Faculty of Science, University of Yaoundé 1, P. O. Box 812, Yaoundé, Cameroon

[2] Centre d'Excellence en Technologies de l'Information et de la Communication (CETIC), University of Yaoundé 1, Yaoundé, Cameroon

Published online: 24 July 2015

Stochastic resonance (SR) is one of the most shining and relatively simple examples of this type of nontrivial behavior of nonlinear systems under the influence of noise. When a system exhibits the phenomenon of SR, the response of the system to a periodic drive input signal shows a resonant dependence on the noise level. SR has been extensively studied theoretically and experimentally around different power system due to its vast applications in many fields. The interest of the SR problem comes from the large range of physical applications that related to it. One can denote, for example, the electronic circuits [3], two-mode ring lasers [4], nanomechanical systems [5], and neuronal systems [6]. Biological systems use SR to their advantage [7] in the fact that the observations of random noise or background fluctuations may be evidence of a source of biological randomness that could potentially be exploited for a functional benefit [8]. This phenomenon has been demonstrated in various systems such as systems with a single potential well [9], bistable systems [10] and more recently in periodic sinusoidal systems [11]. Considerable progress has been made in recent years in understanding SR in periodic potential, but only potential with constant shape such as sinusoidal potential has been used. In some earlier works it has been shown numerically by Reenbohn and co-workers [12,13] that SR indeed occurs in underdamped periodic potential at higher external frequencies. They have studied the energy absorbed by the particle per period of the external field termed as the input energy, which present like an appropriate quantifier of SR [14]. A recent work has been also done by Saikia et al. [15], they considered two model systems for study. In one case, the medium is considered to have uniform friction, whereas in the other case, the friction is considered to be nonuniform. Introduction of a deformable potential in the study of SR is therefore indispensable to observe the effect of the potential shape. However, the occurrence of SR in periodic nonsinusoidal potential has not yet been studied.

In the present work, we use a periodic but nonsinusoidal potential to observe the occurrence of the phenomenon of SR. We consider a variable nonsinusoidal periodic potential introduced some years ago in the context of the solitons [16], recently in the context of bose-Einstein condensate [17] and in nanotribology [18,19]. This potential allows us to consider a variety of the potential shapes. The paper is organized as follows: In Sect. 2, we introduce the model, describe the potential and the evolution of the energy barrier. The observable used as indicator of SR is also presented. In Sect. 3, the results of the numerical simulations are discussed and finally in the last section we conclude the work.

2 Model and Theoretical Approach

Consider the underdamped motion of a particle of mass m in a periodic nonsinusoidal potential and in a medium with friction coefficient γ. This particle is subjected to an external periodic force $F(t) = F_0 + \Delta F cos\omega t$. Taking into account the influence of the noise the dynamics of the particle can be described by the Langevin equation

$$m\frac{d^2x}{dt^2} = -\gamma\frac{dx}{dt} - \frac{\partial V\,(x,r,t)}{\partial x} + \xi\,(t)\,. \tag{1}$$

where

$$V\,(x,r,t) = U_{RP}\,(x,r) - xF\,(t) \tag{2}$$

is the effective potential of the system. In contrast to the simple sinusoidal potential, here we deal with a periodic nonsinusoidal potential namely Remoissenet–Peyrard (RP) potential given by [20]:

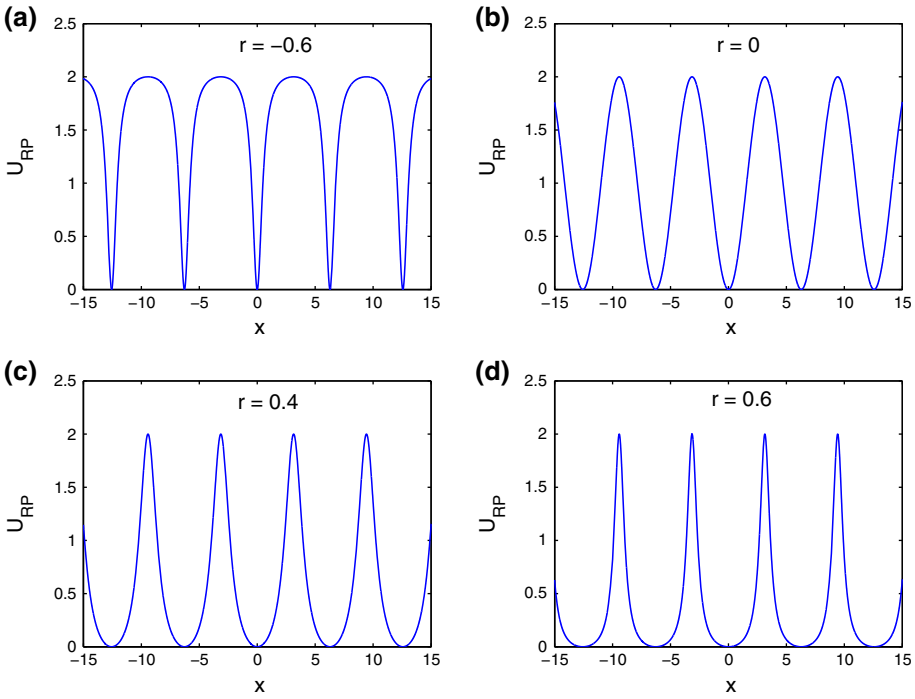

Fig. 1 Illustration of the corrugation potential $U_{RP}(x, r)$ for the values of shape parameter $r = -0.6$ (**a**), $r = 0$ (**b**), $r = 0.4$ (**c**) and $r = 0.6$ (**d**), with $U_0 = 1$. The shape potential depends on the parameter r. When $r = 0$, we have a sinusoidal profile of the potential

$$U_{RP}\,(x, r) = U_0\,(1 - r)^2\,\frac{1 - \cos x}{\left(1 + r^2 + 2r\cos x\right)}. \tag{3}$$

This potential is symmetric and 2π-periodic in x, the shape of the potential is defined by the parameter r with $-1 < r < 1$. U_0 is a constant which measures the amplitude of the potential. The illustration of corrugation potential is given in Fig. 1. When $r > 0$ the nonsinusoidal RP potential has flat bottoms separated by thin barriers (see Fig. 1d for $r = 0.6$), while for $r < 0$, it has the shape of sharp wells separated by flat wide barriers (see Fig. 1a for $r = -0.6$). The common tilted sinusoidal potential used by Reenbohn et al. [12,13] can be deduced from Eq. (3) trough a continuous deformation when the parameter r goes to zero (see Fig. 1b). We would like to mention that $1 - cosx$ and $sinx$ present a difference in phase which does not affect the dynamics of the system. The random fluctuations in the system are represented by $\xi(t)$ which satisfy the statistics: $\langle\xi(t)\rangle = 0$ and $\langle\xi(t)\xi(t')\rangle = 2\gamma T\delta(t - t')$ where the medium temperature T is in units of the Boltzmann constant k_B. Equation (1) may model several physical processes such as the dynamics of a nonlinear mechanical oscillator in deformable substrate. In the following, we use $m = 1$, $U_0 = 1$, $\Delta F = 0.2$, $F_0 = 0.1$ and $\tau = 8$.

The solution for local minimum where the particle resides x_a and the transition point x_b can be determined from $\frac{\partial V}{\partial x} = 0$. Other variables can be obtained from these positions such as the energy barrier ΔV, the frequencies ω_a and ω_b which represent the frequency of the system in the potential minimum x_a and at the top of the barrier located at x_b, respectively. The barrier between any two consecutive wells of the effective potential V disappears ($\Delta V = 0$) when the magnitude of the external field exceeds the critical force F_c. At that time switchings

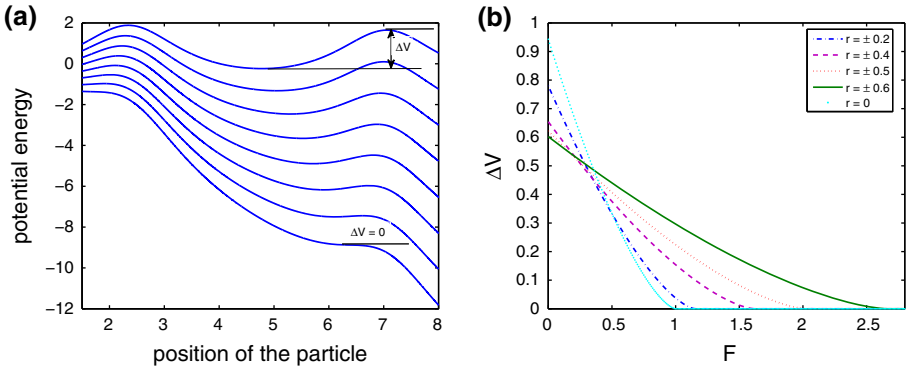

Fig. 2 Schematic illustration of the evolution of the effective potential, showing the decreasing of the energy barrier. From *top to bottom* each curve corresponds to a change in F of 0.22 step starting from 0.05, for $r = 0.2$ (**a**) and illustration of the energy barrier as a function of the external force F, for several potential shapes (**b**)

between the potential wells are possible. A critical point x_c where the barrier vanishes and the critical force F_c can be obtained by solving equations $\frac{\partial V}{\partial x} = 0$ and $\frac{\partial^2 V}{\partial x^2} = 0$. After a few mathematical calculations, the critical force can be deduced as:

$$F_c = \frac{U_0 \left(1 - r^2\right)^2 \sin x_c}{\left(1 + r^2 + 2r \cos x_c\right)^2}, \tag{4}$$

with, $x_c = \pm \arccos\left(\frac{1+r^2-\sqrt{r^4+34r^2+1}}{4r}\right)$ is the instability point.

Figure 2a illustrates the evolution of the effective potential V as a function of the positions x for $U_0 = 1$. Here, the potentials clearly show the presence of an initial minimum (stable particle position) and an initial maximum (unstable particle position). When one take the initial value of external force F from 0.05 to critical force $F_c = 1.15$ corresponding to the shape potential $r = 0.2$, we can see that the energy barrier ΔV decreases and finally vanishes as F equals to F_c.

Assuming that when x_a and x_b converge to critical point (x_c, F_c) the switching event occur around the critical point (x_c, F_c), so $V_{xx}(x_b, F)$ and $V_{xx}(x_a, F)$ can be obtained by Taylor expansion around the critical point,

$$V_{xx}\left(x_b, F\right) = V_{xx}\left(x_c, F_c\right) + V_{xxx}\left(x_b - x_c\right) + V_{xxF}\left(F - F_c\right) + 0\left(\delta x^2\right). \tag{5}$$

However, $V_{xx}\left(x_c, F_c\right) = 0$ and $V_{xxF} = 0$ thus,

$$V_{xx}\left(x_b, F\right) = \left(U_{RP}\right)_{xxx}\left(x_b - x_c\right), \tag{6}$$

here $_{xx}$ indicates the second derivative with respect to x and $V_{xxx} = (U_{RP})_{xxx}$. The energy barrier is defined as,

$$\Delta V = V(x_b, F) - V(x_a, F), \tag{7}$$

therefore for the determination of ΔV, it is important to make a Taylor expansion around (x_c, F_c) as illustrated by Dong et al. [21]:

$$V\left(x, F\right) = V\left(x_c, F_c\right) + \frac{\partial V}{\partial x}\left(x - x_c\right) + \frac{\partial V}{\partial F}\left(F - F_c\right) + \frac{\partial^2 V}{\partial x \partial F}\left(x - x_c\right)\left(F - F_c\right)$$

$$+\frac{1}{2}\frac{\partial^2 V}{\partial x^2}(x-x_c)^2+\frac{1}{2}\frac{\partial^2 V}{\partial F^2}(F-F_c)^2+\frac{1}{2}\frac{\partial^3 V}{\partial x^2 \partial F}(x-x_c)^2(F-F_c)$$
$$+\frac{1}{2}\frac{\partial^3 V}{\partial x \partial F^2}(x-x_c)(F-F_c)^2+\frac{1}{6}\frac{\partial^3 V}{\partial x^3}(x-x_c)^3+\frac{1}{6}\frac{\partial^3 V}{\partial F^3}(F-F_c)^3$$
$$+0\left(\delta x^4\right). \tag{8}$$

At the critical point (x_c, F_c), $V_x = V_{xx} = V_{FF} = V_{xF} = V_{xFF} = V_{FFF} = 0$, thus:

$$V(x_b, F) = V(x_c, F_c) + \frac{\partial V}{\partial F}(F-F_c) + \frac{1}{6}\frac{\partial^3 V}{\partial x^3}(x_b - x_c)^3 \tag{9}$$

and

$$V(x_a, F) = V(x_c, F_c) + \frac{\partial V}{\partial F}(F-F_c) + \frac{1}{6}\frac{\partial^3 V}{\partial x^3}(x_a - x_c)^3. \tag{10}$$

By substituting (9) and (10) into (7), the expression of the energy barrier is given as follows

$$\Delta V = \frac{1}{6}(U_{RP})_{xxx}\left[(x_b - x_c)^3 - (x_a - x_c)^3\right], \tag{11}$$

From (8), since $\dfrac{\partial V(x,F)}{\partial x} = 0$ the relationship between $(F_c - F)$ and $(x_c - x)$ is given by

$$F_c - F = -\frac{1}{2}(U_{RP})_{xxx}(x - x_c)^2. \tag{12}$$

For a given F, where $F < F_c$, x_a is smaller than x_c and x_b is larger than x_c. Thus, we have two relations:

$$x_b - x_c = \sqrt{\frac{2}{-(U_{RP})_{xxx}}}(F_c - F)^{\frac{1}{2}}, \tag{13}$$

and

$$x_a - x_c = -\sqrt{\frac{2}{-(U_{RP})_{xxx}}}(F_c - F)^{\frac{1}{2}}. \tag{14}$$

The energy barrier becomes

$$\Delta V = \frac{2\sqrt{2}}{3}\left(-(U_{RP})_{xxx}\right)^{-\frac{1}{2}}(F_c - F)^{\frac{3}{2}}. \tag{15}$$

Figure 2b shows the evolution of the energy barrier obtained analytically as a function of external force F taken over a large range for several values of shape potential r. For each value of shape potential, we have the critical force F_c given by Eq. (4), thus for $r = \pm 0.2$; $F_c = 1.15$, $r = \pm 0.4$; $F_c = 1.62$, $r = \pm 0.5$; $F_c = 2.02$ and $r = \pm 0.6$; $F_c = 2.65$. One can observe a decreasing of the energy barrier with increasing external force until it vanishes when F is equal to F_c.

Let us consider the amplitude of the periodic force $F(t)$ to be small in the sense that switchings between the potential wells are impossible in the absence of noise $(F(t) < F_c)$ at all time. The fluctuational force $\xi(t)$ causes transitions between neighboring potential wells with a rate given by the Kramers rate,

$$r_K = \frac{\omega_a \omega_b}{2\pi\gamma}\exp\left(-\frac{\Delta V}{T}\right), \tag{16}$$

where ΔV is the heigh of the potential barrier separating two consecutive minima given by (15) and T is the temperature in unit of the Boltzmann constant. Without external force the probability density of switching coincide with the Kramers rate which can permit to have the mean switchings time for potential wells to each potential shape.

Several key quantities in the literature are used to quantify SR such as the spectral power amplitude (SPA) [22], the signal-to-noise ratio (SNR) [23], the residence-time distribution density of a particle in one of the potential wells [24] and the hysteresis loop area (HLA) [25]. HLA is equivalent to the input energy lost by the system to the environment per period of the external force $F(t)$. It is considered as an appropriate measure of SR in an underdamped sinusoidal potential system [26]. As the system is underdamped, the energy is continually dissipated to the environment to which the system is in contact at given temperature. The required energy is supplied by the external field. The energy absorbed by the particle per period of the external field is termed as input energy. This input energy is used as the index of SR, which is defined in a period of the external force as follows [27]:

$$W\left(t_0, t_0+\tau\right)=\int_{t_0}^{t_0+\tau} \frac{\partial V\left(x(t), r, t\right)}{\partial t} dt. \tag{17}$$

The first partial derivative with respect to time t of the effective potential of the system (Eq. 2) gives $\frac{\partial V}{\partial t}=-x\frac{\partial F}{\partial t}$. In addition $dF=\frac{\partial F}{\partial t}dt$ and Eq. (17) can therefore become

$$W\left(t_0, t_0+\tau\right)=-\int_{F(t_0)}^{F(t_0+\tau)} x dF \tag{18}$$

One can then define the expression,

$$W\left(t_0, t_0+\tau\right)=-\oint x dF=A, \tag{19}$$

where A is the magnitude of the HLA. Equation (18) becomes simply,

$$W\left(t_0, t_0+\tau\right)=\int_{t_0}^{t_0+\tau} x\left(t\right) \omega \Delta F \sin\left(\omega t\right) dt. \tag{20}$$

The average input energy per period, $\overline{W}$, averaged over an entire trajectory is

$$\overline{W}=\frac{1}{N_1}\sum_{n=0}^{n=N_1} W\left(n\tau, (n+1)\tau\right)=\overline{A}. \tag{21}$$

Using (20), Eq. (21) becomes

$$\overline{W}=\frac{1}{N_1}\left(\int_0^{\tau} x\left(t\right) \omega \Delta F \sin\left(\omega t\right) dt+\cdots+\int_{N_1\tau}^{(N_1+1)\tau} x\left(t\right) \omega \Delta F \sin\left(\omega t\right) dt\right). \tag{22}$$

Therefore,

$$\overline{W}=\frac{1}{N_1}\int_0^{(N_1+1)\tau} x\left(t\right) \omega \Delta F \sin\left(\omega t\right) dt, \tag{23}$$

here N_1 represent the number of periods of $F(t)$ and has taken equal to 10^5 in all the simulation.

Since $x(t)$ is a stochastic variable it is unreasonable to expect a sensible hysteresis loop over a period of the field. Moreover, when averaged over the entire duration of a trajectory, a well defined hysteresis loop $\bar{x}(F(t_i))$ and its area is obtained:

$$\bar{x}\left(F\left(t_i\right)\right) = \frac{1}{N_1} \sum_{n=0}^{n=N_1} x\left(F\left(n\tau + t_i\right)\right), \tag{24}$$

for all $[0 \leq t_i < \tau]$.

At the lowest temperature $\overline{W}$ depends very strongly on the initial conditions $(x(0), v(0))$. However it is always sensible to ensemble average $\overline{W}$ over all possible initial conditions and obtain the average input energy per period $\langle \overline{W} \rangle$.

3 Numerical Results

In order to understand the dynamical processes of the present system, Eq. (1) has been integrated numerically with fourth-order Runge–Kutta algorithm for stochastic processes developed by Kasdin [28]. Initial velocity $\dot{x}(0) = 0$ for all cases and the initial positions $x(0)$ are chosen at 99 equispaced points x_i, $i = 1, 2, ..., 99$, between 0 and 2π. The drive (signal) frequency $\omega = \frac{2\pi}{\tau}$ $(\tau = 8)$ is chosen to be close to the natural frequency at the bottom of the wells of the potential. We focus our attention on the phenomenon of SR. System can achieve SR by modulating system parameters m, U_0, ΔF, γ, F_0, and r. It is assumed that the signal amplitude of the external force is small enough that, in the absence of any fluctuation force, it is insufficient to force a particle to move one well to another.

The set of numerical results for several shape of the potential, which describes SR is depicted in Fig. 3. These figures illustrate the variation of the average input energy $\langle \overline{W} \rangle$ as a function of temperature for the values of $\gamma = 0.2$, $\gamma = 0.3$, $\gamma = 0.5$ and for six shapes of the potential namely, $r = -0.4$ (Fig. 3a), $r = -0.2$ (Fig. 3b), $r = 0$ (Fig. 3c), $r = 0.2$ (Fig. 3d), $r = 0.4$ (Fig. 3e) and $r = 0.6$ (Fig. 3f). These curves increase until reaching a maximum and decrease gradually as the temperature increases, thus showing a signature feature of SR. For these three values of γ each curve displays typical maximum average of the input energy. We note that for all these values of r the phenomenon of stochastic resonance is exhibited through the peaks. We observe from Fig. 3a that the peaks of resonance are less defined and the maximum value of the average input energy $\langle \overline{W} \rangle_{max}$ increases as γ increases. We can also see that the same value of the average input energy is reached at lower temperature despite the difference value of the damping coefficient γ. The temperature T_{SR} of occurrence of stochastic resonance also increases with γ. The same behavior is observed in Fig. 3b with the shape potential $r = -0.2$, but in this case the peaks of resonance are well defined. When the shape parameter r increases, the peaks become more pronounced and quite broad as reflected by Fig. 3c, d for $r = 0$ and $r = 0.2$. We notice that temperature T_{SR} increases with γ like the case of $r = -0.4$ but contrary on Fig. 3a, the maximum of the average input energy $\langle \overline{W} \rangle_{max}$ decreases rapidly when γ increases. Let us specify that, when the temperature T is too small $(T << T_{SR})$, the switching events become very rare; thus the interwell transitions are hardly visible. However, beyond T_{SR}, the interwell dynamics become more frequent. Single maxima are reached at different value of the temperature. There is, however, a remarkable difference between the nature of motion of the particle at the temperature T_{SR} of maximum of the average input energy $\langle \overline{W} \rangle_{max}$ for different values of the shape parameter r.

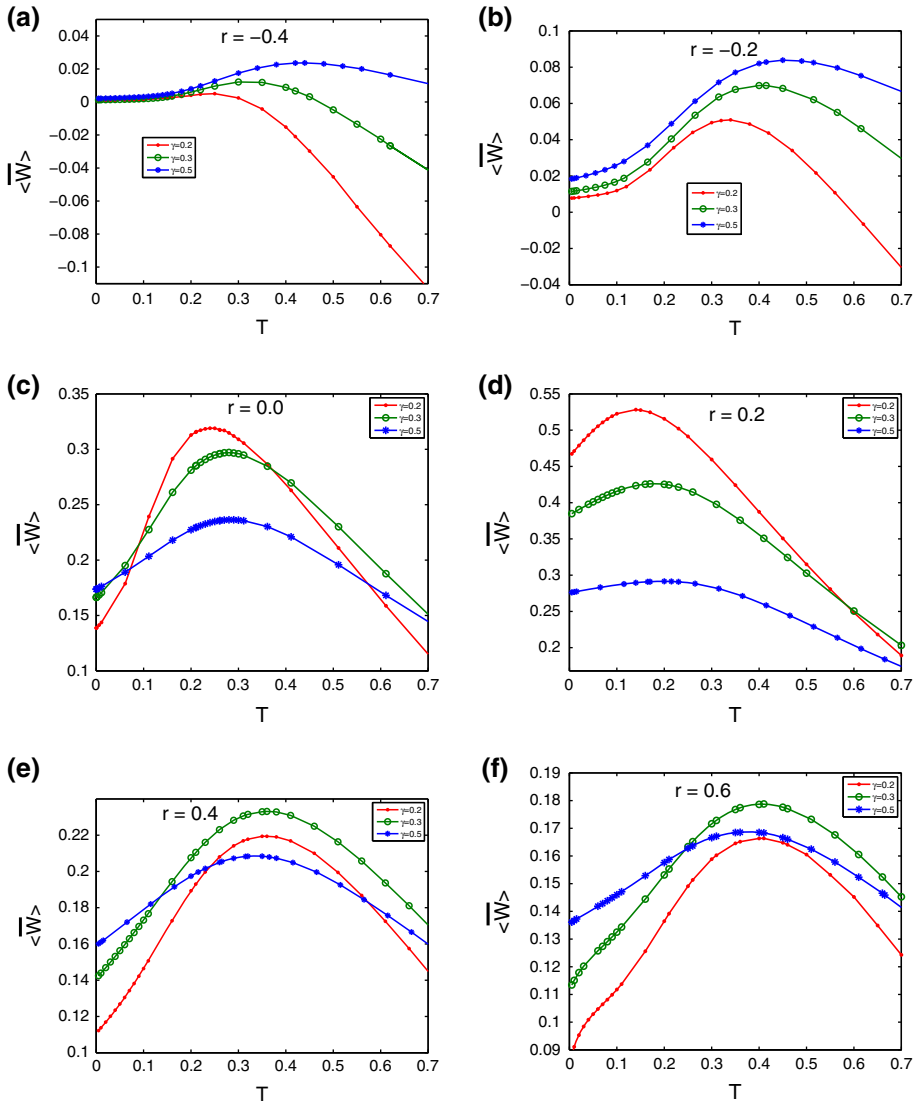

Fig. 3 Plot of $\langle \overline{W} \rangle$ as a function of T, for values of $\gamma = 0.2$, $\gamma = 0.3$ and $\gamma = 0.5$ for $r = -0.4$ (**a**), $r = -0.2$ (**b**), $r = 0$ (**c**), $r = 0.2$ (**d**), $r = 0.4$ (**e**), and $r = 0.6$ (**f**). Other parameters are $m = 1$, $U_0 = 1$, $\Delta F = 0.2$ and $F_0 = 0.1$

In order to gain a good appreciation of the effect of the shape parameter and the friction coefficient, other calculations are done for a large range of parameters γ and r. The effect of the different shape potential on the SR as well as of the damping coefficient is depicted in Fig. 4. Therefore, by giving a value of the shape parameter r, there is a range of the parameter γ where the phenomenon of SR does not occur. For low values of the shape parameter r ($r < -0.6$), SR does not occur for all parameter γ. This may be due to the suitable choice of the other parameters of the system m, U_0, ΔF, F_0 and in particular to the judicious choice of the period τ of the external periodic force. The position of the input

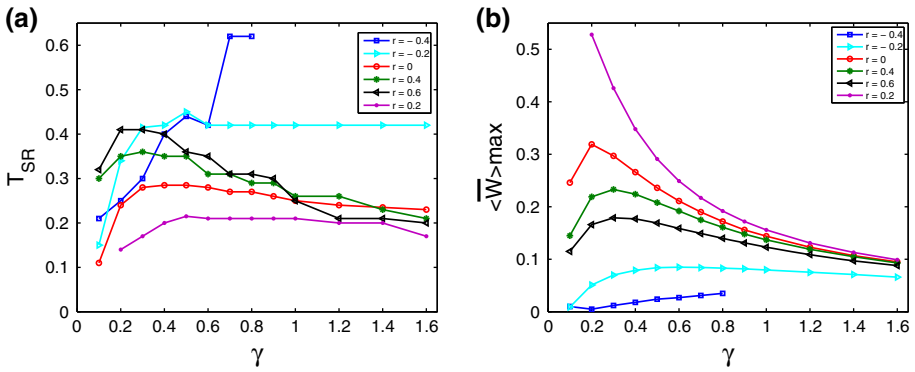

Fig. 4 Plot of the variation of T_{SR} as a function of γ (**a**) and the variation of $\langle\overline{W}\rangle_{max}$ as a function of γ (**b**)

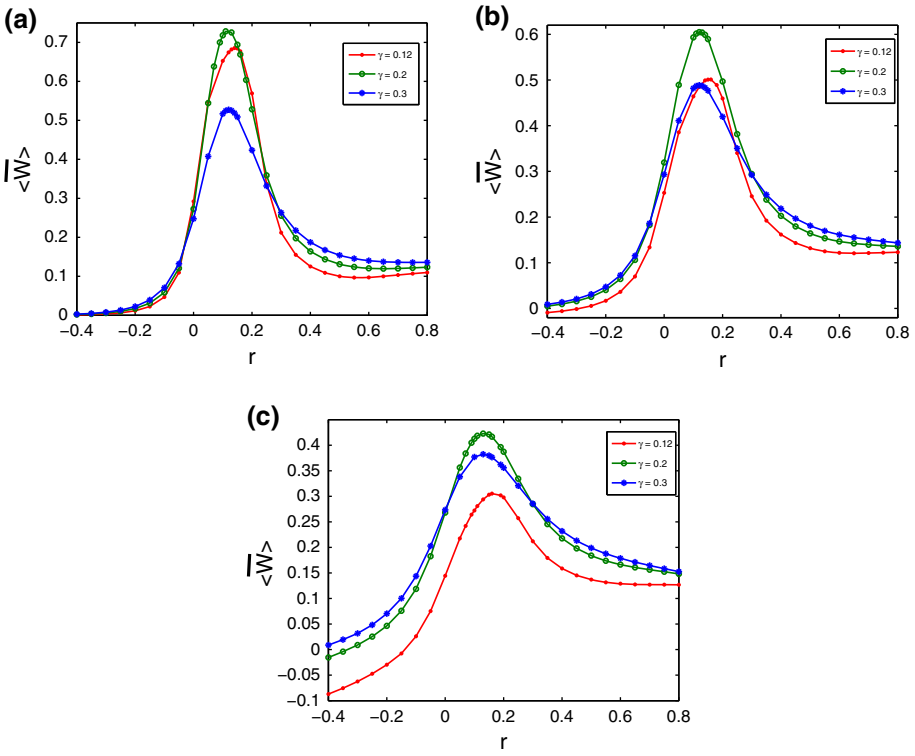

Fig. 5 Plot of the variation of $\langle\overline{W}\rangle$ as a function of shape potential r for $T = 0.14$ (**a**), $T = 0.24$ (**b**) and $T = 0.4$ (**c**). Other parameters are $m = 1$, $U_0 = 1$, $\Delta F = 0.2$ and $F_0 = 0.1$

energy $\langle\overline{W}\rangle$ peaks is also dependent on the parameter r as well as on the parameter γ. This dependence is shown in Fig. 4a where the T_{SR} is represented as a function of the parameter γ for several shape parameters. As one can see from Fig. 4b, when γ is high the value of $\langle\overline{W}\rangle_{max}$ converges towards 0.1. It is also noted from Fig. 4b the reduced of SR peak when the parameter γ increases, however for small value of γ, one can also notice a small increasing

of SR peak when γ is less than 0.2 in certain range of the parameter r. A high value of $\langle \overline{W} \rangle_{max}$ is obtained for low values of γ and when r goes to 0.2.

For further investigation, the average input energy $\langle \overline{W} \rangle$ as a function of the shape parameter r is simulated using some resonance temperature T_{SR}. This shows more clearly the effects on the input energy by varying the shape of the potential. Figure 5 shows that the highest value of the input energy can be obtained for $r = 0.11$ with $\gamma = 0.2$. One can see that the input energy shows a maximum as a function of the shape potential r, these maxima are obtained around $r = 0.13$. It is very clear from Fig. 5 that the average of the input energy $\langle \overline{W} \rangle$ for the parameter $\gamma = 0.2$ is generally higher than the other values of the parameter γ. When the shape parameter r is lower than -0.2 ($r < -0.2$) or higher than 0.4 ($r > 0.4$), the values of the input energy $\langle \overline{W} \rangle$ are generally closed together.

4 Conclusion

We have studied SR over a wide class of periodic nonsinusoidal systems. The analytical prediction of the energy barrier as a function of the shape potential was shown. The variation of the shape of the potential affect the occurrence of the SR of the system. There is a range of shape potential where SR does not occur, in particular where $r < -0.6$. For $r > -0.6$, the occurrence of the SR depends on the value of the damping coefficient γ. It is important to point out that the position of the input energy peaks depend crucially on the shape of the potential. Our results indicate that the deformed version of this model can provide some degree of physical understanding of the SR.

References

1. Gammaitoni, L., Hanggi, P., Jung, P., Marchesoni, F.: Stochastic resonance. Rev. Mod. Phys. **70**, 223–287 (1998)
2. Benzi, R., Parisi, G., Sutera, A., Vulpiani, A.: Stochastic resonance in climatic change. Tellus **34**, 10–16 (1982)
3. Fauve, S., Heslot, F.: Stochastic resonance in a bistable system. Phys. Lett. A **97**, 5–7 (1983)
4. McNamara, B., Wiesenfeld, K., Roy, R.: Observation of stochastic resonance in a ring laser. Phys. Rev. Lett. **60**, 2626–2629 (1988)
5. Badzey, R.L., Mohanty, P.: Coherent signal amplification in bistable nanomechanical oscillators by stochastic resonance. Nature **437**, 995 (2005)
6. Longtin, A.: Stochastic resonance in neuron models. J. Stat. Phys. **70**, 309–327 (1993)
7. Wiesenfeld, K., Moss, F.: Stochastic resonance and the benefits of noise: from ice ages to crayfish and SQUIDS. Nature (London) **373**, 33–36 (1995)
8. Ghosh, P.K., Bag, B.C., Ray, D.S.: Interference of stochastic resonances: splitting of Kramer's rate. Phys. Rev. E **75**, 032101 (2007)
9. Stocks, N.G., McClintock, P.V.E., Soskin, S.M.: Observation of zero-dispersion peaks in the fluctuation spectrum of an underdamped single-well oscillator. Europhys. Lett. **21**, 395 (1993)
10. McNamara, B., Wiesenfeld, K.: Theory of stochastic resonance. Phys. Rev. A **39**, 4854–4869 (1989)
11. Dykman, M.I., Luchinsky, D.G., Mannella, R., McClintock, P.V.E., Stein, N.D., Stocks, N.G.: Stochastic resonance: linear response theory and giant nonlinearity. J. Stat. Phys. **70**, 463–478 (1993)
12. Reenbohn, W.L., Pohlong, S.S., Mahato, M.C.: Periodically driven underdamped periodic and washboard potential systems: dynamical states and stochastic resonance. Phys. Rev. E **85**, 031144 (2012)
13. Reenbohn, W.L., Mahato, M.C.: Relative stability of dynamical states and stochastic resonance in a sinusoidal potential. Phys. Rev. E **88**, 032143 (2013)
14. Saikia, S., Roy, R., Jayannavar, A.M.: Work fluctuations and stochastic resonance. Phys. Let. A **369**, 367–371 (2007)
15. Saika, S., Jayannavar, A.M., Mahato, M.C.: Stochastic resonance in periodic potentials. Phys. Rev. E **83**, 061121 (2011)

16. Peyrard, M., Remoissenet, M.: Solitonlike excitations in a one dimensional atomic chain with a nonlinear deformable substrate potential. Phys. Rev. B **26**, 2884–2886 (1982)
17. Alexander, T.J., Salerno, M., Ostrovskaya, E.A., Kivshar, Y.S.: Matter waves in anharmonic priodic potentials. Phys. Rev. A **77**, 043607 (2008)
18. Kenmoe, G.D., Kofane, T.C.: Frictional stick-slip dynamics in a nonsinusoidal Remoissenet-Peyrard potential. Eur. Phys. J. B **55**, 347–357 (2007)
19. Kenmoe, G.D., Tchaptchet, E.D., Kofane, T.C.: Thermal effect on atomic friction with deformable substrate. Tribol. Lett. **55**, 533–542 (2014)
20. Kivshar, Y.S., Salerno, M.: Modulational instability in the discrete deformable nonlinear Schrodinger equation. Phys. Rev. E **49**, 3543 (1994)
21. Dong, Y., Perez, D., Gao, H., Martini, A.: Thermal activation in atomic friction: revisiting the theoretical analysis. J. Phys **24**, 265001 (2012)
22. Lindner, B., Schimansky, L.: Coherence and stochastic resonance in a two-state system. Phys. Rev. E **61**, 6103 (2000)
23. Li, P., Nie, L.R., Shu, C.Z., Hu, S., Shao, Q.: Effect of correlated dichotomous noises on stochastic resonance in a linear system. J. Stat. Phys. **146**, 1184–1202 (2012)
24. Gammaitoni, L., Marchesoni, F., Santucci, S.: Stochastic resonance as a bona fide resonance. Phys. Rev. Lett. **74**, 1052–1055 (1995)
25. Mahato, M.C., Shenoy, S.R.: Hysteresis loss and stochastic resonance: a numerical study of a double-well potential. Phys. Rev. E **50**, 2503 (1994)
26. Kim, Y.W., Sung, W.: Does stochastic resonance occur in periodic potentials? Phys. Rev. E **57**, 6237–6240 (1998)
27. Sekimoto, K.: Kinetic characterisation of heat bath and the energetics of thermal ratchet models. J. Phys. Soc. Jpn. **66**, 1234 (1997)
28. Kasdin, N.: Runge-Kutta algorithm for the numerical integration of stochastic differential equations. J. Guid. Control Dyn. **18**, 114 (1995)

Physica A 472 (2017) 25–31

Contents lists available at ScienceDirect

Physica A

journal homepage: www.elsevier.com/locate/physa

Effect of coupling on stochastic resonance and stochastic antiresonance processes in a unidirectionally *N*-coupled systems in periodic sinusoidal potential

Y.J. Wadop Ngouongo [a,*], G. Djuidjé Kenmoé [a,b], T.C. Kofané [a,b]

[a] *Laboratory of Mechanics, Materials and Structures, Department of Physics, Faculty of Science, University of Yaounde I, P.O. Box 812, Yaounde, Cameroon*

[b] *Centre d'Excellence en Technologies de l'Information et de la Communication (CETIC), University of Yaounde I, Yaounde, Cameroon*

HIGHLIGHTS

- SR and SAR in *N*-coupled particles in periodic sinusoidal potential.
- It is always advantageous to consider a nonlinear coupling in a system.
- Influence of the coupling on the SR and SAR phenomena.
- The apparition of SR is affected by the coupling and the choice of the frequency of the excitation force.
- Effect of the chain size on SR and SAR.

ARTICLE INFO

Article history:
Received 25 July 2016
Received in revised form 20 October 2016
Available online 30 December 2016

Keywords:
Stochastic resonance
Stochastic antiresonance
Hysteresis loop area
Noise
Efficiency

ABSTRACT

This work presents the characterization of stochastic resonance (SR) and stochastic antiresonance (SAR) in terms of hysteresis loop area (HLA). In connection with SR and SAR phenomena, we study the dynamics of a chain of particles coupled by nonlinear springs in a periodic sinusoidal potential. The dependence of the coupling parameter as well as the system size on SR and SAR is analysed. We consider the role played by the nonlinear coupling on the SR. We show that there is a range of coupling parameter where only SAR is observed, after this range the SR can occur, however, there also exists a range where neither SAR nor SR appear. It is noted that the maximum and the minimum of the average input energy increases with the coupling parameter. Also demonstrate that there exists an optimal value of the number of particles *N* for which the average input energy of the first particle reaches the saturation.

1. Introduction

The general trend of a noise is to weaken the effect of a signal. In the year 1981, the Italian physicists Benzi, et al. [1] showed that, in sharp contrast to this trend, a noise of suitable strength can amplify the response of a weak coherent signal in a system with a large energy barrier. The effect of noise has been intensively investigated in nonlinear systems. Several models used to study this significant property of noise consist of a bistable potential [2] or periodic potential [3] in which a Brownian particle is present. This type of behaviour known under the name of phenomenon of stochastic resonance is a cooperative

* Corresponding author.
E-mail addresses: yannickwadop@yahoo.fr (Y.J. Wadop Ngouongo), kdjuidje@yahoo.fr (G. Djuidjé Kenmoé), tckofane@yahoo.com (T.C. Kofané).

http://dx.doi.org/10.1016/j.physa.2016.12.015
0378-4371/

phenomenon arising from the interplay between deterministic and random dynamics in a nonlinear system wherein the coherent response to a deterministic monochromatic signal can be enhanced by the presence of an optimal amount of noise. When the response of the system to a periodic drive input signal exhibits a maximum dependence on the noise level, one speaks of the phenomenon of SR. It has been largely shown to occur in electronic circuits [4], lasers [5], nanomechanical systems [6], and neuronal systems [7] to mention a few. This phenomenon has been demonstrated in various systems such as a vegetation ecological system with time delay [8] and system of coupled neurons [9]. Moreover, on the basis of a qualitative analysis, it has been revealed in [10] that a stochastic antiresonance (SAR) can exist. It consists in that the nonlinear system response to an input signal on the input-noise intensity is minimum rather than maximum. Stochastic antiresonance has been found to occur in a theoretical model equation proposed for the transmission of a periodic signal mixed with a noise through a static nonlinearity [11], squid axons model equation (Hodgkin–Huxley model equation) [12], the time evolution of interacting qubits of quantum systems [13] and certain piece-wise linear systems [14]. One of the main characteristics used to identify SR phenomena is the hysteresis loop area (HLA) [15]. The study of the SR phenomenon by HLA, in the framework of nonlinear-response theory based on the input energy lost by the system to the environment per period of the external force, has been studied by Reenbohn et al. [16]. Dan et al. [17] have also shown that the input energy is a good quantifier of SR.

In some earlier works it has been shown by S. Scarsoglio and co-workers [18] that spatio-temporal SR indeed induces patterns in wetland vegetation dynamics. SR and Ghost-SR have been also studied by S. Rajamani et al. [19] in a unidirectionally coupled and small-world networks. The behaviour of order parameter of the system in dependence on the coupling has been analysed in the coupled stochastic system [20]. In a recent work multiple resonance and antiresonance in the N-coupled Duffing oscillators with nearest neighbour coupling has been done [21]. In this paper, the case of the dynamics of N-coupled stochastic system in periodic sinusoidal potential is of our interest. We use a periodic sinusoidal potential to explore the possibility of occurrence of SR and SAR in term of HLA and to analyse the behaviour of the efficiency which is a conversion of the energy in the system. Our objective is twofold. First we want to show that the nonlinearity of the coupling can bring the SR in the system. Second, we emphasize the role of the system size. The rest of paper is organized as follows: in the next section we explain some details, the model that we have considered in this work and the numerical procedure, while the results and discussion are presented in Section 3. Section 4 concludes the work.

2. Model and numerical procedure

Consider a chain of N particles coupled via nonlinear springs moving unidirectionally in a periodic sinusoidal potential $U(x) = -u_0 \sin(x)$ in a medium with friction coefficient λ. Each particle has a mass m_i $(i = 1, 2, \ldots, N)$ and is driven by an external periodic force $F(t)$ of frequency ω. Let $x_i(t)$ be the coordinates of these particles. Taking into account the force caused by the thermal fluctuation representing the noise $\xi_i(t)$ and by using the fundamental relation of dynamics, the equations of motion of the N particles can be described by the following system of the Langevin equations

$$\begin{cases} m_1\ddot{x}_1 + \lambda\dot{x}_1 - u_0\cos(x_1) + k\left(1 + \varepsilon\sin(x_1 - x_2)\right)(x_1 - x_2) = F_0\cos(\omega t) + \xi_1(t) \\ \quad i = 2, 3, \ldots., N-1 \\ m_i\ddot{x}_i + \lambda\dot{x}_i - u_0\cos(x_i) + k\left(1 + \varepsilon\sin(x_i - x_{i-1})\right)(x_i - x_{i-1}) \\ \quad + k\left(1 + \varepsilon\sin(x_i - x_{i+1})\right)(x_i - x_{i+1}) = F_0\cos(\omega t) + \xi_i(t) \\ m_N\ddot{x}_N + \lambda\dot{x}_N - u_0\cos(x_N) + k\left(1 + \varepsilon\sin(x_N - x_{N-1})\right)(x_N - x_{N-1}) = F_0\cos(\omega t) + \xi_N(t)\,. \end{cases} \tag{1}$$

In this system first and last particles are not connected each other. We use dimensionless variables, where identical mass $m_i = m = 1$ is assigned to each particle and the amplitude of the sinusoidal potential is $u_0 = 1$. The coupling is represented by the parameters k which is the linear part and ε the nonlinear part, if $\varepsilon = 0$, one finds the usual linear coupling. The interaction force resulting from local interaction between adjacent particles in coupled chain derived from the interaction part of the inner energies. Similar interaction can be observed in a PT(parity-time) symmetry model [22] where the polarization angle of the motion in the top chain of the double Frenkel–Kontorova (FK) chains determines the relative strength of the couplings. The fluctuation forces in the system are zero-mean independent Gaussian white noises and satisfy the following statistics: $\langle\xi_i(t)\rangle = 0$ and $\langle\xi_i(t)\xi_i(t')\rangle = 2\lambda T\delta(t - t')$ $i = 1, 2, \ldots, N$, the temperature T is in units of the Boltzmann constant k_B. Eqs. (1) may model several physical processes such as a driven coupled mechanical oscillator in sinusoidal substrate.

Quantities such as signal-to-noise ratio (SNR), input–output gains, cross-correlation, HLA are useful to characterize the signature of the SR. The HLA is of our interest, although Gudyma et al. [23] have shown that it is possible the induced by noise collapse of hysteresis loop. Following the stochastic energetics formulation of Sekimoto [24], the energy absorbed by each particle in a period of the external field is termed as input energy or work done by the field and is calculated as

$$W_i\left(t_0, t_0 + \frac{2\pi}{\omega}\right) = -\int_{F(t_0)}^{F\left(t_0 + \frac{2\pi}{\omega}\right)} x_i dF. \tag{2}$$

Using the expression of the external force, the input energy becomes,

$$W_i\left(t_0, t_0 + \frac{2\pi}{\omega}\right) = \int_{t_0}^{t_0 + \frac{2\pi}{\omega}} x_i(t)\,\omega F_0\sin(\omega t)\,dt = A_i \tag{3}$$

where A_i is the magnitude of the HLA corresponding to each particle. The input energy per period, $\overline{W}_i$, averaged over an entire trajectory is

$$\overline{W}_i = \frac{1}{N_1}\sum_{n=0}^{n=N_1} W_i\left(\frac{2\pi n}{\omega}, \frac{2\pi\,(n+1)}{\omega}\right). \tag{4}$$

The number of periods N_1 of the driving force $F(t)$ has taken equal to 10^5 in all the simulation. It has also been shown in Ref. [21] that it is possible to calculate the conversion of energy called efficiency η in the system as

$$\eta = \frac{\langle\dot{x}\rangle^2}{\left|\langle\dot{x}^2\rangle - T\right|}. \tag{5}$$

A fourth-order Runge–Kutta algorithm for stochastic processes developed by Kasdin [25] is implemented to solve numerically Eqs. (1). The system is initialized with the particles placed at the uniform separation and their initial velocities are null $\dot{x}_i(0) = 0$. The Eqs. (1) are integrated over a time long enough of $N_1 + 1$ periods. By numerically calculating Eqs. (3) and (4), we obtain the average input energy $\langle\overline{W}_i\rangle$ which is computed by averaging $\overline{W}_i$ over all the trajectories. We focus our attention on the occurrence of the phenomena of the SR and the SAR in the main objective to deduce information on microscopic properties of the system from the observed dynamics of the particles. System can achieve each dynamics by taking various values of the system parameters F_0, λ, k, ε and ω. It is assumed that the signal amplitude of the external forces is weak. Here the term weak means that in absence of noise the periodic force alone is unable to move particles from one well to other one.

3. Results and discussion

It is noted that in the absence of noise, there exists a critical value of $F = F_c$ at which cross-well orbits begin to occur. However, in the absence of noise and at a value fixed $F \ll F_c$ the motion is confined to one well alone. But an adequate value of the noise intensity helps to synchronize the output of the system with the external force. The system then exhibits the behaviour similar to that of the noise free case but slightly perturbed by the noise. This type of behaviour occurs for $T < T_c$, where T_c is the critical value of T at which cross-well behaviour occurs. When T just above T_c, the switching is not periodic, particles switch irregularly and rarely between two consecutive wells. Whereas as the value of T increases further, the switching between the wells increases. At $T > T_c$, almost periodic switching is observed. The periodicity of the noise-induced oscillation of the particles is the same as the periodicity of the driving force. This is the signature of the SR. Further increase of the noise intensity produces a loss of coherence. For sufficiently large values of T, the motion is strongly dominated by the noise. In this case intermittent dynamics disappears and the trajectory jumps erratically between the wells.

3.1. Effect of the parameter k

Let us first consider that the coupling is linear $\varepsilon = 0$. In order to evaluate the constructive role of noise, we plot in Fig. 1 the average input energy $\langle\overline{W}_1\rangle$ of the first particle for various values of k and for $N = 50$. Throughout Fig. 1(a) plotted for a frequency $\omega = 0.785$, one observes that initially the curves of $\langle\overline{W}_1\rangle$ increase with increasing T, reach a maximum then decrease until attain a minimum and then again increase gradually with T. This maximum displays a signature feature of the phenomenon of SR whereas the minimum shows the SAR phenomenon. For an other frequency $\omega = 1$ as illustrated in Fig. 1(b) and (c) SR disappears. Fig. 1(c) is for $\varepsilon = 0.1$ indicating that even for weak nonlinear coupling ε, the SR phenomenon does not occur for $\omega = 1$. The judicious choice of the frequency is thus very important for the appearance of the SR. The system is then able to oscillate coherently with subthreshold periodic input signals in a wide frequency range. We therefore seek to find values of parameters k and ε such that the system is able to oscillate coherently with sub-threshold periodic input signals in a wide frequency range. In order to achieve our goal, we choose a frequency ω ($\omega = 1$) for which there is no SR without the nonlinear coupling and see how the inclusion of the nonlinear coupling brings SR in the system. For that let us take $\varepsilon = 0.5$.

Fig. 2 depicts the evolution of $\langle\overline{W}_1\rangle$ as a function of the temperature T when $\varepsilon = 0.5$ and for different values of the parameter k. In Fig. 2(a) plotted for $k = 0.05, 0.1, 0.2, 0.3$ and 0.31, the curves of $\langle\overline{W}_1\rangle$ only present a minimum when T is increased for the values of $k \leq 0.3$. However, for $k = 0.31$ $\langle\overline{W}_1\rangle$ also exhibits a maximum. Therefore for k between 0 and 0.3 denoted by k_{SAR} the phenomenon of stochastic antiresonance only occurs. For the values of $k = 0.32, 0.4, 0.5, 0.55, 0.59, 0.6$ and 0.62 represented here on Fig. 2(b), first $\langle\overline{W}_1\rangle$ curves start to decrease with increasing T, reach a minimum then increase until attain a maximum when $k \in]0.3, 0.6[$, however when $k = 0.6$ and 0.62 $\langle\overline{W}_1\rangle$ only displays a maximum. This demonstrates that there is a range of k noted k_{SAR+SR} for which SAR and SR appear. One then notes that when k increases from the value 0.32, it is observed that SAR disappears gradually while only the SR takes place. It is also interesting to point that the phenomenon of SR gradually disappears and does not occur for a certain range of k as shown in Fig. 2(c). We can then more clearly notice that the average input energies of occurrence of the SAR ($\langle\overline{W}_1\rangle_{SAR}$) as well as SR ($\langle\overline{W}_1\rangle_{SR}$) increase whereas the temperature of occurrence of SAR ($T_{1_{SAR}}$) as well as that of the SR ($T_{1_{SR}}$) decrease as k is increased. In Fig. 2(d) and (e) are presented the hysteresis loop in the plane ($x1 - F$) for the temperatures $T = 0.001$ (Fig. 2(d)), $T = 0.2$ (Fig. 2(e))

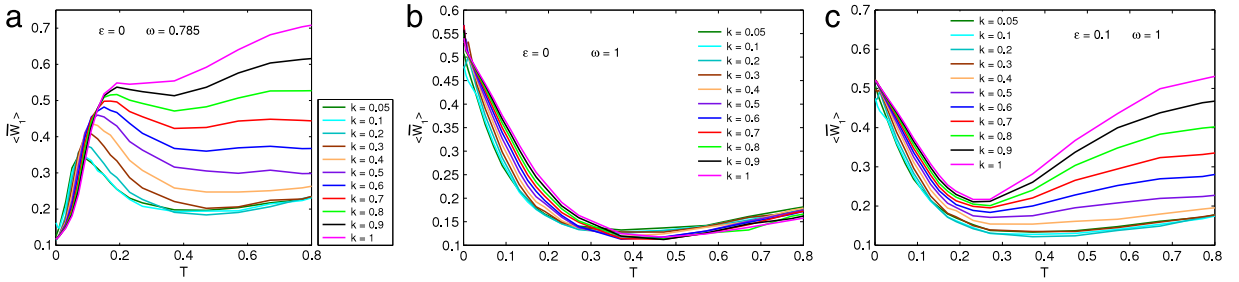

Fig. 1. Variation of $\langle \overline{W}_1 \rangle$ as a function of T for various values of k from 0.05 to 1 when $\varepsilon = 0$ and $\omega = 0.785$ (a); $\varepsilon = 0$ and $\omega = 1$ (b); $\varepsilon = 0.1$ and $\omega = 1$ (c). Other parameters are $F_0 = 0.2$, $N = 50$ and $\lambda = 0.2$.

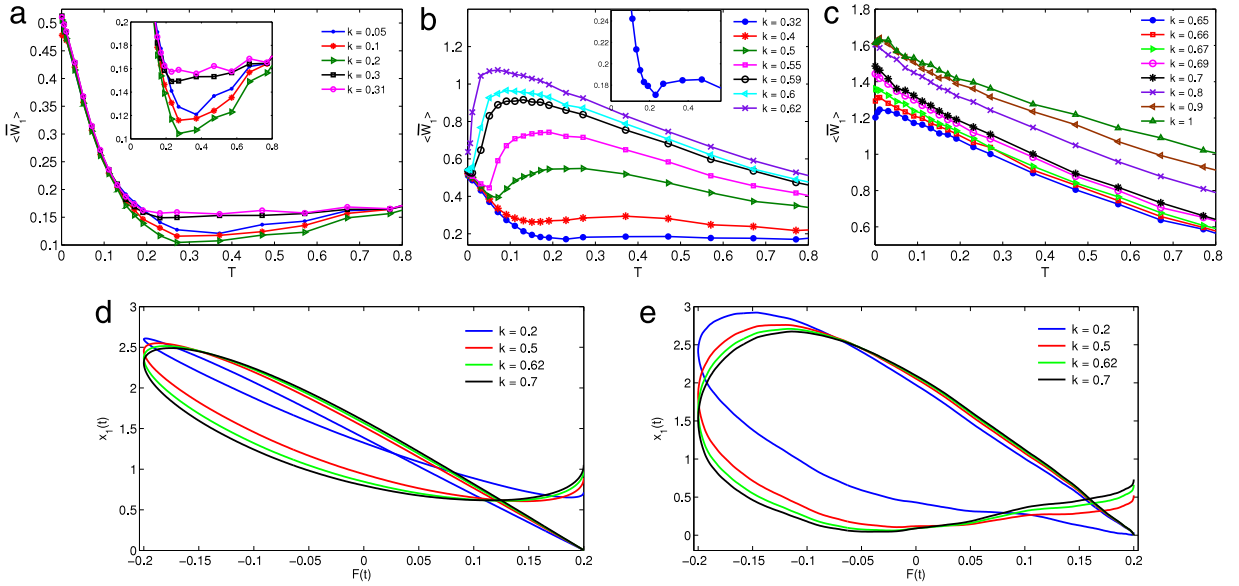

Fig. 2. Variation of $\langle \overline{W}_1 \rangle$ as a function of T for several fixed values of k and for $\varepsilon = 0.5$. Hysteresis loop in the plane (x_1, F) for four values of k indicated on figure and for $T = 0.001$ (Fig. 2(d)), $T = 0.2$ (Fig. 2(e)). Other parameters are $\omega = 1$, $F_0 = 0.2$, $N = 50$ and $\lambda = 0.2$.

and for several fixed values of k. The hysteresis loop size of the system increases with k, this is in agreement with the results observed in the calculations of the areas of these hysteresis loops.

For a more comprehensive description of the effect of k, we present the dependence of $\langle \overline{W}_1 \rangle$ on both T and k in Fig. 3(a). As one can see the increasing of k until a certain range can reduce the constructive effect of the noise. What explains the fact that there exists the values of k which destabilize systematically the occurrence of SR and SAR. This may be due to the apparition of a new phenomenon in the system for this range of k which will come to destroy the SR and SAR phenomena. We observe from Fig. 3(a) that the position of the $\langle \overline{W}_1 \rangle$ peaks and the minima of $\langle \overline{W}_1 \rangle$ crucially depend on the parameter k. These dependences are exhibited in Fig. 3(b) in which $T_{1_{SR}}$ and $T_{1_{SAR}}$ are displayed as a function of the parameter k. We can also observed the evolution of $\langle \overline{W}_1 \rangle_{SR}$ and $\langle \overline{W}_1 \rangle_{SAR}$ when k is increased as presented in Fig. 3(c). Where it is noted that the increasing of the parameter k amplifies the maximum and the minimum of $\langle \overline{W}_1 \rangle$. Furthermore, $T_{1_{SR}}$ and $T_{1_{SAR}}$ as well as $\langle \overline{W}_1 \rangle_{SR}$ and $\langle \overline{W}_1 \rangle_{SAR}$ are found to depend nonlinearly on k.

We numerically computed the response of the last particle denoted as $\langle \overline{W}_N \rangle$ for the particular values of k indicated in Fig. 4(a). In this figure $\langle \overline{W}_N \rangle$ illustrates different kind of dependence on the parameter k. We see that $\langle \overline{W}_N \rangle$ only displays SAR when $k = 0.2$ whereas for $k = 0.62$ only SR is exhibited, however for $k = 0.5$ both SR and SAR occur but for $k = 0.7$ none of the two phenomena is not occurred. For several values of k we plot in Fig. 4(b) the temperatures $T_{N_{SR}}$ and $T_{N_{SAR}}$ then in Fig. 4(c) $\langle \overline{W}_N \rangle_{SR}$ and $\langle \overline{W}_N \rangle_{SAR}$. Observe that $\langle \overline{W}_N \rangle_{SR}$ and $\langle \overline{W}_N \rangle_{SAR}$ behave almost the same way than $\langle \overline{W}_1 \rangle_{SR}$ and $\langle \overline{W}_1 \rangle_{SAR}$. That is not the case with the temperatures at which SR and SAR occur. To understand the general behaviour of the system, we examine the mean value $\langle \overline{W}_m \rangle$ of the average input energies of all particles as a function of T for the values of k used in Fig. 4(a). Throughout Fig. 5(a), one notices that for each value of the linear parameter k the phenomena of SR and SAR occur but with the amplitudes very lower than the one's obtained with the first and last particle. Point out that although SR and SAR does not occur for the first and last particle when $k = 0.7$, we notice that they occur through the system. The efficiency

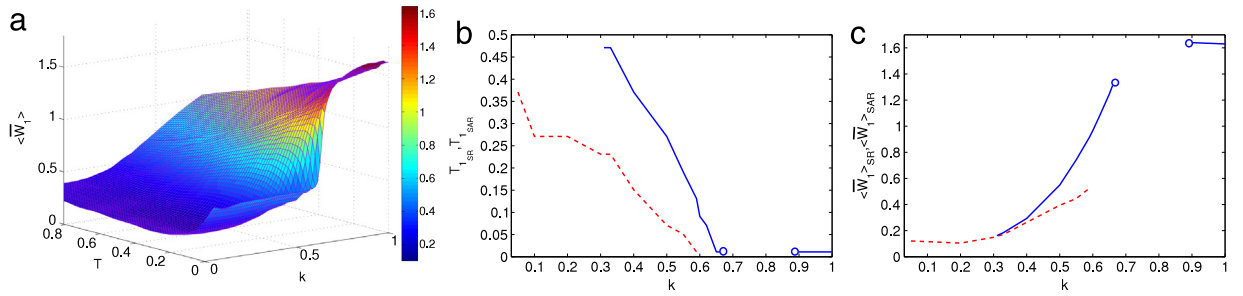

Fig. 3. Dependence of $\langle \overline{W}_1 \rangle$ on the parameter k and temperature T (a), plot of the variation of $T_{1_{SR}}$ and $T_{1_{SAR}}$ as a function of k (b) and variation of $\langle \overline{W}_1 \rangle_{SR}$ and $\langle \overline{W}_1 \rangle_{SAR}$ as a function of k (c). Other parameters are $\omega = 1$, $\varepsilon = 0.5$, $F_0 = 0.2$, $N = 50$ and $\lambda = 0.2$.

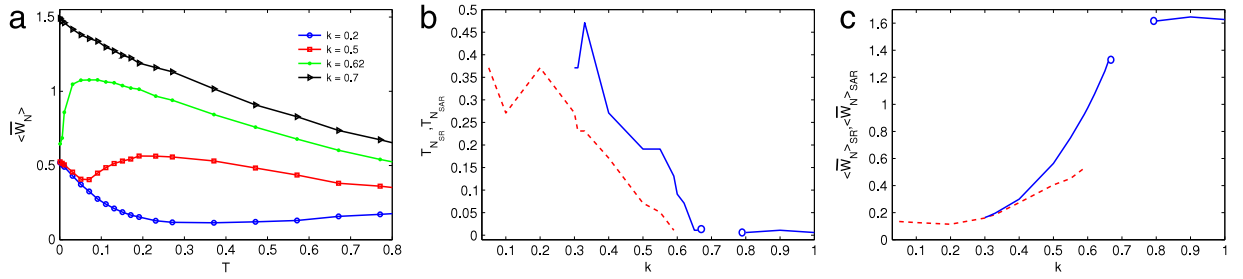

Fig. 4. $\langle \overline{W}_N \rangle$ as a function of T for the values of $k = 0.2$, 0.5, 0.62 and 0.7 (a), plot of the variation of $T_{N_{SR}}$ and $T_{N_{SAR}}$ as a function of k (b) and variation of $\langle \overline{W}_N \rangle_{SR}$ and $\langle \overline{W}_N \rangle_{SAR}$ as a function of k (c). The parameters are the same as for Fig. 3.

η which is the ratio of the dissipated power associated with the directed motion of the particles against friction, and the input power from the time-periodic forcing is investigated as in Ref. [26]. We plot in Fig. 5(b) the variation of η as a function of the temperature T for the values of k indicated in Fig. 5(a). As one can see, η exhibits the peaks and the minima as the case of the mean value $\langle \overline{W}_m \rangle$. We also note a similarity on the position on these peaks and these minima.

3.2. Effect of the chain size N

Having established the interdependence between coupling and phenomena of SR and SAR. In this section we turn our attention on the effect of the chain size for a value of $k = 0.58$ where SR and SAR phenomena are observed. In order to explore the significant influence of the number of particles N on the average input energy $\langle \overline{W}_1 \rangle$ of the first particle, one plots in Fig. 6 the variation of $\langle \overline{W}_1 \rangle$ as a function of the temperature T for several sizes of the chain. Fig. 6(a) illustrates a typical curve for a given value of N, in each of the cases, it can be seen that there is two extrema for which $\langle \overline{W}_1 \rangle$ takes its minimum value and the other where $\langle \overline{W}_1 \rangle$ is maximal. This shows that the output of the system has a nontrivial dependence on its size. Then note that when T increases $\langle \overline{W}_1 \rangle$ exhibits a resonant and antiresonant behaviour. This demonstrates that the first particle displays the SR and SAR phenomena. For too large N, the curves of $\langle \overline{W}_1 \rangle$ are closed together. Thereby point that the depth of the minimum of $\langle \overline{W}_1 \rangle$ decreases and moves towards its value at $T = 0$ when N is increased, however the maximum of $\langle \overline{W}_1 \rangle$ increases with N until reaches the saturation. Also remark that the temperature $T_{1_{SAR}}$ at which SAR occurs, decreases very weakly when N is increased whereas $T_{1_{SR}}$ decreases more rapidly. In order to gain a good appreciation of the effect of the number of particles N, we depict the dependence of $\langle \overline{W}_1 \rangle$ on the number of particles N and the temperature T in Fig. 6(b). The position of the minima and peaks of energy $\langle \overline{W}_1 \rangle$ depend of N. This dependence is shown in Fig. 7(a) where T_{SR} and T_{SAR} are represented as a function of N. The amplitudes of these minima and these peaks also strongly depend of N as illustrated in Fig. 7(b).

4. Concluding remarks

In this work, we have investigated the stochastic resonance and stochastic antiresonance unidirectionally dynamics of the N-coupled systems in periodic sinusoidal potential. Each particle displays a particular behaviour. The variation of the coupling parameter as well as the number of particles affect the occurrence of the SR and the SAR in the system namely the first and the last particle. Dealing first with the first particle, we have shown that for a certain frequency ω the increasing of the coupling can bring SR. Also found that there is a range of coupling parameter where only SAR is observed, where both SAR and SR occur, where only SR is observed and where neither SAR nor SR does not appear. That is also the case for the last particle. However, the mean value $\langle \overline{W}_m \rangle$ of the average input energies of each particle shows typical SR and SAR but with the

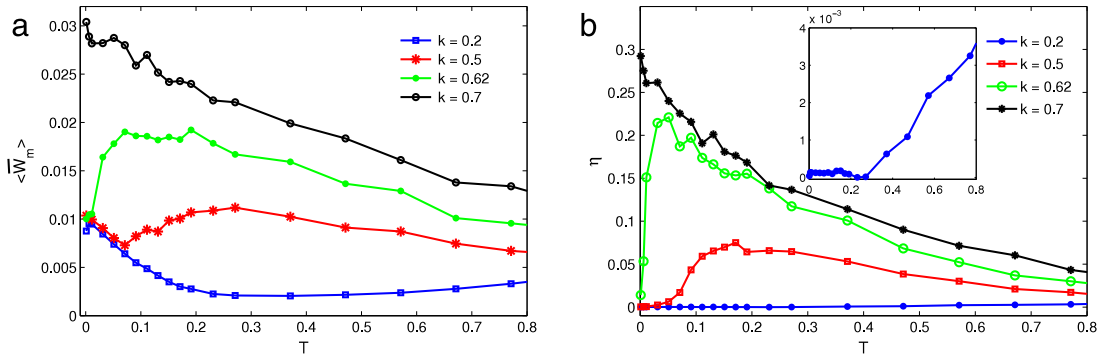

Fig. 5. Plot of the mean $\langle \overline{W}_m \rangle$ (a) and the efficiency η (b) as a function of T for the values of k indicated on the figure. The parameters are the same as for Fig. 3.

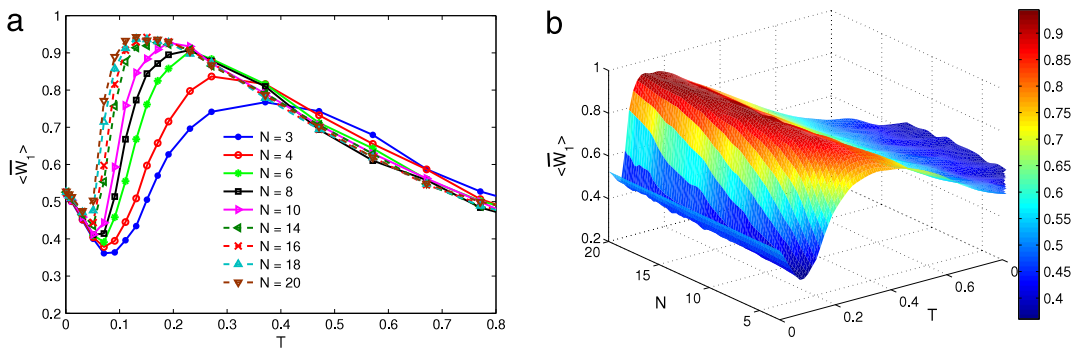

Fig. 6. Plot of $\langle \overline{W}_1 \rangle$ as a function of T for several values of N (a) and dependence of $\langle \overline{W}_1 \rangle$ on the number of particle N and temperature T (b). Other parameters are $\omega = 1$, $\varepsilon = 0.5$, $F_0 = 0.2$, $k = 0.58$ and $\lambda = 0.2$.

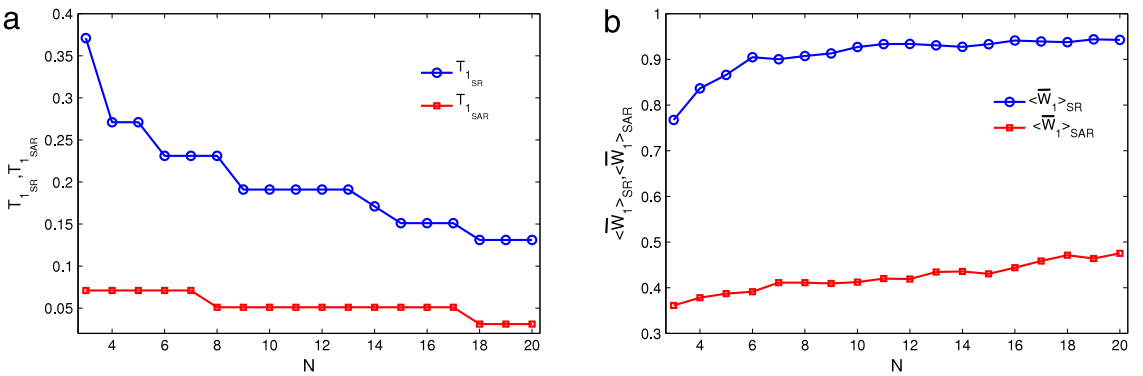

Fig. 7. Variation of $T_{1_{SR}}$ and $T_{1_{SAR}}$ (a) and $\langle \overline{W}_1 \rangle_{SR}$ and $\langle \overline{W}_1 \rangle_{SAR}$ (b) as a function of N. Other parameters are $\omega = 1$, $\varepsilon = 0.5$, $F_0 = 0.2$, $k = 0.58$ and $\lambda = 0.2$.

very weak amplitudes. By exploring the behaviour of the efficiency as T is increased, one notices that the efficiency almost behaves as $\langle \overline{W}_m \rangle$, one can ask: Can we use the efficiency to characterize the SAR and SR phenomena? It has been also shown that the increasing of the chain induces the increasing of the average input energy of the first particle. SR can be obtained in a periodic potential even for a system of complex particles. Our results indicate that the form of the coupling as well as the length of the chain can provide some degree of physical understanding of the SR and SAR.

References

[1] R. Benzi, A. Sutera, A. Vulpiani, J. Phys. A 14 (1981) 453.
[2] B. McNamara, K. Wiesenfeld, Phys. Rev. A 39 (1989) 4854.
[3] G. Djuidje Kenmoé, Y.J. Wadop Ngouongo, T.C. Kofané, J. Stat. Phys. 161 (2015) 475.

[4] S. Fauve, F. Heslot, Phys. Lett. A 97 (1983) 5.
[5] B. McNamara, K. Wiesenfeld, R. Roy, Phys. Rev. Lett. 60 (1988) 2626.
[6] R.L. Badzey, P. Mohanty, Nature 437 (2005) 995.
[7] H. Zhanga, T. Yang, Y. Xu, W. Xu, Eur. Phys. J. B 88 (2015) 125.
[8] Q. Han, T. Yang, C. Zeng, H. Wang, Z. Liu, Y. Fu, C. Zhang, D. Tian, Physica A 408 (2014) 96.
[9] E. Yilmaz, M. Uzuntarla, M. Ozer, M. Perc, Physica A 392 (2013) 5735.
[10] M. Evstigneev, P. Reimann, V. Pankov, R.H. Prince, Europhys. Lett. 65 (2004) 7.
[11] F.C. Blondeau, Phys. Lett. A 232 (1997) 41.
[12] L.S. Borkowski, Phys. Rev. E 82 (2010) 041909.
[13] D.P.K. Ghikas, A.C. Tzemos, Int. J. Quantum Inf. 10 (2012) 1250023.
[14] N.V. Agudov, A.V. Krichigin, Radiophys. Quantum Electron. 51 (2008) 812.
[15] M.C. Mahato, A.M. Jayannavar, Physica A 248 (1998) 138.
[16] W.L. Reenbohn, S.S. Pohlong, C.M. Mahato, Phys. Rev. E 85 (2012) 031144.
[17] D. Dan, A.M. Jayannavar, Physica A 345 (2005) 404.
[18] S. Scarsoglio, P. D'Odorico, F. Laio, L. Ridolfi, Ecol. Complexity 10 (2012) 93.
[19] S. Rajamani, S. Rajasekar, M.A.F. Sanjuán, Commun. Nonlinear Sci. Numer. Simul. 19 (2014) 4003.
[20] Iu. Gudyma, et al., Eur. Phys. J. B 87 (2014) 205.
[21] R. Jothimurugan, K. Thamilmaran, S. Rajasekar, M.A.F. Sanjuan, Nonlinear Dynam. (2015). arXiv:1510.01564 [nlin.CD].
[22] J. Cuevas-Maraver, B.A. Malomed, P.G. Kevrekidis, Symmetry 8 (2016) 39. http://dx.doi.org/10.3390/sym8060039.
[23] Iu. Gudyma, et al., Physica B 486 (2016) 44.
[24] K. Sekimoto, J. Phys. Soc. Japan 66 (1997) 6335.
[25] N. Kasdin, J. Guid. Control Dyn. 18 (1995) 114.
[26] L. Machura, M. Kostur, P. Talkner, J. Łuczka, F. Marchesoni, P. Hänggi, Phys. Rev. E 70 (2004) 061105.

Physica A 527 (2019) 121321

Contents lists available at ScienceDirect

Physica A

journal homepage: www.elsevier.com/locate/physa

Dynamics of a particle periodically driven in the deformable potentials: Stochastic resonance

Y.J. Wadop Ngouongo [a,*], G. Djuidjé Kenmoé [a,b], T.C. Kofané [a,b]

[a] Laboratory of Mechanics, Materials and Structures, Department of Physics, Faculty of Science, University of Yaounde I, P.O. Box 812, Yaounde, Cameroon

[b] Centre d'Excellence en Technologies de l'Information et de la Communication (CETIC), University of Yaounde I, Yaounde, Cameroon

HIGHLIGHTS

- SR in ASDP and DWDP systems.
- The apparition of double SR is observed in the ASDP system.
- As a function of the shape parameter, input energy can exhibit one or two narrow band.
- As a function of the shape parameter, input energy distribution can be bimodal nature.
- Chaos can destroy the SR phenomenon.
- The amplitude of the external force for which switching between wells begin strongly depends of the shape parameter.

ARTICLE INFO

Article history:
Received 10 October 2018
Received in revised form 23 April 2019
Available online 29 April 2019

Keywords:
Stochastic resonance
Chaos
Hysteresis loop area
Noise
Deformable potentials

ABSTRACT

In connection with stochastic resonance (SR), we study the dynamics of a particle in the asymmetric deformable potential (ASDP) and double well deformable potential (DWDP). The phenomenon of SR is known to occur in sinusoidal and some nonsinusoidal systems. However, the question of the occurrence of SR in the ASDP and DWDP systems has not been resolved. This numerical work presents the characterization of stochastic resonance in terms of hysteresis loop area (HLA) in both the models. The average input energy displays a double SR peak as a function of temperature in the ASDP model and one peak of SR which occurs at weak temperature in the DWDP model. The presence of Chaos is also investigated in DWDP system where we show that the Chaos can destroy the SR phenomenon.

1. Introduction

A physical system can be constituted by a single particle. When this particle is trapped in a potential well and driven by an external force, a variety of phenomena can be realized such as synchronization [1–4], chaos and bifurcation [5–8] and recently vibrational resonance [9]. The effect of resonance is to produce a large vibration. Adding the noise (thermal fluctuation force) the system can exhibit several behaviors such as negative mobility [10], diffusion [11] and stochastic resonance (SR) [12]. The optimal periodic response of a system to an external periodic drive as a function of noise strength is referred as stochastic resonance. The researchers of all domain and the engineers exploit this phenomenon nowadays as an instrument for their specific purposes. This phenomenon has been experimentally observed in electronic circuits [13],

* Corresponding author.
E-mail addresses: yannickwadop@yahoo.fr (Y.J. Wadop Ngouongo), kdjuidje@yahoo.fr (G. Djuidjé Kenmoé), tckofane@yahoo.com (T.C. Kofané).

https://doi.org/10.1016/j.physa.2019.121321
0378-4371/

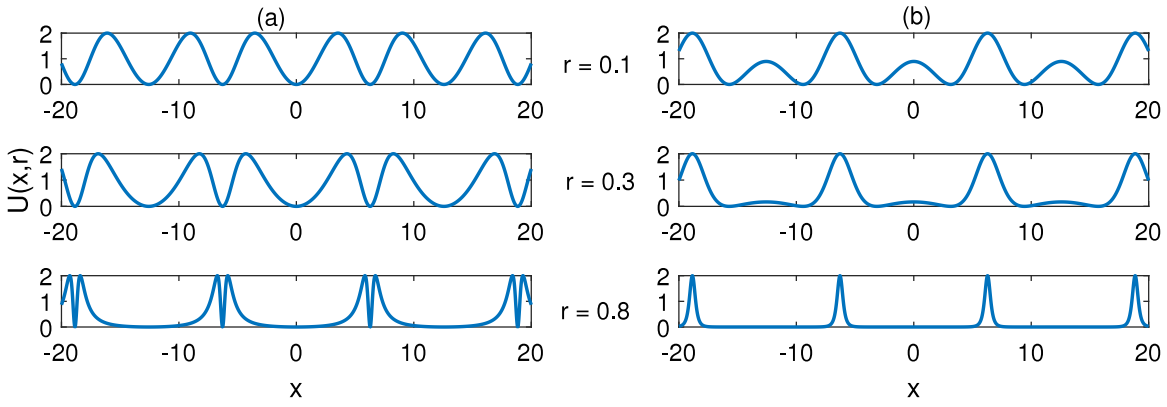

Fig. 1. Illustration of the nonlinear deformable potentials $U(x, r)$ as a function of x for the values of r indicated on the figure and for the two models: (a) ASDP, (b) DWDP. The shape of the potential depends on the parameter r.

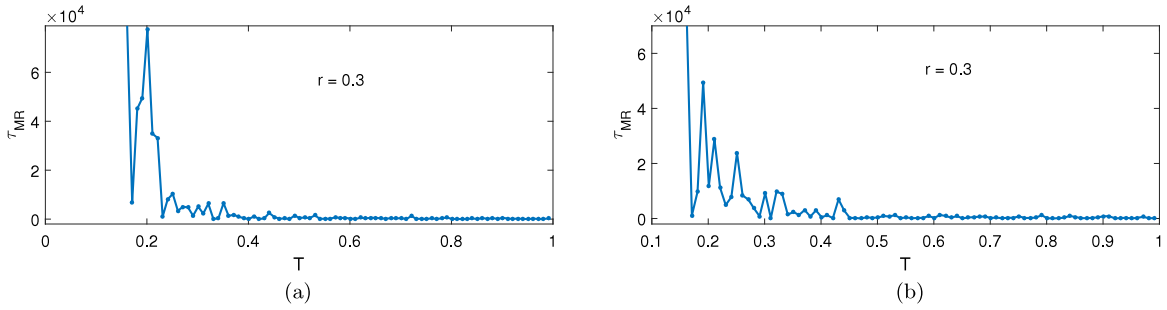

Fig. 2. Mean residence time τ_{MR} of the particle in the initial well for ASDP system (a) and double well for DWDP system (b) as a function of T when $r = 0.3$. Other parameters are $M = 1$, $U_0 = 1$, $\gamma = 0.2$, $A_0 = 0.2$ and $F_0 = 0.1$.

lasers [14], nanomechanical systems [15], and neuronal systems [16] just to mention a few. It has also been studied in various systems such as systems with a single potential well [17], bistable systems [18], sinusoidal systems [19,20] and more recently non-sinusoidal periodic system by Djuidje et al. [21]. Nonlinear excitation in one dimensional have recently attracted much attention in the study of the sinusoidal confined systems. However, the deformable systems present a particular interest in the study of some physical phenomena. In real systems, as for instance Josephson junctions, incommensurate systems, charge-density wave condensates, or crystals with dislocations, the shape of the potential can deviate strongly from a sinusoidal one. In this context, introducing a one-dimensional model with nonlinear periodic deformable potential, it has recently been shown that the shape of the substrate potential is an important factor in the modeling of physical systems [22]. These kinds of potential have already been used in the context of the solitons [23].

Most of the studies in the field of trapped particles are modeled by physical systems having a rigid shape on-site substrate potential. Nevertheless, these systems with periodic structure, although interesting, describe realistic system only with some approximations. To obtain a physically more realistic periodic substrate for trapped particles, the effects of physical parameter such as temperature and pressure should be take into account. It then appears necessary to consider the deformable character of the medium in trapped particles. In the present work, we consider the nonlinear periodic deformable potentials which generalize three models; the Remoissenet–Peyrard potential model previously considered in the context of SR where we have shown the effect of the shape of potential on SR [21], the asymmetric deformable potential (ASDP) model recently introduced in the study of the vibrational resonance [24] and double well deformable potential (DWDP) model in order to analyze the dynamics of the particle in the two last systems and to explore the possibility of occurrence of SR in these systems. This question of SR in these systems is ours, has not yet been considered. To attain one of our main objectives in the goal to solve the real problem around this topic, we use the hysteresis loop area (HLA) [25,26] which is equivalent to the input energy lost by the system to the environment per period of the external force. Several key quantities in the literature are also utilized as the appropriate measures of SR.

This paper is organized as follows: In Section 2, we introduce the theoretical models of the particle moving along the deformable traveling-wave potentials. Present the different potentials and establish the Langevin equations which describe the dynamic of the particle in each deformable potential models. In Section 3, the quantities of ours interest such as the input energy and observable used as indicator of SR are displayed. We compute the mean residence time for a variety of the potential and numerical results of the input energy of the systems. The full probability distribution of the

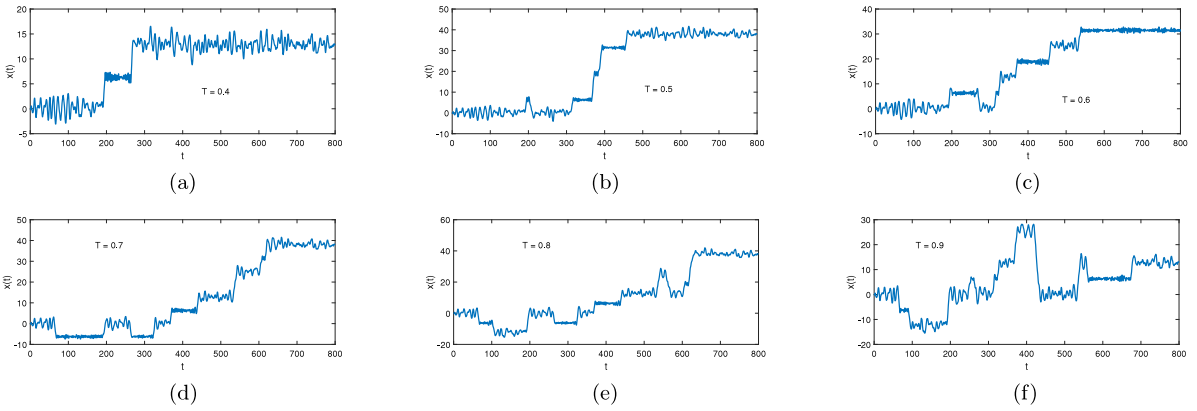

Fig. 3. Trajectories $x(t)$ versus time t for ASDP model and for $r = 0.3$ at various values of the temperature. Other parameters are $M = 1$, $U_0 = 1$, $\gamma = 0.2$ and $F_0 = 0.1$.

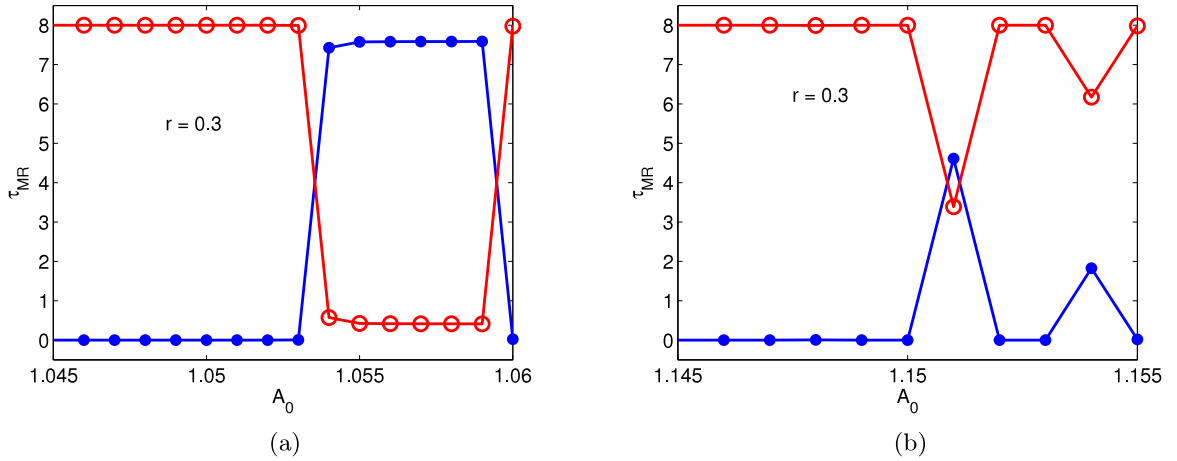

Fig. 4. Mean residence time in the initial well (blue circle line) while the red dot line is the mean residence time of the particle out of the initial well as a function of amplitude of external force A_0 in the absence of noise for $r = 0.3$ and for the both models: (a) ASDP , (b) DWDP (initial double well). Other parameters are $M = 1$, $U_0 = 1$, $\gamma = 0.2$ and $F_0 = 0.1$.

input energy of system, the stochastic resonance using the hysteresis loop area are also analyzed. Finally, our results are summarized and concluded in Section 4.

2. Model description and numerical procedure

In this work, we consider a particle of mass M moving along a periodic deformable potential $U(x, r)$ and in a medium with friction coefficient γ. This particle is subjected to an external periodic force $F(t) = F_0 + A_0 \cos(\omega t)$ and the thermal fluctuation force $\xi(t)$. The dynamics of the particle can be described by the Langevin equation as

$$M\frac{d^2x}{dt^2} = -\gamma\frac{dx}{dt} - \frac{\partial U(x,r)}{\partial x} + F_0 + A_0\cos(\omega t) + \xi(t). \tag{1}$$

The on-site dimensional potential $U(x, r)$ represents the nonlinear periodic deformable potential generalized given in Ref. [23]:

$$U(x,r) = A(r)\frac{1+e\cos x}{\left[1+r^2+2r\cos(x/m)\right]^p} \tag{2}$$

where r is a shape parameter with range $-1 < r < 1$, $A(r)$ is a normalizing amplitude; m, p are integers and $e = \pm 1$. When $A(r) = U_0(1-r)^2$, $m = p = 1$, $e = -1$ and $-1 < r < 1$ we get the potential recently studied [20]. For $A(r) = U_0(1-r^2)^2$, $m = p = 2$, $e = -1$ and $0 < r < 1$ one has an asymmetric deformable potential (ASDP), illustrated in Fig. 1(a) for various values of r. This potential presents two successive wells which are not same with, respectively, a flat and sharp bottom.

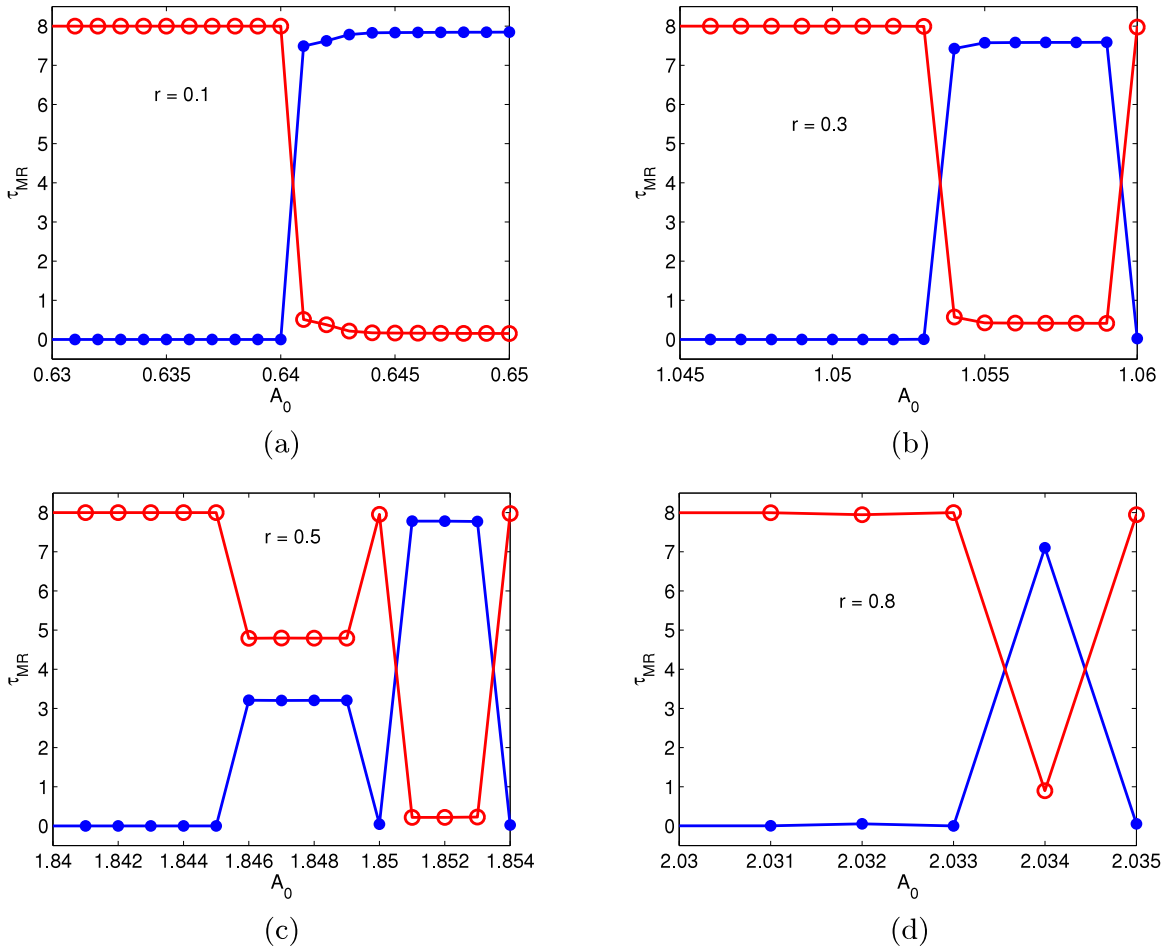

Fig. 5. Mean residence time in the initial well (blue circle line) while the red dot line is the mean residence time of the particle out of the initial well as a function of amplitude of external force A_0 in the absence of noise for $r = 0.1$ (a), $r = 0.3$ (b), $r = 0.5$ (c) and $r = 0.8$ (d) in the ASDP model. Other parameters are $M = 1$, $U_0 = 1$, $\gamma = 0.2$ and $F_0 = 0.1$.

Whereas for $A(r) = U_0(1-r)^4$, $m = p = 2$, $e = 1$ and $0 < r < 1$ we obtain a double-well deformable potential (DWDP) plotted in Fig. 1(b).

The random fluctuations in the system are represented by $\xi(t)$ which satisfy the statistics: $\langle \xi(t) \rangle = 0$ and $\langle \xi(t)\xi(t') \rangle = 2\gamma T\delta(t-t')$ where the medium temperature T is in units of the Boltzmann constant k_B. Eq. (1) may model several physical processes such as the dynamics of a nonlinear mechanical oscillator in deformable substrate. Below we use $M = 1$, $U_0 = 1$, $A_0 = 0.2$ and $F_0 = 0.1$. A fourth-order Runge–Kutta algorithm for stochastic processes developed by Kasdin [27] is implemented to solve numerically Eq. (1). We take the initial velocities $\dot{x}(0) = 0$ for all cases and the initial positions $x(0)$ are chosen between 0 and 4π. The drive (signal) frequency $\omega = \frac{2\pi}{\tau}$ ($\tau = 8$) is taken to be close to the natural frequency at the bottom of the wells of the potential. The Eq. (1) is integrated over a time long enough of $N_1 + 1$ periods.

Quantities such as signal-to-noise ratio (SNR), input–output gains, cross-correlation, HLA are useful to characterize the signature of the SR. The HLA is of our interest. Following the stochastic energetics formulation of Sekimoto [28], the energy absorbed by the particle in a period of the external field is termed as input energy or work done by the field and is calculated as

$$W\left(t_0, t_0 + \frac{2\pi}{\omega}\right) = -\int_{F(t_0)}^{F\left(t_0+\frac{2\pi}{\omega}\right)} x dF \tag{3}$$

Using the expression of the external force, the input energy becomes,

$$W\left(t_0, t_0 + \frac{2\pi}{\omega}\right) = \int_{t_0}^{t_0+\frac{2\pi}{\omega}} x\,(t)\,\omega A_0 \sin(\omega t)\,dt = A \tag{4}$$

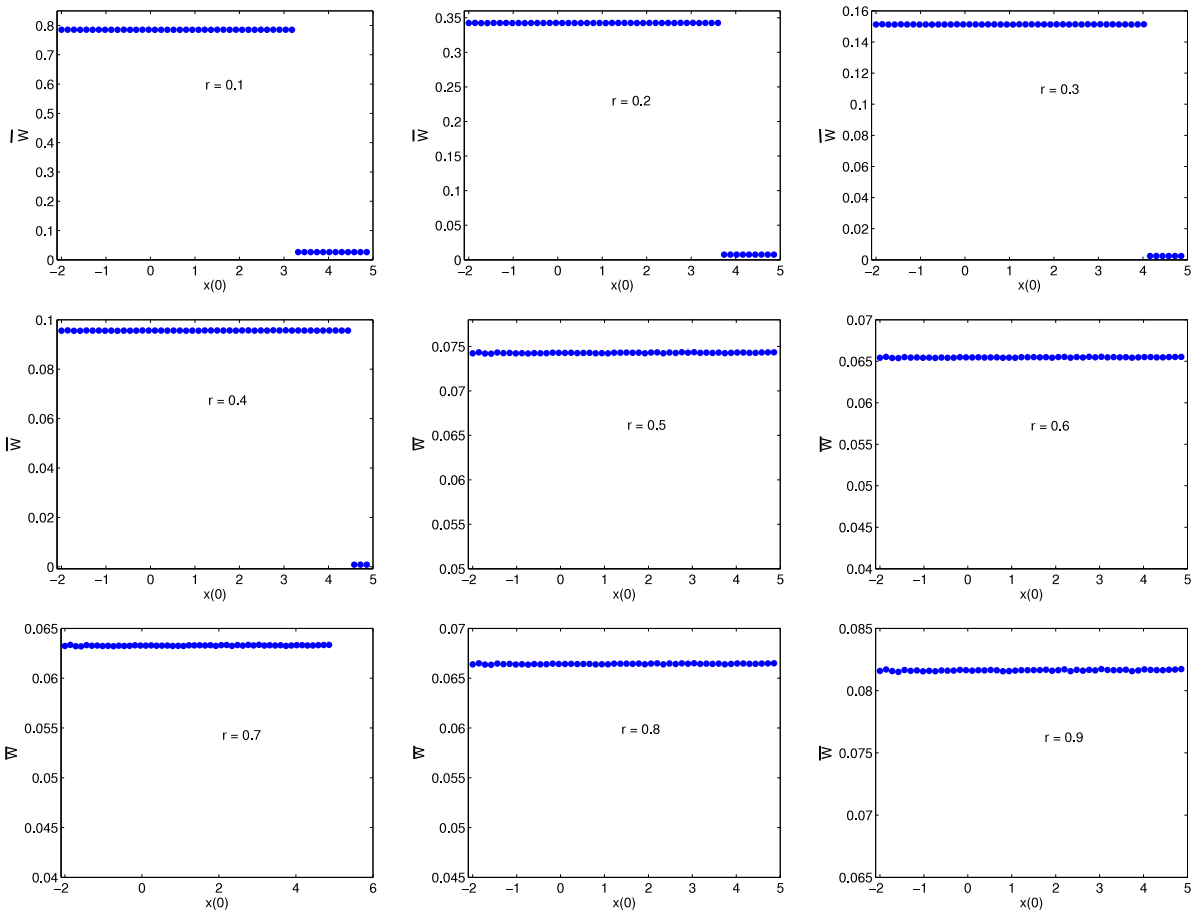

Fig. 6. Variation of the input energy $\overline{W}$ with initial positions $x(0)$ at a temperature $T = 0.01$ for ASDP system and for various values of shape parameters r. Other parameters are $M = 1$, $U_0 = 1$, $\gamma = 0.2$, $A_0 = 0.2$ and $F_0 = 0.1$.

where A is the magnitude of the HLA corresponding to each particle. The input energy per period, $\overline{W}$, averaged over an entire trajectory is

$$\overline{W} = \frac{1}{N_1} \sum_{n=0}^{n=N_1} W\left(\frac{2\pi n}{\omega}, \frac{2\pi\,(n+1)}{\omega}\right) \tag{5}$$

The number of periods N_1 of the driving force $F(t)$ has taken equal to 10^5 in all the simulation. In order to deduce information on microscopic properties of the ASDP and DWDP systems from the observed dynamics of the particle, we focus our attention on the occurrence of the phenomena of the SR. System can achieve each dynamics by taking various values of the system parameters F_0, γ, A_0 and ω. In the following, we present the results of our numerical calculations and analyze how the particle trajectories in the ASDP and DWDP systems from mean residence time, and hence the input energy and the input energy distribution, are affected by the shape parameter r. We examine the occurrence of SR in the ASDP and DWDP models.

3. Numerical results

One of the objectives is to deduce information on the properties of the system to understand how the particle stays in a well before switching to another well; this refers to mean residence time τ_{MR}. For a weak amplitude of the external force and in the absence of noise, the motion of the particle is confined to a well or an equilibrium state. That is, before the noise induced dynamics (or even the external force), the residence time of the system in each well is infinite (τ_{MR} is much larger than the period). Fig. 2(a) and (b) illustrate numerically computed τ_{MR} on each well for at set of $n * \tau$ transitions ($n = 5000$) as a function of the temperature T when $x(0) = 0$, $r = 0.3$ and $A_0 = 0.2$. At the weak values of T, there is no switching and so τ_{MR} is infinite and the number of times that the particle jumped from initial well to another well is zero in both the systems. At appropriate optimum noise intensity a periodic switching between the wells

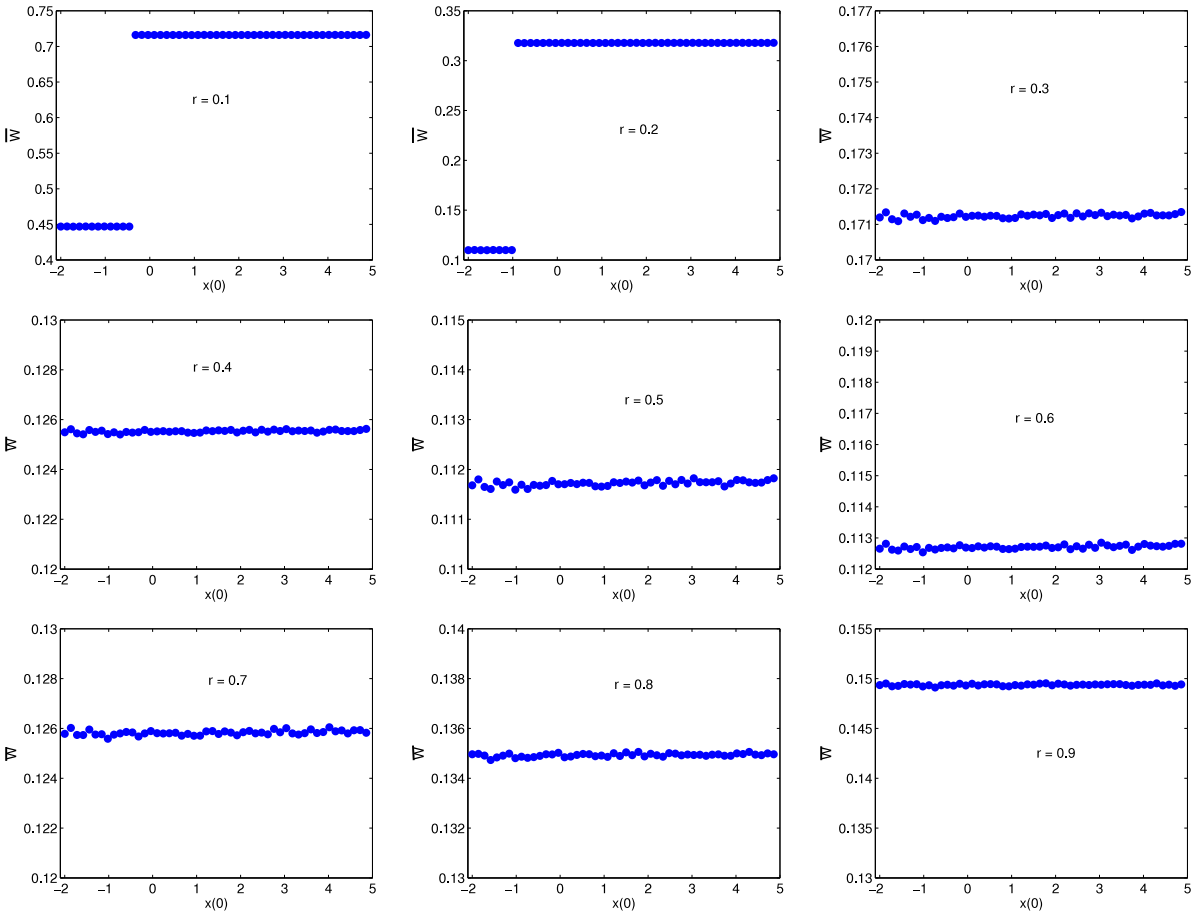

Fig. 7. Variation of the input energy $\overline{W}$ with initial positions $x(0)$ at a temperature $T = 0.01$ for DWDP system and for various values of shape parameters r. Other parameters are $M = 1$, $U_0 = 1$, $\gamma = 0.2$, $A_0 = 0.2$ and $F_0 = 0.1$.

take place. This noise-induced phenomenon is called SR [29–31]. In each of these two potentials, far before resonance $\tau_{MR} \gg n/2$. At resonance where HLA becomes maximum $\tau_{MR} = n/2$. $\tau_{MR} \ll n/2$ for far after resonance. one can remark that τ_{MR} is nonmonotonical, this is clearly explained by the behavior of the trajectories $x(t)$ in Fig. 3, plotted for various temperatures. Where in some case, although the particle go out of the initial well, it can return in this well with the time. By considering the temperature $T = 0$, we calculate τ_{MR} for different values of the amplitude of the external force A_0. Fig. 4 represents the mean residence time of the particle on each well (circle line) and the mean residence time out of the initial well (dot line) computed for one period of the external force as a function of A_0 for $r = 0.3$. we observe that when $A_0 < A_{0s}$, A_{0s} being the value of A_0 at which switching starts, the mean residence time of the particle out of the initial well (dot line) is null whereas the mean residence time in the initial well is equal to τ. This means that the probability to find the particle in initial well is equal to 1. We then note that the normalized residence time (τ_{MR}/τ) is equal to 1, this means no switching occurs and the trajectories are intrawell in nature. One can note that the value of A_0 for which switching between wells begin strongly depends of the shape parameter as shown in Fig. 5 plotted for ASDP system.

3.1. Input energy and input energy distribution of the systems

3.1.1. Input energy

At the lowest temperature $\overline{W}$ depends very strongly on the initial positions $x(0)$. We then present an investigation of the variation of the input energy profile averaged over a trajectory as a function of the initial positions $x(0)$ in the ASDP and DWDP models for several shape parameters and for a temperature $T = 0.001$. As a function of the shape of the potential, $\overline{W}$ can display two or one narrow band. In the case of ASDP system, we observe that the curves of $\overline{W}$ are confined to two narrow bands when $r < 0.5$, and gradually increasing r, $\overline{W}$ makes a transition towards only one narrow band as shown in Fig. 6. However, the input energy $\overline{W}$ clearly displays two bands for $r < 0.3$ and one band for $r > 0.3$ in the DWDP model as illustrated by Fig. 7. In fact, for a shape of potential given a band of $\overline{W}$ corresponds to a state of

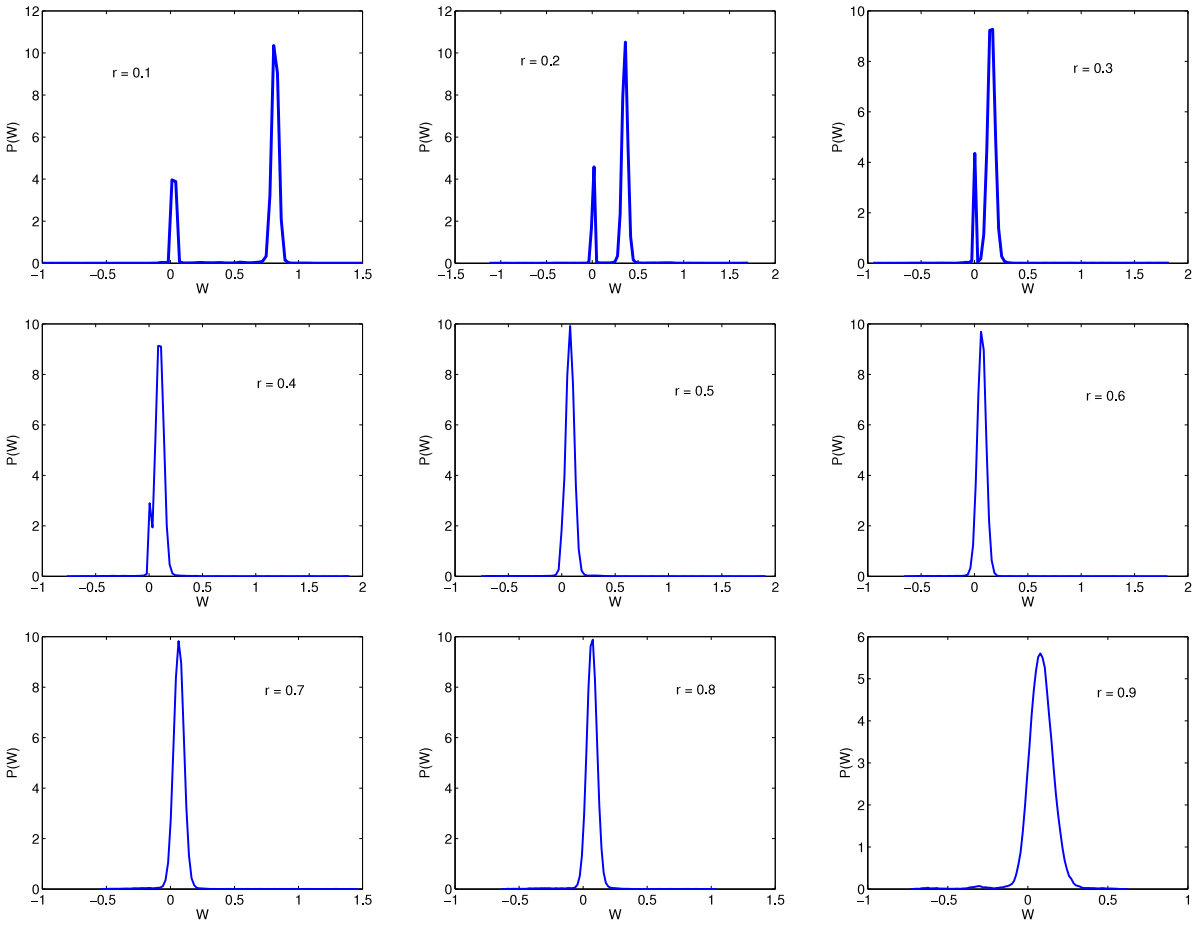

Fig. 8. Input energy distribution $P(W)$ at a temperature $T = 0.01$ for ASDP model and for various values of shape parameters r. Other parameters are $M = 1$, $U_0 = 1$, $\gamma = 0.2$, $A_0 = 0.2$ and $F_0 = 0.1$.

Table 1
Values of $\overline{W}$ band of the ASDP and DWDP systems for various values of r.

r	ASDP	DWDP
0.1	0.026 ; 0.785	0.446 ; 0.716
0.2	0.007 ; 0.342	0.109 ; 0.317
0.3	0.002 ; 0.151	0.171
0.4	0.0008 ; 0.095	0.125
0.5	0.074	0.111
0.6	0.065	0.112
0.7	0.063	0.125
0.8	0.066	0.134
0.9	0.081	0.149

energy in which the particle can be found. It has been shown in Ref. [20] that the two narrow bands observed on $\overline{W}$ curves correspond to the existence of two dynamical states distinctly identified by the phase difference between the external force and the trajectory $x(t)$. Table 1 shows a summary of the values of $\overline{W}$ bands for the ASDP and DWDP systems when r is varied. The behavior of $\overline{W}$ is then controlled by the parameter r. Of course, for both the systems, it is important to point that for the values of r where two bands appear, the upper band gradually diminishes, then disappears and joins the lower band as r is increased. Thereby, one can say that some states have made a transition to another states. The shape parameter influence is then similar to the action of temperature in thermodynamic equilibrium systems and leads to the effective reducing of the depths of potential well. Although considering a entire space period of these systems where both the wells are included, the behavior of $\overline{W}$ is not affected. In order to know how the input energy is distributed in the system, in following we examine the behavior of input energy distribution.

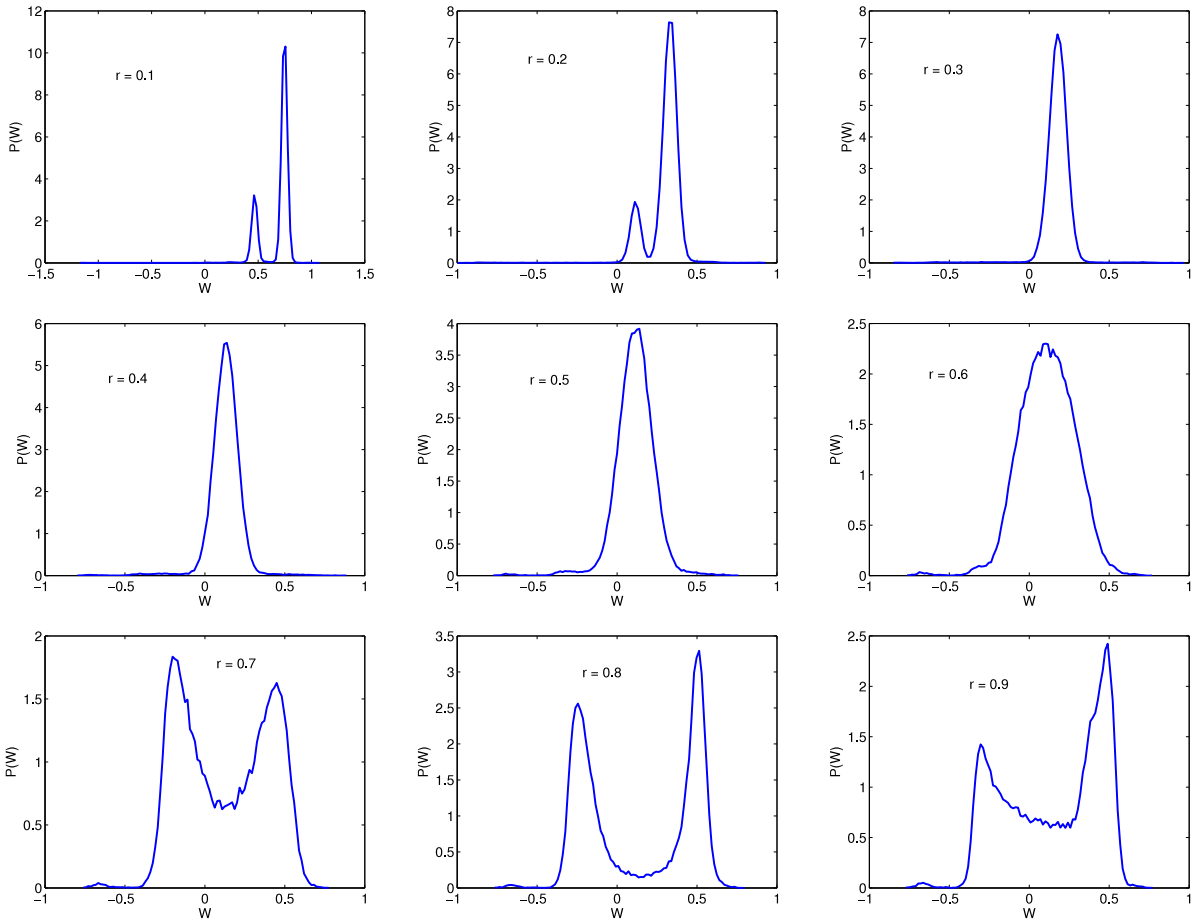

Fig. 9. Input energy distribution $P(W)$ at a temperature $T = 0.01$ for DWDP model and for various values of shape parameters r. Other parameters are $M = 1$, $U_0 = 1$, $\gamma = 0.2$, $A_0 = 0.2$ and $F_0 = 0.1$.

3.1.2. Input energy distribution

The distribution can carry important information about the system and mainly the stochastic resonance. The values of W are different depending on whether during the particular period of $F(t)$, input energy has then a well-defined distribution. One can compute the input energy distribution over ensembles with different initial position $x(0)$. In Fig. 8, the distribution of W is exhibited for various shape parameters r at a temperature $T = 0.001$ for ASDP system. As we can see the peaks of $P(W)$ are quite sharp. The nature of $P(W)$ depends of the value of r, thus $P(W)$ displays a bimodal distribution when $r < 0.5$. The height of the first peak decreases with r, this peak gradually disappears yet to lose completely from $r = 0.5$. Therefore, for $r > 0.4$ the input energy distribution $P(W)$ changes from two peaks to only one and their width increases with r. All these peaks are exactly centered at the values of $\overline{W}$ bands. The apparition of $P(W)$ peaks then obeys at the behavior of $\overline{W}$. For DWDP system, two peaks are observed when $r < 0.3$, $P(W)$ peaks also obey at the behavior of $\overline{W}$. Nevertheless, for $r > 0.6$, it is interesting to note that, although $\overline{W}$ is consisted of only one band, $P(W)$ has a bimodal nature. Thereby there is no longer any relationship between $P(W)$ and $\overline{W}$. That can be due to weird nature of the hysteresis loops. $P(W)$ is unimodal for the other values of r as illustrated in Fig. 9. When $r > 0.6$, In both the models, the height of the peaks nonmonotonically depends of r. These distributions can also provide many informations about the number of state having a well-defined input energy. Notice the intrusion of W into the negative value. The increase of negative region of $P(W)$ goes hand in hand with increasing r. In both the systems the position of peaks varies along with the changing of the shape of the potential that is because the shape parameter affects the values of the input energy.

3.2. Hysteresis loop area: stochastic resonance

In this section we focus our attention on the phenomenon of stochastic resonance which is a manifestation of the constructive role of the noise. This phenomenon requires three ingredients: a weak coherent signal, a noise source and

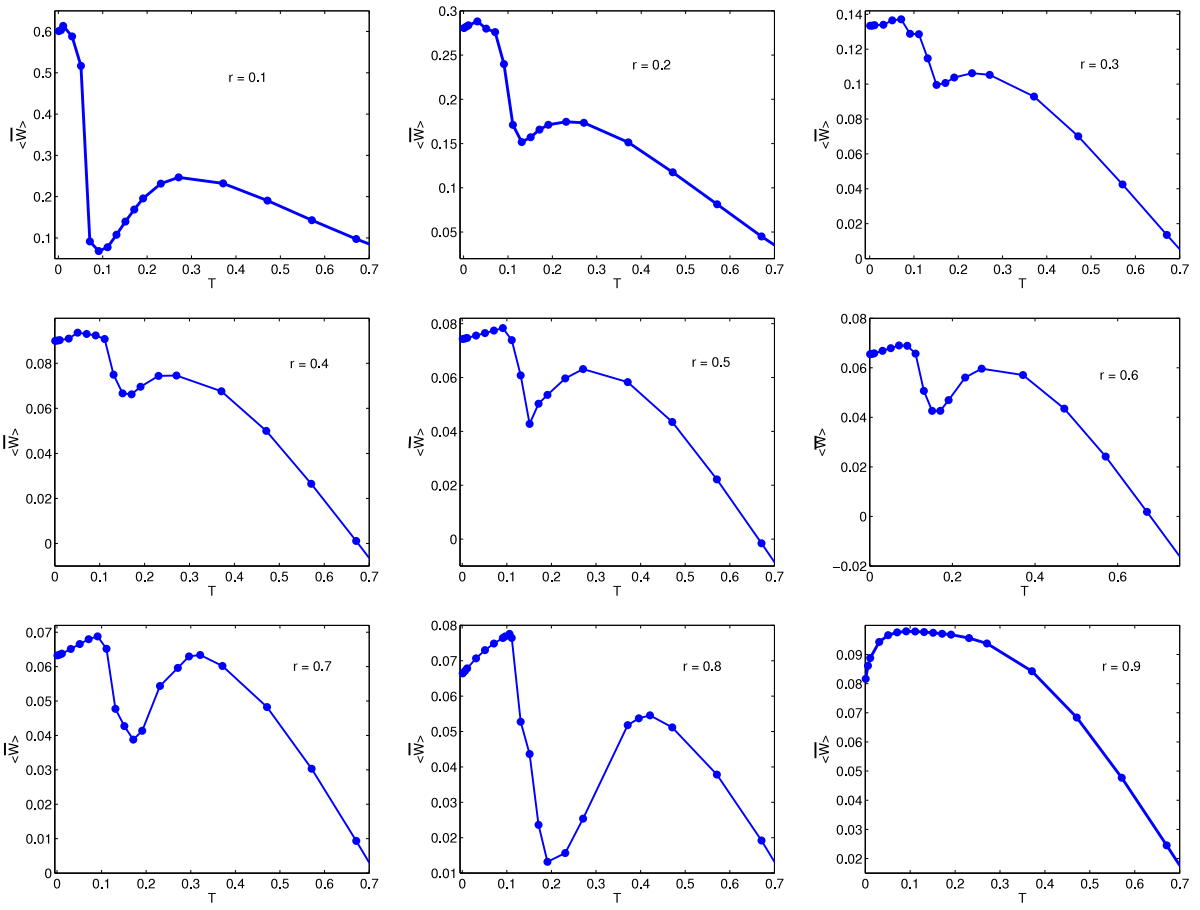

Fig. 10. Variation of $\langle\overline{W}\rangle$ as a function of T for ASDP system and for various values of shape parameters r. Other parameters are $M = 1$, $U_0 = 1$, $\gamma = 0.2$, $A_0 = 0.2$ and $F_0 = 0.1$.

an energetic activation barrier. In order to characterize the SR phenomenon, we use the hysteresis loop whose the area will allow to quantify it. Hysteresis loop closely resemble an ellipse. The hysteresis loops are different for various trajectories depending on the duration of the dynamics and shape of the potential. By numerically calculating Eqs. (3) and (4), one obtains the average input energy $\langle\overline{W}\rangle$ which is computed by averaging $\overline{W}$ over ensemble with different initial position. For several values of the shape parameters we plot in Fig. 10 the variation of the average input energy $\langle\overline{W}\rangle$ as a function of the temperature for ASDP case. The curves of $\langle\overline{W}\rangle$ initially increase, reach a maximum, decrease until attain a minimum, increase again until an other maximum and then gradually decrease with T. $\langle\overline{W}\rangle$ then displays two maxima whose the energy of the first is higher. In the literature, it is known that one maximum characterizes the phenomenon of SR, thus two maxima cannot be only a simple SR but rather a double SR. The cooperative effect of noise and external force does then show up. Due to finite tilting force F_0 the ASDP system illustrates two resonant temperatures for a wide range of shape parameter r. The first peak appears at the weak temperature namely at the limit of the deterministic. This peak has nothing to do with usual mechanical resonance, but it just associated to the intra-well dynamics, where less favorable conditions for transitions between wells are realized. Thus the temperature of occurrence of this first peak is not enough to allow to the particle to across the potential barrier. Second peak arising at higher temperature, relates to the classical SR phenomenon which is due to the mechanism of synchronization of the periodic external force with the activated inter-well dynamics. However, for $r = 0.9$, $\langle\overline{W}\rangle$ not exhibits two peaks of resonance but only one. In the DWDP case the behavior of $\langle\overline{W}\rangle$ is quite different from the one obtained for the ASDP model. As displayed in Fig. 11, $\langle\overline{W}\rangle$ exhibits a maximum as T is increased. The phenomenon of SR then occurs in this system for any value of r excepted for $r = 0.3$ where the curve of $\langle\overline{W}\rangle$ is monotonic. This no appearance of SR phenomenon for $r = 0.3$ is certainly due to the choice of the parameter's systems. To confirm that, let us take $\gamma = 0.12$ in the case of $r = 0.3$, where SR did not occur. The system clearly defines a peak of resonance, SR then takes place as depicted in Fig. 12(a). In this model, SR appears at lower temperatures than the ASDP system. The average input energy as well as temperature of occurrence of the SR strongly depend of r. each of both the systems gets the particular properties under the effects of noise and external force. Moreover, it is necessary to point that in this kind of system, there is generally competition between the phenomena such as the Chaos and the

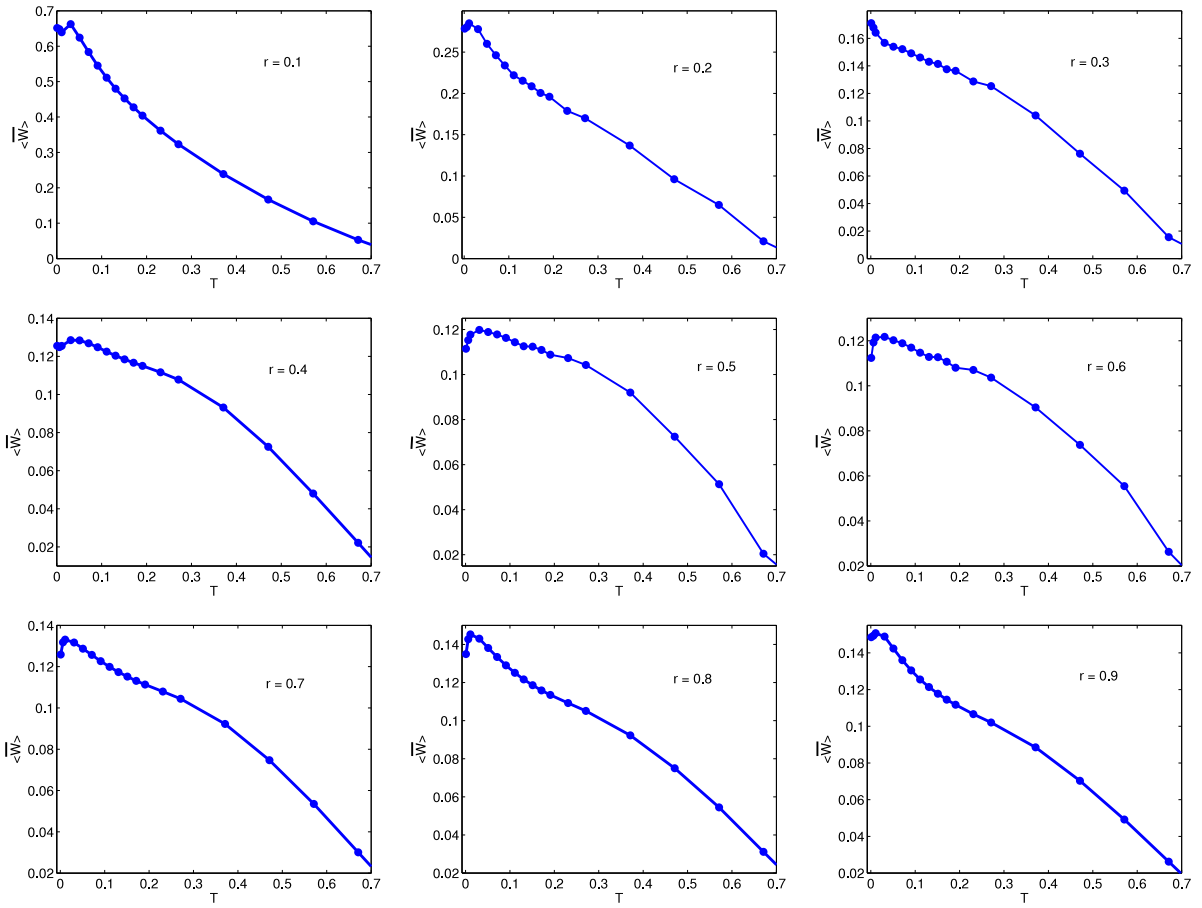

Fig. 11. Variation of $\langle \overline{W} \rangle$ as a function of T for DWDP system and for various values of shape parameters r. Other parameters are $M = 1$, $U_0 = 1$, $\gamma = 0.2$, $A_0 = 0.2$ and $F_0 = 0.1$.

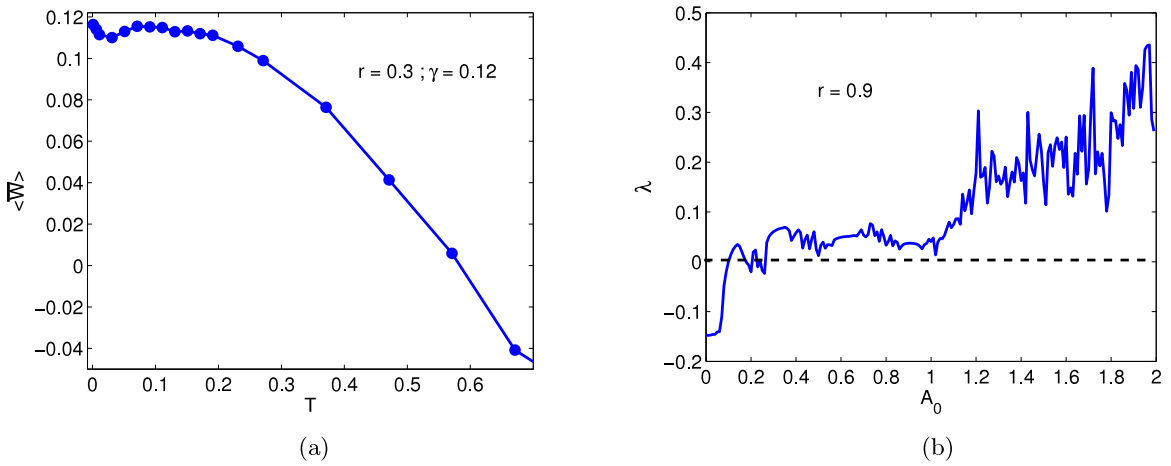

Fig. 12. Variation of $\langle \overline{W} \rangle$ as a function of T in the DWDP system for $r = 0.3$ and $\gamma = 0.12$ (a). Evolution of Lyapunov exponent λ with A_0 for $r = 0.9$ and $\gamma = 0.2$ (b). Other parameters are $M = 1$, $U_0 = 1$, $A_0 = 0.2$ and $F_0 = 0.1$.

stochastic resonance for example. What is the case for the DWDP system, for which we study the system's state from the Lyapunov exponent which is a good indicator of Chaos in dynamical system. For $r = 0.9$, one plots in Fig. 12(b) the Lyapunov exponent λ as a function of the amplitude of the external force A_0. Dashed line separates the domain where

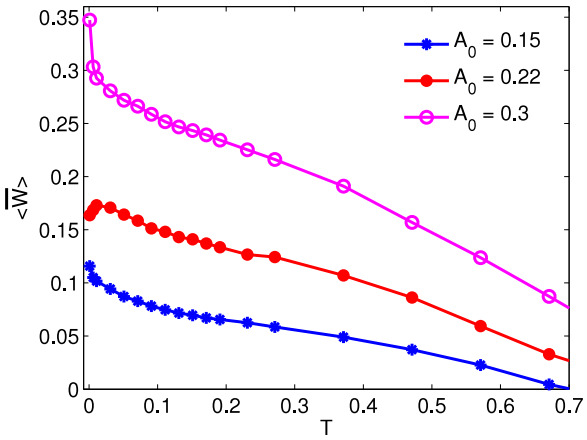

Fig. 13. Plot of $\langle \overline{W} \rangle$ with T in the DWDP model for $r = 0.9$ and for the values of A_0 indicated on the figure. Other parameters are $M = 1$, $U_0 = 1$, $\gamma = 0.2$ and $F_0 = 0.1$.

the Chaos is present ($\lambda > 0$) and the other hand where it is absent ($\lambda < 0$). Taking the values of $A_0 = 0.15$, 0.22 and 0.3, mainly where the Chaos is present in the system, we investigate the variation of $\langle \overline{W} \rangle$ with T in Fig. 13. Remark that SR appears for $A_0 = 0.22$ and does not occur for the two others values. Thus, the Chaos is responsible of the destruction of the SR phenomenon in the system when $A_0 = 0.15$ and $A_0 = 0.3$. Nevertheless it is not enough sufficient to prohibit the SR when $A_0 = 0.22$.

4. Concluding remarks

We have explored SR dynamics of two deformable models namely ASDP and DWDP for which the shape of the potential of each model is mainly defined from the shape parameter r. The mean residence time, the input energy as well as input energy distribution have been analyzed at low temperature in these both models. Our findings indicate that in the absence of the noise the amplitude of the external force at which the switching begin strongly depends of the potential shape. For each of the two models, $\overline{W}$ can be confined to two bands and only one as a function of r and $P(W)$ can have a bimodal or unimodal nature. For DWDP model, $P(W)$ gets a bimodal nature although $\overline{W}$ displays only one band when $r > 0.6$. We have noticed the presence of a double SR in the ASDP model for each value of r excepted for $r = 0.9$. However, SR only appears at weak temperatures in the DWDP case. Investigation of Chaos in the DWDP model for $r = 0.9$ is done in order to show that the disappearance of SR in the system can be due to Chaos. It would be interesting to study the interdependence between the Chaos and SR in the deformable systems in the goal to get some degree of physical understanding of the SR.

References

[1] U. Parlitz, Int. J. Bifurcation Chaos 3 (1993) 703.
[2] U.E. Vincent, A.N. Njah, O. Akinlade, A.R.T. Solarin, Chaos 14 (2004) 1018.
[3] Z. Zhang, X. Wag, M.C. Cross, Phys. Rev. E 65 (2002) 056211.
[4] A.P. Munuzuri, V. Perez-Munuzuri, M. Gumez-Gestena, L.O. Chua L O, V. Perez-Villar, Int. J. Bifurcation Chaos 5 (1995) 17.
[5] A. Kenfack, Chaos Solitons Fractals 15 (2003) 205.
[6] J. Kozlowski, U. Parlitz, W. Lauterborn, Phys. Rev. E 51 (1995) 1861.
[7] U.E. Vincent, A. Kenfack, Phys. Scr. 77 (2008) 045005.
[8] T. Hikihara, K. Torri, Y. Ueda, Phys. Lett. A 281 (2001) 155.
[9] T.L.M. Djomo Mbong, M. Siewe Siewe, C. Tchawoua, Commun. Nonlinear Sci. Numer. Simul. 22 (2015) 228.
[10] L. Machura, M. Kostur, P. Talkner, J. Łuczka, F. Marchesoni, P. Hänggi, Phys. Rev. E 70 (2004) 061105.
[11] A.M. Fopossi Mbemmo, G. Djuidjé Kenmoé, T.C. Kofané, Physica A 496 (2018) 1.
[12] Y.J. Wadop Ngouongo, G. Djuidjé Kenmoé, T.C. Kofané, Physica A 472 (2017) 25.
[13] S. Fauve, F. Heslot, Phys. Lett. A 97 (1983) 5.
[14] B. McNamara, K. Wiesenfeld, R. Roy, Phys. Rev. Lett. 60 (1988) 2626.
[15] R.L. Badzey, P. Mohanty, Nature 437 (2005) 995.
[16] H. Zhanga, T. Yang, Y. Xu, W. Xu, Eur. Phys. J. B 88 (2015) 125.
[17] N.G. Stocks, P.V.E. McClintock, S.M. Soskin, Europhys. Lett. 21 (1993) 395.
[18] B. McNamara, K. Wiesenfeld, Phys. Rev. A 39 (1989) 4854.
[19] M.I. Dykman, D.G. Luchinsky, R. Mannella, P.V.E. McClintock, N.D. Stein, N.G. Stocks, J. Stat. Phys. 70 (1993) 463.
[20] S. Saika, A.M. Jayannavar, M.C. Mahato, Phys. Rev. E 83 (2011) 061121.
[21] G. Djuidje Kenmoé, Y.J. Wadop Ngouongo, T.C. Kofané, J. Stat. Phys. 161 (2015) 475.
[22] M. Peyrard, M. Remoissenet, Phys. Rev. B 26 (1982) 2886.
[23] M. Remoissenet, Phys. Rev. B 29 (1984) 6.
[24] U.E. Vincent, T.O. Roy-Layinde, O.O. Popoola, P.O. Adesima, P.V.E. McClinkton, Phys. Rev. E 98 (2018) 6.

[25] M.C. Mahato, A.M. Jayannavar, Physica A 248 (1998) 138.
[26] M. Evstigneev, P. Reimann, C. Schmitt, C. Bechinger, J. Phys.: Condens. Matter 17 (2005) S3795.
[27] N. Kasdin, J. Guid. Control Dyn. 18 (1995) 114.
[28] K. Sekimoto, J. Phys. Soc. Japan 66 (1997) 6335.
[29] L. Gammaitoni, P. Hänggi, P. Jung, F. Marchesoni, Rev. Modern Phys. 70 (1998) 223.
[30] R. Benzi, G. Parisi, A. Sutera, A. Vulpiani, Tellus 34 (1982) 10.
[31] R. Benzi, G. Parisi, A. Sutera, A. Vulpiani, SIAM J. Appl. Math. 43 (1983) 565.